THE RELATIONSHIP OF AURORAL HYDROGEN EMISSIONS TO AURORAL MORPHOLOGY

A

DISSERTATION

Presented to the Faculty of the
University of Alaska in Partial Fulfillment
of the Requirements
For the Degree of
DOCTOR OF PHILOSOPHY

by

William J. Stringer, M.S.
College, Alaska

May 1971

THE RELATIONSHIP OF AURORAL HYDROGEN EMISSIONS

TO AURORAL MORPHOLOGY

APPROVED:

Hilbert E. Belon

Daniel W. Swift

J. Neal Davis

Gerald J. Romick
Chairman

John P. Mount (acting)
Department Head

APPROVED: C. Rubelk
Dean of the College of Mathematics,
Physical Sciences and Engineering

DATE: Dec 6 73, 1971

L. Lee
Vice President for Research and Advanced Study

TABLE OF CONTENTS

ABSTRACT

During the winters of 1964-65 and 1965-66 a north-south chain of meridian scanning photometers was operated in Alaska along the dipole 256° meridian effectively gathering auroral spectral photometric data between dipole latitudes 60° and 75°. This work presents the analysis of auroral H-beta and N_2^+ 4278 Å MSP measurements as representative of precipitation of energetic protons and electrons. In order to illustrate the conclusions drawn on the basis of this analysis, plots of zenith intensity from dipole latitude 60° to 75° of H-beta and N_2^+ 4278 Å have been prepared for every fifteen minutes during the night of January 20/21, 1966.

When examined in terms of the auroral substorm model, it is found that the most predictable feature of the aurora is the "hydrogen arc". In the evening sector it is always the most equatorward auroral feature. "Break up" always originates in the midnight sector when a narrow, bright, electron-produced arc appears within the broad (~ 2° of latitude) hydrogen arc near its poleward edge.

The electron-proton region "cross-over" in the morning sector was found to represent a statistical averaging including periods of "cross-over" following substorms and periods of superposition of electron and proton emissions during quiet auroral conditions. The "cross-over" occurs approximately thirty minutes following a substorm when the hydrogen arc vanishes and auroral patches occur in its place. During this time, hydrogen emission intensities peak polewards of the peak emission of electron-related emissions.

Further analysis of specific auroral features has indicated that narrow discrete regions of hydrogen emission coincident with very bright

electron-produced auroral arcs are produced by electron impact on atmospheric hydrogen atoms.

In order to interpret H-beta emissions in terms of precipitation of energetic protons, it was necessary to investigate the fraction of true hydrogen H-beta emission measured by an interference filter photometer. The first step was to obtain and analyze experimental H-beta line profiles. The profile analysis shows that the N_2 VK 2-15 band contaminates H-beta line profiles and therefore H-beta photometric measurements. This also answers a long-standing problem regarding the asymmetry of doppler profile measurements of the H-beta line taken from the magnetic horizon: removal of the N_2 VK 2-15 band produces a symmetric profile.

The second step was an analysis of other auroral emissions which contaminate H-beta auroral photometric measurements. The combined results of these two steps are: 1. Some regions of the galaxy can yield several hundred rayleighs of H-beta. Auroral H-beta measurements should not be made with these galactic regions as a background. 2. The N_2 VK 2-15 band contributes a variable amount of contamination depending on auroral electron flux. The variation is from a few percent at H-beta intensities of 300R to 25 percent at H-beta intensities of 1000R. 3. Spectral emissions from ionized atomic oxygen (OII) and atomic nitrogen (NI) contribute contaminations which are at the most equal to 10 and 3 percent of the total signal recorded. 4. Auroral background continuum contamination was estimated at half the contamination due to the N_2 VK 2-15 band. In conclusion, the total contamination of H-beta photometric measurements with the filters used here is no more than 50% for even the brightest auroras.

In order to investigate the total number flux of protons in the aurora, simultaneous auroral H-beta observations and in situ auroral proton measurements were compared with theoretical predictions relating proton precipitation and photon production. It was found that great fluxes of low energy protons are precipitated in some auroras. The consequence of this result is that the total auroral particle flux may be neutral or vary about neutrality.

ACKNOWLEDGEMENTS

This thesis bridges several areas of auroral research. It is not the result of a single experiment or a single set of observations. Hence, data and assistance were obtained from many individuals. This work was begun under the direction of Professor A. E. Belon and chiefly utilizes photometric data obtained by him and Dr. G. J. Romick. Professor Belon was absent during the central portion of the study and in his absence Dr. Romick became permanent advisor. However, Professor Belon remained actively interested in the research and rejoined my committee upon his return. I wish to thank him for his interest and guidance throughout my graduate career.

I wish to thank Dr. G. J. Romick for overall direction, patience and good humor during this undertaking. In particular, the photometric and spectographic results benefited greatly from his knowledge and guidance.

Professor D. W. Swift helped improve the general readability of the manuscript and in particular the organization and data interpretation of Chapter V. Dr. T. N. Davis read the manuscript critically and suggested many improvements in style and content. I assume responsibility for any errors which may remain despite the very much appreciated efforts of these gentlemen.

Mr. D. D. Wallis and Mr. N. B. Brown cooperated to help obtain the hydrogen H-beta emission line profiles used here. They also have helped me through discussions and useful suggestions. Thank you, Don and Neal.

Dr. Lyle Broadfoot, Kit Peak Observatory, provided the synthetic VK 2-15 band profile used. Dr. Robert Wax, TRW Systems, through helpful discussions gave insight to auroral rocket measurements and made several useful suggestions. Dr. Allen Johnstone cooperated toward interpretation of simultaneous rocket and ground-based measurements of auroral protons. These persons have my sincere thanks.

I would like to thank Professor Keith Mather, Director of the Geophysical Institute for his continuing interest and encouragement of all students and his support of the auroral research program at the Geophysical Institute.

Many other persons at the Geophysical Institute have helped greatly through either direct aid or by merely providing a friendly and cooperative atmosphere. In particular, I would like to thank the special photo section under Mr. Russ Beach, the steno section under Mrs. Margaret McCoy, our draftsman, Mrs. Shirley Wilson and special typist, Miss Alice Hupprich.

Special thanks go to Miss Judy Holland who came to my aid on many occasions.

I also thank my wife, Sandra, for not only domestic support of my research but on many occasions throughout my graduate career technical support as well.

This work was supported by the following National Science Foundation contracts or grants: GA 1660, GA 10144, GA 4597, and GA 28404.

LIST OF ILLUSTRATIONS

Generally, College and Fort Yukon data are available throughout the night. The Bar-I photometer did not contribute data until 0414 150° WMT.

Fig. 5.3 Parts 1a through 6b. Corresponding all-sky camera photographs and photographs of oscilloscope display of horizon-to-horizon scan of 5577 [OI] (top trace) and H-beta (bottom trace) illustrating various phases of a substorm which occured as a "break-up" at zenith at L.T. 0132, Nov. 2, 1965. (Belon and Romick, private communication).

Fig. 5.4 Parts a through g. Model of H-beta emissions during the auroral substorm. Relative H-beta emission contours are shown on plastic overlay covering a reproduction of the Akasofu (1964) auroral substorm model. (The substorm drawing for part f is a modified Akasofu drawing). Regions of discrete bright hydrogen emission are shown as solid lines. The boundary of pure proton precipitation (to the west) and mixed proton and electron precipitation (to the east) is shown as a dotted line.

Fig. 6.1 Horizon-to-horizon photometric scan in H-beta (left) and N_2^+ 4278 (right) obtained at College near local midnight, Oct. 29, 1970. The photometer output is displayed in three linear gains for each emission. The narrow, bright region of H-beta shows a deflection of .75 inch on the most sensitive gain while N_2^+ 4278 shows a deflection of 2.5 inches on the next highest gain. Hence the ratio of N_2^+ 4278 to H-beta is approximately 30 to 1.

Fig. 6.2 Scalings in relative intensity of 6704 (N_2), 5577 [OI] and H-beta against 4278 (N_2^+) of the bright arc in figure 4.3, parts 4b and 4c. Arrows indicate sequence of scalings from bottom of arc through peak emission to high altitude portions of arc.

Fig. 6.3 Estimated densities of atmospheric hydrogen from Bates and Nicolet, 1950, (top) and Bowman et. al., 1970 (bottom).

Fig. 6.4 Differential cross section for H-alpha production due to electron bombardment. (Kieffer, 1969).

Fig. 6.5 Profile showing normalized volume emission rate of λ 5577 [OI], λ 6300 [OI] and λ 3914 (N_2^+) versus altitude for a narrow auroral arc with peak emission at 110 km and lower border at 100 km altitude. (Romick and Belon, 1967).

Fig. 6.6 Schematic representation of satellite measurements of precipitating protons and electrons and simultaneous spectographic observations of H-alpha and λ 5577 [OI] at L.T. 2208 Nov. 9, 1966. (Romick and Sharp, 1967).

Fig. 6.7 (Top, right hand) Current distribution based on results of vector magnetometer flight (shown as curved line) above an auroral arc. (Cloutier, et. al., 1970).
(Center) Explanation of current distributions based on observed and inferred particle precipitation patterns. The Davidson (1965) charge-exchange spreading calculations have been used to produce hydrogen emission contours.
(Bottom) Predicted pattern of H-beta and N_2^+ 4278 auroral emissions resulting from particle precipitation patterns indicated.

Fig. D.1 Photograph of analog device constructed to show the field of view in the celestial sphere of a photometer scanning the 256° dipole meridian at a specified local time.

LIST OF TABLES

Table 5.1 Six minute scalings of horizontal component of College Magnetogram for Jan. 21, 1966 U.T.

CHAPTER I.

Review of Optical Emissions Related to Particle Precipitations

I.1 Introduction

Auroral spectrographic studies have historically utilized the emissions observed in auroras to investigate problems principally of aeronomical interest. The morphology of bright auroral features has been studied to gain knowledge of mechanisms responsible for a particle injection into the atmosphere from the magnetosphere or beyond. It is widely recognized, however, that the bright auroral features photographed for such purposes are caused by injected electrons. Spectrographic studies have indicated the injection of energetic protons as well as electrons during auroras.

A complete picture of the morphology of magnetospheric processes responsible for the aurora requires knowledge of proton precipitation patterns as well as the electron precipitation patterns deduced from auroral photographs. One method of obtaining this information is a systematic monitoring of both hydrogen and electron-associated optical emissions in the aurora. This thesis presents the results of such a study performed by means of interference filter photometers.

In view of the relatively low intensity of the auroral hydrogen emission it was necessary, before analyzing the photometric data, to first consider other sources of optical emissions occurring in the same spectral region as the observed hydrogen emission and to develop an analytical method to subtract this "contamination" from the signal received. Part of this analysis necessitated the acquisition of high resolution spectral "profiles" of the hydrogen emission line and the neighboring spectral regions. With the aid of these results, measurements of true hydrogen emissions

and electron-produced emissions were compared within the framework of the auroral substorm model proposed by Akasofu (1964, 1965). The result was the development of a model of proton precipitation during the substorm.

The study of magnetospheric processes requires that ultimately the hydrogen emissions and electron-produced emissions be related to the flux and energy spectra of the incident particles. A coordinated experiment comparing measured hydrogen emission intensities with direct measurements of protons in an aurora was performed. The results of this experiment have been found to be consistent with theoretical predictions relating energetic auroral protons and hydrogen emissions.

The relationship between auroral hydrogen emissions and injected protons was then used to investigate specific features of the auroral "hydrogen arc", and to relate them to patterns of electron and proton precipitation. Owing to their importance in auroral theories, the questions of flux neutrality and proton-electron cross-over behaviors are examined in detail.

The subject matter of this thesis overlaps considerably the disciplines of magnetospheric physics and aeronomy. In order to present the discussions of H-beta contamination, line profiles, the general substorm picture, and the effects of the interaction of the magnetic field on the pattern of precipitating protons with some degrees of continuity, a brief review of pertinent but diverse background material is presented in this introductory chapter.

1.2 Historical Background

The history of the identification of hydrogen lines in the auroral spectrum and the discovery that their line profile indicated the incidence of fast protons onto the atmosphere is somewhat uncertain. Chamberlain (1961) was probably most correct when he credited the identification of atomic hydrogen lines in the auroral spectrum to Vegard (1939), the recognition that these lines were broadened to Gartlein in 1948 (see Gartlein, 1950) and the actual measurement of displaced doppler profiles to Meinel (1950).

Vegard (1939) published a letter to Nature showing a portion of a spectrogram containing a broad bump with a spike at 4860 Å which was icentified as H-beta and a well-pronounced line at 6563 Å which was identified as H-alpha. In this note Vegard stressed two statements - "...occasionally considerable quantities of hydrogen are present in the auroral region." and "...The occurrence of strong hydrogen lines must be due to showers of hydrogen or to a kind of hydrogen radiation occasionally coming from the sun." The principle theme of this note was the formation of noctilucent clouds and a mechanism he had proposed some years earlier that occasionally hydrogen "showers" increase the hydrogen density in the upper atmosphere to make the formation of water vapor possible.

Apparently, C. W. Gartlein attended the 1948 Oslo Assembly of the I.V.G.G. where he presented spectrographic data indicating doppler broadening of hydrogen lines observed near the horizon. He interpreted this as indicating "...the presence of hydrogen in violent random motion during many auroras."

During the great aurora of August 18, 1950, Meinel (1950) obtained, a spectrogram from the zenith sky showing a definitely doppler-displaced hydrogen profile indicating incoming hydrogen velocities of 3200 km/sec. This was interpreted as due to incoming protons.

General acknowledgement that at times, at least, incoming energetic protons could be associated with the aurora led to speculation that protons could be the cause of the aurora and considerable effort was spent investigating this possibility. Chamberlain (1961) and Eather (1967) have reviewed this history extensively and it is unneccessary to repeat it in detail here. Generally, calculations (Chamberlain, 1961) began to show that the small flux of protons observed, as inferred from the intensity of hydrogen emissions, simply could not produce all the emissions found in the aurora. Later, balloon and rocket-borne detectors measured Bremsstrahlung x-rays at high altitudes indicating precipitation of high-energy electrons into the atmosphere. As the possibility rose that energetic electrons precipitated into the atmosphere could be the primary source of auroral emissions, consideration of the role of protons diminished.

Romick and Elvey (1958), using all-sky camera photographs and spectrograms from a HUET C-1 flint glass prism spectrograph, described what are still considered here to be the essential characteristics of auroral hydrogen emission. This picture was developed further a little later by Rees, Belon and Romick (1963). The general features observed for dipole latitudes $\sim 65°$ were:

1) Hydrogen emission is associated with a broad diffuse weak auroral arc located always to the south of bright, more active electron-associated arcs during the early evening.

2) The hydrogen region moves equatorward in the evening and returns poleward in morning.

3) During or just after auroral breakup hydrogen emission diminishes in those regions where patches form and if it is to be found anywhere it is located poleward at that time.

Montbriand (1969) reviews the history of the development of the morphology of hydrogen emissions crediting the above authors with the results listed and indicates that these observations were verified by Montbriand (1961), Montbriand and Vallance-Jones (1962), Stoffregen and Derblom (1962) and Omholt, Stoffregen and Derblom (1962).

However, several areas of controversy or misunderstanding have arisen. A series of auroral observations by Montalbetti (1959), Eather and Jacha (1966) and Eather and Sandford (1966) concluded that the hydrogen emission was contained in a wide-spread (7° latitude) mantle of aurora not associated with any particular auroral form. Also Eather (see Eather 1967) severely disputed many observations of hydrogen intensities greater than 150 rayleighs. A "cross over" of hydrogen emission was proposed by Stoffregen and Derbolm (1962), supported by some authors and disputed by others (Eather and Sandford (1966)). By this time much of the controversy has been resolved and it is hoped that this present work will resolve even further the areas of disagreement which had arisen.

Early auroral hydrogen measurements were utilized to determine the number and energy spectrum of injected protons from laboratory measurements of the intensities of hydrogen spectral lines emitted in the process of bombarding atmospheric gases with energetic protons. During the last decade a number of direct measurements of auroral protons have been made by means of rocket-borne detectors. In pre-

paration for the discussion in Chapter V of an experiment relating hydrogen intensity measurements and direct proton measurements, recent in situ measurements of auroral protons are reviewed briefly.

1.3 Direct Particle Measurements

Auroral electron and proton energies have been measured directly by means of rockets and polar-orbiting satellites. Miller (1969) reviewed published results including those appearing between 1960 (McIlwain, 1960) and 1969 (Chase, 1969) and produced a diagram containing all these results displayed on logarithmic scales of number versus energy. This diagram is reproduced here as figure 1.1, which also incorporates the results obtained by Bernstein, et. al. (1969) and Johnstone (1970).

In general, it can be noted without reference to individual papers that the older measurements were made with particle detectors which were insensitive to low energy particles. The data from these measurements were generally fit to energy spectral laws of the form $N = N_o e^{\frac{-E}{E_o}}$

Where N is the number of protons having an energy E, and E_o is a constant called the characteristic energy of the distribution of protons. The data shown here are the derived spectral laws. In general, the characteristic energy of these exponential laws was near the lower detector threshold energy. A power law fit (straight line on this figure) may have been applied just as well in some cases, since the deviation from a straight line is very small.

Both Bernstein, et. al. (1969), and Johnstone (1970) attempted several fits to their data but found only a power law to fit well. The reason researchers have been reluctent to use power law fits to particle spectra is that the integrand becomes infinite at low energies.

Fig. I.1 Measured differential energy spectra of auroral protons.

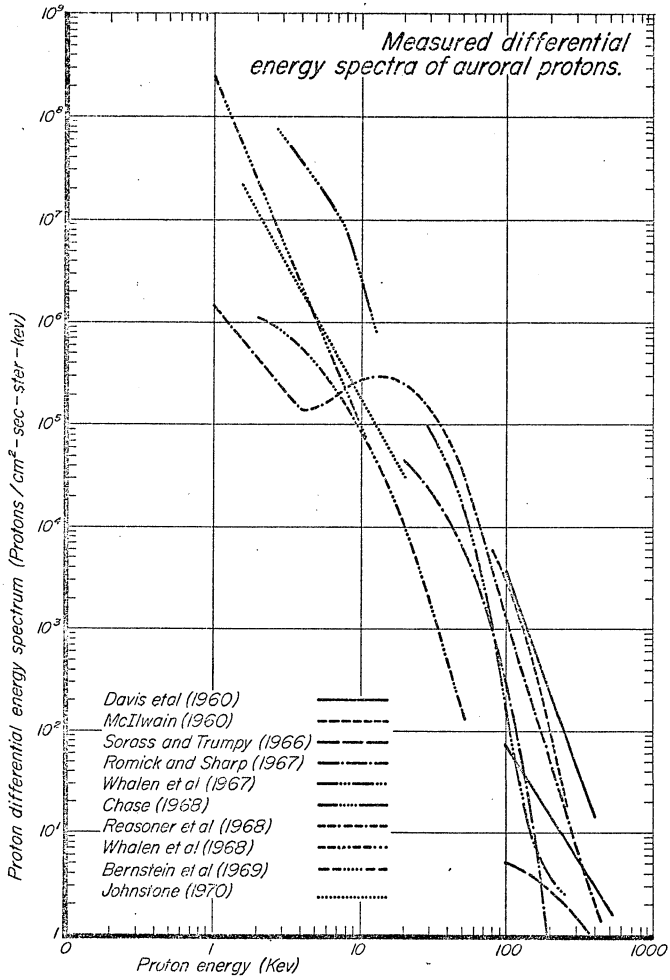

This point will be the topic of one section of Chapter IV. Whereas former experimenters found that they could match up their data with exponential spectra - if the characteristic energy were low enough - the more recent measurements at lower energies forced abandonment of all attempts at exponential fits.

The proton spectrum data in figure I.1 were taken over a moderately wide range of auroral environments. Yet, in general, with the exception of Whalen's and Reasoner's low energy data, there seems to be a general trend for proton spectra to follow power law energy distributions similar to Johnstone's from at least 1 or 2 kev to 200 kev.

Ground-based hydrogen emission measurements and low altitude (<300 km) rocket measurements reflect the spatial distribution of protons after they have entered the atmosphere. This measured distribution can be considerably different from the distribution of injected protons above the atmosphere.

I.4 Charge-Change Spreading of an Injected Proton Beam

The behavior of protons upon entering the earth's atmosphere has been treated theoretically by Davidson (1965). A Monte Carlo method was used to compute the latitudinal dispersion in the auroral zone of 5 to 20 kev protons injected on a field line, having a magnetic latitude of 67° at the earth's surface with two model pitch angle distributions. Neutral hydrogen atoms resulting from charge-exchange at altitudes of 500 to 300 km were found to travel large distances across field lines before ionization again confined them to a spiral path downward. As this process (illustrated in figure I.2) is repeated, a diffusion process takes place that spreads the original proton sheet into a region several hundred kilometers wide.

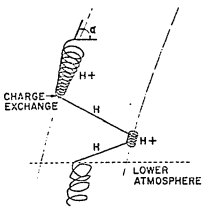

Fig. 1.2 The trajectory of a low-energy proton entering the earth's atmosphere. Near the end of the path, charge changes become so frequent that the orbit is nearly a spiral corresponding to an effective charge less than one electronic charge. (Davidson, 1965).

The results were found to depend upon the initial pitch angle distribution assumed. The two pitch angle distributions employed by Davidson are defined as follows. If α is the angle measured at the equatorial plane between the proton velocity vector and the magnetic field line, the distribution which is defined as being "isotropic" is uniform over values of α between 0° and 3°. (Protons with values of $\alpha > 3°$ are "mirrored" before reaching the atmosphere.) The distribution which is defined as "$\sin^{-1}$" signifies a population of protons proportional to $\sin^{-1} \alpha$ between 0° and 3° in the equatorial plane. At the top of the atmosphere the first distribution is truly isotropic because protons with $\alpha > 3°$ are reflected back to the equatorial plane; the second distribution is sharply peaked in the direction of the incident beam of protons.

Figures 1.3 and 1.4 show the latitudinal distribution of the resulting H-alpha emission for both pitch angle distributions. There is considerable difference between the width of the region of peak hydrogen intensity for isotropic and $\sin^{-1}$ pitch angle distributions. (As will be discussed in Chapter IV, $\sin^{-1}$ pitch angle distributions are highly unlikely.)

Davidson concluded that the results were relatively independent of injection energy provided that the proton energy is less than that at which the charge exchange cross section begins to fall rapidly. Figure 1.5 shows these cross sections for hydrogen and oxygen. The behavior of the nitrogen cross section is similar to those shown. The point worth noting here is that between 10 kev and 100 kev the ionization cross section decreases by two orders of magnitude while the change exchange cross section is relatively unchanged.

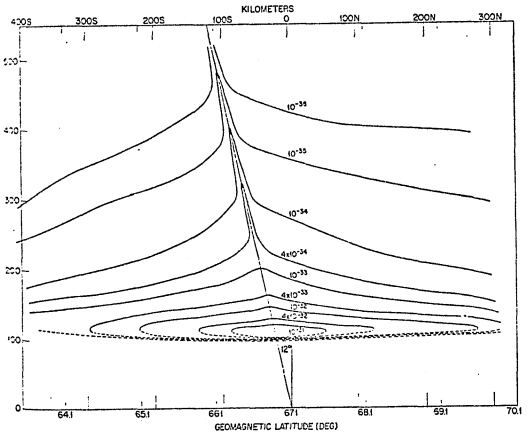

Fig. 1.3 The energy density (in ergs per cubic centimeter per injected proton) of Balmer α emission excited by protons and hydrogen atoms entering the atmosphere from above. The injection pitch angle distribution is isotropic. The proton injection energy is 10 kev. (Davidson, 1965).

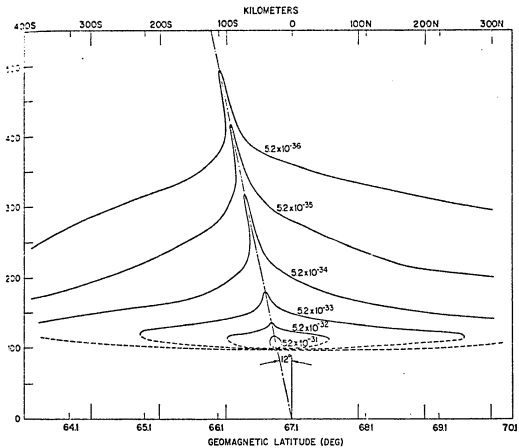

Fig. 1.4 The energy density (in ergs per cubic centimeter per injected proton) of Balmer α emission excited by 10 kev protons and hydrogen atoms entering the atmosphere from above. An injection pitch angle distribution proportional to $(\sin)^{-1}$ was assumed. (Davidson, 1965).

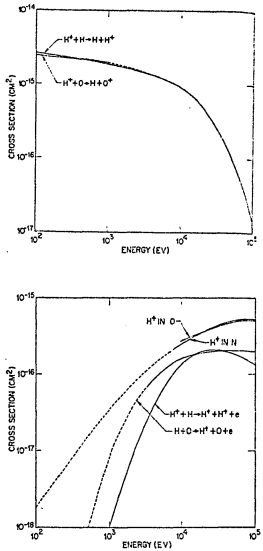

Fig. I.5 (Top) Charge-exchange cross sections. Measured values of charge-exchange cross section for proton-oxygen collisions are extrapolated above 1 kev to lie nearly on the curve that best fits the experimental and theoretical results for protons on hydrogen atoms.

(Bottom) Ionization cross sections. The curves shown for oxygen and nitrogen are one-half the measured stopping powers per molecule in the molecular gas, divided by 35 ev per ion pair. Plausible extrapolations are indicated by dashed lines below 10 kev. (Davidson, 1965).

TABLE I.I

Altitude, km	$H^+ \rightarrow H$		$H^+ \rightarrow H$	
	5 kev	100 kev	5 kev	100 kev
700	9900			
600	4300			
500	490		10,000	
400	98		2,000	
300	19	300	300	100
200	4	50	30	16
180	2	$\sim$ 25		
150	1	$\sim$ 10	5	
120	0.2			

Table I.I Mean free path in km for charge change of 5 kev protons (Davidson, 1965) compared with estimated values for 100 kev (using CIRA atmosphere tables) at various altitudes in the atmosphere.

Table 1.1 gives Davidson's mean free paths for charge exchange processes of 5 kev protons and hydrogen atoms for various altitudes in the atmosphere. Added to Davidson's values are values for 100 kev protons computed for comparison purposes for later discussions here. In particular note that, whereas the mean free path for neutralization is increased, the mean free path for ionization is decreased for 100 kev protons. Hence one expects rather severe changes in the spatial extent of the emission region due to change of proton energy from 10 kev to 100 kev.

This charge-change beam spreading does not occur to injected electrons. On the basis of this behavioral difference alone one also expects a difference in general character between hydrogen emission regions and regions of auroral emissions related to precipitated electrons. One major object of this work is to relate the behavior of these two types of emission regions in the aurora. The behavior of the electron-produced emission regions is that of the visually or photographically observed auroral features - hydrogen emissions being below the visual and photographic threshold. The behavior of visually observed auroral features has been documented and described in terms of the auroral substorm model.

1.5 The Dynamic Behavior of the Aurora

1.5.1 The auroral substorm

Akasofu (1964, 1965) has documented a recurring auroral substorm which determines the behavior of the aurora throughout the nighttime sector. All-sky camera photographs taken simultaneously throughout

the entire polar region indicate that the auroral system regularly undergoes an expansion and contraction centered near dipole (dp) midnight. The behavior of the aurora throughout the nighttime sector of the auroral belt is governed by the phase of this substorm: The expansive phase starts by a sudden increase in brightness of the part of some quiet arc which is near the dp midnight meridian. Thereafter, within 10-30 minutes this arc and the ones to the north take part in a rapid bulging motion toward the dp pole. Simultaneous with the auroral substorm, a magnetic substorm is found on magnetograms. The area covered by the substorm is much larger than the area effectively covered by a single all-sky camera or seen by a single observer. Therefore, the phases of the substorm appear differently to different observers, depending upon their location relative to the substorm. Akasofu has described a substorm as seen from four observing stations at various dp times with respect to the center of the substorm.

The early evening side. If the substorm is rather weak, the homogeneous arcs characterizing the quiet-time early evening display may not be affected at all, or a slight increase in luminosity and a hint of inhomogeneity may be noticed in the arcs. If the substorm is of moderate strength, the number and luminosity of the arcs increases. Yet, the arcs do not undergo a major displacement from the vicinity of the auroral zone even though rays and other inhomogeneous features appear. The H component of the geomagnetic field may increase corresponding with a weak eastward electrojet. If the substorm is of considerable magnitude, the arcs here show ray structure or westward-traveling folds. The arcs spread all over the latitude strip customarily occupied by the

aurora. The eastward current is definitely indicated and coronal-type structures may be seen north of the auroral zone.

The evening side. Even during quiet times in the evening sector (2200-2300 dp) some motion and inhomogeneity is evident in the auroral arcs. When a moderate substorm takes place--centered about 2 to 3 hours in local time to the east--the number and luminosity of the arcs increase and westward-traveling folds can be seen. With increasing substorm intensity, the folds transform from wave motion along the arcs to markedly folded distortions in the arc which become very large and cause wholesale displacement of the arc. In this case the arc is said to undergo a pseudo breakup. Even here, however, there is not a large change of the magnetic field. If the substorm is very intense, instead of being severely folded, the arcs are actually broken up and the resulting arc segments drift rapidly toward the west. In this case the H component of the field undergoes a sharp decrease indicating a large westward auroral electrojet.

The morning side. During a substorm of moderate strength, the characteristics are most identifiable in the morning sector. The activation and auroral luminosity are greatest here. The arc may fold in an irregular way or actually break up. Arc segments and other forms drift eastward. Many isolated rays and coronal bundles appear and the background luminosity increases. On the northern border of the expanding bulge new arcs form and move northward rapidly. This expansive bulge can extend to quite high latitudes ($\sim 75°$ dp).

The late morning side. If the substorm is weak, the arcs merely increase in brightness. If the substorm is of greater strength, the arcs in the auroral zone and to the south are likely to break up, and the segments dissolve into patches resembling cumulus clouds, which drift eastward. The more northern arcs retain a curtain-like structure. At the end of the active expansive stage many of the arcs on the early evening side disappear or become faint. On the morning and late morning side a number of faint and diffuse arcs tend to be found in a patchy aurora which form after the expansion. Many of the arcs which advanced northward during the expansive stage now return toward the auroral zone.

1.5.2 The behavior of the aurora in the low latitude sector of the auroral oval . . .quiet periods of class I and class II.

At times during the IGY (Akasofu, 1964) periods of several days were found with no magnetic storms yet polar magnetic substorms occurred. If no substorms occurred, these periods were called quiet periods of class I. The auroral displays at these times consisted of faint arcs seen mainly in the vicinity of midnight. During the IGY there were periods of relative quiet between substorms (which may or may not be associated with a magnetic storm having a sudden commencement). These quiet periods Akasofu called quiet periods of type II. They are characterized by faint bands in the vicinity of 75° dp in the midnight sector, faint arcs in the evening side at auroral zone latitudes and broken patches and faint bands in the midnight and morning sectors of the auroral zone.

1.5.3 The model

Based on the observations outlined briefly in the above two sections, Akasofu has proposed a model to show the auroral features which may be seen in the field of view of a single all-sky camera placed at some location in the vicinity of the substorm. In figure 1.6 the discrete auroral forms of the entire auroral cap are depicted for six different times with respect to the time of a substorm. The small circle shown gives the segment of the substorm which would be seen at these different times by an all-sky camera fixed on the earth. A typical magnetogram (horizontal component, H) and the aurora as observed with an all-sky camera are shown.

It can be seen that an all-sky camera and magnetic station at one location will see a different version of the substorm than similar instruments at other locations. During the time interval shown in these figures, three substorms took place. The first all-sky photograph is of early evening aurora during a type II quiet period. The next shows a mid-evening all-sky photograph just to the west of a medium-strength substorm at the end of the expansive stage. The third again shows a type II quiet period, while the fourth shows the sky as seen from a location just on the morning side of a developing substorm. Note that while at the time of the second photograph a small return current was indicated on the magnetogram, here a large westward electrojet appears. The fifth view is again of a type II quiet period. (Note the recovery of the magnetogram and the absence of any current.) The sixth frame shows the sky in the mid-morning with a substorm in progress in the midnight sector. Note that here, too, a rather strong electrojet is indicated by the magnetogram.

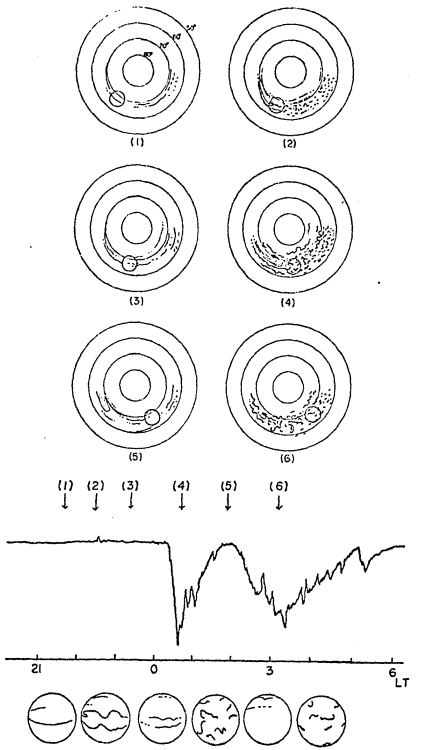

Fig. 1.6 A model distribution of auroras over the northern polar region illustrating the dynamic behavior of the polar auroral substorm. (Akasofu, 1964).

1.6 Auroral Hydrogen Measurements

Recently, Montbriand (1969) has described a morphology of the hydrogen emission region on the basis of the auroral substorm for increasing levels of substorm activity. His results were obtained from the analysis of spectographic data from a north-south chain of meridian spectographs located across the auroral zone.

The results described in this thesis for the location of the hydrogen emission zone agree with the location of the zone found by Montbriand, and it is unnecessary to reproduce his figures. The observations reported here utilized calibrated photometric data and the results have extended the morphology of hydrogen during the substorm to include relative hydrogen intensities. Regions of pure proton precipitation have been identified, and absolute intensity measurements have been interpreted in terms of actual number fluxes of injected protons.

One of the basic contributions of this thesis is absolute intensity measurements of hydrogen emission in the aurora. To achieve these absolute measurements it was first necessary to perform a detailed analysis of auroral emissions which may contaminate the hydrogen H-beta line emissions monitored by photometric measurements. This analysis entailed obtaining profiles of intensity versus wavelengths of the H-beta line and the immediate spectral vicinity, and then identifying and removing contaminating emissions. Such a contamination analysis has not been performed before and will therefore be described in detail.

CHAPTER II

H-beta Profile Measurement, Contaminating Emissions

2.1 Introduction

The early hydrogen line profiles (Meinel, 1950 ; Vegard, 1955 ; and Gartlein and Sprague, 1957) were obtained from microdensitometer tracings of spectrograms and did not yield much detail. However, it was quickly realized (Gartlein and Sprague, 1957 ; Vegard, 1955 ; Omholt, 1956 ; and Chamberlain, 1961) that analysis of the line profiles could yield some information regarding energy and pitch angle distributions of the protons. Some attempts were made at such an analysis (Chamberlain, 1961) but the results were far from satisfactory.

In the early 1960's, scanning spectrophotometers were developed and more satisfactory profiles were obtained. (See Eather, 1967, for a review of these measurements). This author's initial interest in H-beta line profiles stemmed from concern that the H-beta photometric measurements to be used in the analysis of the role of protons in the auroral substorm might be significantly contaminated by other auroral emissions. It was also thought to be useful to obtain a set of zenith and horizon profiles to determine absolute total line intensities from photometric measurements (See Appendix A). This chapter contains discussion of the major contaminants of H-beta in quantitative fashion, the removal of these contaminants from profiles obtained at College and, finally, the analysis of the resulting corrected profiles in preparation for the general discussion of the contamination of H-beta photometric signals.

2.2 Contaminating Emissions

2.2.1 The Vegard-Kaplan 2-15 band

For some time it has been recognized that there is a molecular band head near 4835 Å and that the associated band degrades toward longer wavelengths. Vegard and Kvifte (1945) originally ascribed the emissions as due to H_2. Later , it was found to be the 2-15 band of the forbidden Vegard-Kaplan system of N_2. The fact that the VK 2-15 band underlies the H-beta line has often been used to discredit observations indicating intensity fluctuations or even great intensities (>500R) of H-beta. These arguments have always been qualitative but nevertheless damaging to reported observations. Evidently, the problem of removing the VK 2-15 band from H-beta line profile measurements has not been discussed previously. Most published profiles show smoothed data. Those which show raw data indicate that the H-beta profile was determined by the best smooth curve which could be drawn under a plot of the instrumental signal output.

The Vegard Kaplan band system of N_2 results from a first-order forbidden transition from the $A^3\Sigma_u^+$ state to the $X^1\Sigma_g^+$ state. The lifetime for this transition has variously been reported from as long as 30 seconds (Oldenberg et. al. 1961) to as short as 2 seconds (Shemansky and Carelton 1969). The particular band under consideration here, the 2-15 band, has its band head at 4835 Å and degrades toward longer wavelengths for over 100 Å. (See figure 2.2). The band has two P and R branches each and no Q branch. The result is a rather complicated structure.

Broadfoot (private communication) has calculated on the basis of Broadfoot and Hunten's (1964) intensity measurements and theoretical

considerations by Shemansky (1969), intensity ratios for the VK system. If the total VK system emissions have an intensity of 15KR, approximately 3KR will appear in the $V^1 = 2$ level, and of this 3% or 90R will appear in the VK 2-15 band. Using a maximum observed intensity of 20KR for the 6704 Å I PG (5-2) band of N^2 (Romick, private communication) and the relative intensity and vibrational distribution for the N^2 B state from the paper by Broadfoot and Hunten (1964) gives a possible total VK emission of 72 KR. Thus, the total VK 2-15 band intensity would be 450 R. This is probably the maximum intensity expected for the 2-15 band.

2.2.2 Auroral OII lines

Introduction

Contamination by atomic emission lines of ionized oxygen of H-beta line profiles and photometric data could possibly be comparable in magnitude to contamination due to the VK 2-15 band. The wave lengths of the OII lines lying in the vicinity of the H-beta profile, their identification, line strength and estimated maximum intensity are given in Table 2.1.

Table 2.1

λ	Transition Array	Multiplet	Line Strength (S)	Est. Max. Int. (R)
4861	$2p^3p^1-2p^2\ (^1D)\ 3d^1$	#57 $^2p^o-^2D$	8.3	26R
4871	$2p^3p^1-2p^2\ (^1D)\ 3d^1$	#57 $^2p^o-^2D$	14.9	42R
4857	$2p^3 3p-2p^2\ (^3P)\ 3d$	#29 $^4s^o-^4D$	7.16	22R
4865	$2p^3 3p-2p^2\ (^3P)\ 3d$	#29 $^4S^o-4D$	2.67	8R

Intensities of the OII lines

Possible intensities of these atomic lines were estimated by means of their line strength and that of the OII line at 4189 Å which was identified on Chamberlain's (1961) auroral spectral atlas. The intensity of 4189 Å (OII) was estimated at 500 R on the basis of nearby lines whose intensity had been given. This line belongs to the same transition array as 4861 Å and 4871 Å (OII). While this transition array has only been tentatively identified as belonging to the auroral spectrum, the transition array to which 4856 Å and 4865 Å (OII) belong is well known in the auroral spectrum.

Gal'perin (1959) indicates the presence of 4856.8 Å (OII) on an experimental H-beta profile. While no absolute intensities were given, its amplitude was approximately 1/5 the peak R/Å (rayleighs per angstrom) of the H-beta profile. A total assumed H-beta emission of 1000 R corresponds to a peak emission of approximately 44 R/Å for the instrument-broadened 4856 Å (OII) line. Using Gal'perin's published instrumental width, this peak emission yields approximately 30 R for the total 4856 Å (OII) emission. Hence, the intensity estimated here (Table 2.1), 22 R, may be taken as a reasonable value for this emission, especially since the above estimate is based on spectra taken during the very bright aurora of February 18/19, 1958, and also because it is very unlikely that the H-beta profile reported by Gal'perin was obtained under H-beta intensities greater than 500 R.

2.2.3 Auroral NI lines

Neutral lines of atomic nitrogen are listed at 4846.7 Å and 4850.5 Å but have never been observed in the laboratory (Remy, et. al., 1960).

Because of the great uncertainty of their existence, the NI lines were not considered in the H_β profile analysis. These lines will be discussed again in Chapter III.

2.2.4 Auroral background continuum

The possibility of an auroral background continuum is discussed in the next chapter. The existence of a continuum which is rather uniform in intensity over a portion of the spectrum has no effect on the H-beta line profile analysis which is under discussion here since it only changes the background level which is subtracted from the data by graphical methods.

2.3 H-beta Line Profile Measurement

2.3.1 Instrumentation

The line profiles reported here were measured by means of a 0.75 meter f/4 scanning spectrophotometer of the Ebert-Fastie design (Fastie, 1952). The stationary instrument is provided with an optical head assembly consisting of two mirrors, one of which may be turned in elevation. Rotation of the entire head assembly permits the azimuthal component of "aiming". In the configuration used for this experiment, unfocused auroral light is reflected onto the 10.5 cm curved entrance slit by the optical head assembly. The field of view is approximately 14° square. The diffraction grating used is 20 cm by 15 cm and blazed at 5000 Å with 1200/lines/mm.

The grating is driven by a 6 rpm motor through a cam which is so constructed as to provide scans which are linear in Å / sec. Light from the curved exit slit is reformed by means of a fiber optics system to the round configuration of the face plate of an RCA 7265 photomultiplyer having S-20 photocathode response. The photomultiplyer is thermally stabilized at -20° C by a commercial thermoelectric system. The output

signal is amplified by a Keithley 417 electrometer and recorded simultaneously with time and scan-encoding data on magnetic tape. A digital summing device, ("Enhancetron" manufactured by Nuclear Data) can be used in real time or in playback to add successive scans when the signal-to-noise ratio is such that its use is warranted. The direct scan output or the summed scans can then be printed on an x-y plotter. Simultaneous with these measurements, a meridian scanning photometer scanning from horizon to horizon along the dipole meridian every 10 seconds was operated to provide absolute intensity measurements.

H-beta line profiles were obtained on approximately 30 nights during the winter of 1968-69. From these nights, 14 profiles were selected for analysis. The criterion for selection was the apparent signal-to-noise ratio. Not all of the profiles selected in this way were as well-behaved as profiles which have been previously published.

2.3.2 Removal of instrument function and contaminating emissions from H-beta line profiles

The method employed for removal of the instrument function from the H-beta profile was adapted from Bracewell (1955). This method is essentially a graphical method of deconvoluting the convolution of two smooth, well-behaved functions, one of which is known. Hence, the deconvoluted profile could not be expected to exhibit sharp atomic lines which had been convoluted by the instrument function. Therefore, all contaminating emissions were convoluted with the instrument function and then subtracted from the raw profile. The uncontaminated profile was then de-convoluted.

Removal of the VK 2-15 band

Synthetic VK 2-15 band spectra were obtained from Broadfoot (private communication) for several temperatures. The band representing T = 900° was chosen for this analysis because it corresponds to the probable altitude (150-180 km) of the VK 2-15 emission. The empirical method chosen for removal of possible VK 2-15 contamination was as follows. The synthetic VK 2-15 band had been specified in terms of intensity for every third of an angstrom. Hence the raw data were scaled in thirds of angstroms to remove some noise but in no way to affect the basic information contained. The VK 2-15 band was convoluted with the instrument function and subtracted from the scaled profile with peak intensity equal to 0.1, 0.2, ---, 0.5 times the peak intensity of the scaled profile. The results were then renormalized for comparison purposes. The criterion for selecting the modified profile which reflected the subtraction of the proper amount of VK 2-15 was to require that the dark currents on both sides of the profile be made equal by the subtraction of the VK 2-15. (Note that the band extends far to the red of the H-beta profile). Hence subtraction of too much VK 2-15 causes, after renormalization, the dark current on the blue side of the H-beta profile to be raised above that on the red side. Figure 2.1 shows the plotted output of 70 summed zenith profile scans. Figure 2.2 shows the summed scans as scaled and normalized (dashed) and the result of subtraction of convoluted VK 2-15 band of peak intensity 0.1 (a), 0.2 (b), and 0.3 (c) that of the dashed H-beta profile. The modified profiles were then renormalized. Examination of the figure shows that case a represents the subtraction of too little VK 2-15 while case c represents the subtraction of too much VK 2-15. The proper VK peak intensity appears

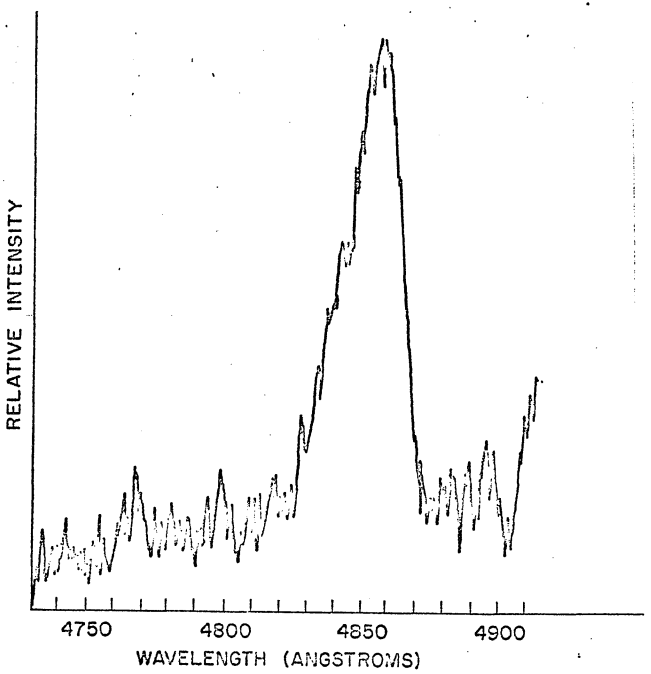

Fig. 2.1 H-beta emission doppler profile observed at zenith. This profile is the sum of 70 spectrophotometer scans across the wavelength interval shown. The duration of each scan was 8 seconds.

Fig. 2.2 (Top) Result of subtracting N_2 VK 2-15 band from H-beta profile shown in figure 2.1. The VK 2-15 band has been subtracted in amounts corresponding to a peak band intensity of 10 percent (a), 20 percent, (b), and 30 percent (c) the peak intensity of the H-beta profile. In each case the dotted line represents the unaltered profile while the solid line is the result of subtraction. All profiles shown are normalized.
(Bottom) Result of convolutions of N_2 VK 2-15 band with Ebert spectrophotometer instrument function (smooth curve). (Amount shown represents that subtracted from middle profile above). VK 2-15 band rotational structure resolved to thirds of angstroms is shown as histogram (Broadfoot, private communication).

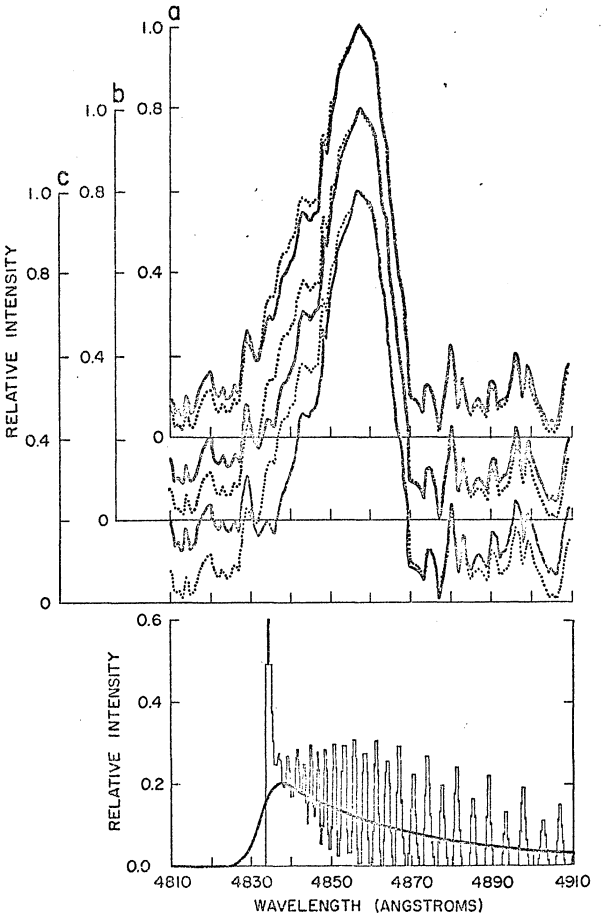

to be near two tenths the peak H-beta intensity (case b). Figure 2.2 also shows the VK 2-15 band with resolution 1/3 Å and the result of the convolution of the band with the instrument function. The amplitude of the 2-15 band in this figure represents the amount subtracted in the case of an assumed ratio VK 2-15 / H-beta = 0.2. This ratio was found to be appropriate for most of the profiles analyzed in this manner.

Removal of the OII lines

The four OII lines were normalized with respect to their relative intensity and convoluted with the instrument function. The result of this convolution was subtracted from the modified profile resulting from the VK 2-15 subtraction. The result of the convolution of these lines with the instrument function is shown in figure 2.3. The intensity of these lines was estimated on the basis of the discussion in section 2.2.2. The peak amplitude of the convoluted OII lines was less than 5% the peak amplitude of the H-beta profile.

Removal of the instrument function

The effect of removing the instrument function was quite small; that is, the profile was narrowed only slightly and the peak amplitude was made slightly greater. Since removal of the convoluted OII lines acted to lower the peak of the profile, the effect of removal of the instrument function was somewhat negated.

Figure 2.3 shows the result of subtraction of the OII lines from figure 2.2b and deconvolution. Although spikes and fluctuations can still be seen on the profiles, they should be regarded as the effect of random noise. Generally, the noise pulses are too narrow to have been true signals passed through the instrument function.

Fig. 2.3 (Top) Result of convolution of OII spectral lines with Ebert spectrophotometer instrument function. Relative intensities of OII lines are those listed in Table 2.1.

(Bottom) Result of subtraction of convoluted OII lines from H-beta profile (solid line). Subtracted amount of convoluted OII lines shown above. H-beta profile used was result of subtraction of N_2 VK 2-15 with peak intensity 20 percent the peak H-beta profile intensity. (Middle profile figure 2.2, top). Dotted line represents smooth profile drawn to fit uncorrected profile shown in figure 2.1. Both curves have been subjected to deconvolution for Ebert spectrophotometer instrument function.

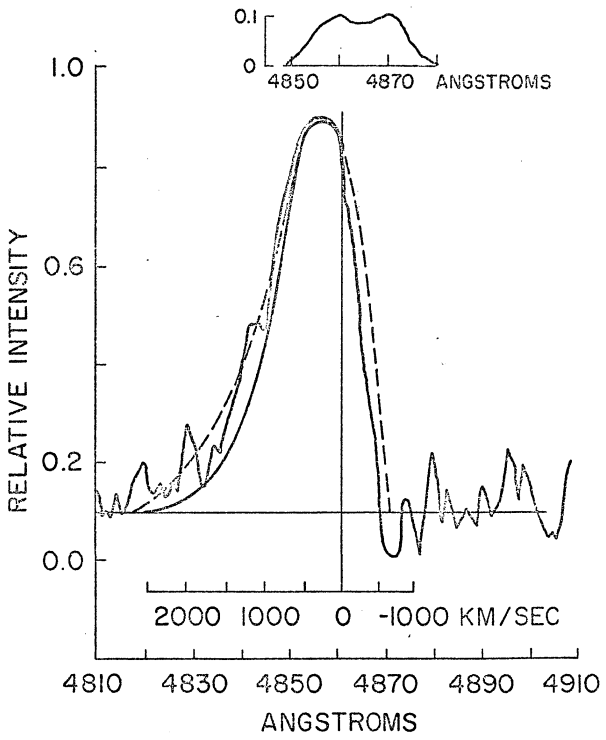

Discussion of effect of removal of contamination and instrument function from H-beta profiles.

Figure 2.3 shows smooth curves corresponding to the shape of the zenith profile before (smoothed from fig. 2.1) and after removal of the VK 2-15, OII lines and deconvolution. In this case, the change was only slightly significant on the blue side of the profile. A horizon profile was taken several minutes after the zenith profile discussed above. Each of these profiles was taken from what was, at that time, by far the region of brightest hydrogen emission in the sky along the magnetic meridian. This region moved from magnetic zenith to the magnetic horizon within a matter of minutes, thus providing a complete set of profiles under stable instrumental conditions.

Figure 2.4 shows the scaled horizon profile before (dashed) and after the VK 2-15 was removed. Figure 2.5 shows the horizon profile after removal of contamination and deconvolution. By this process the horizon profile has been made more symmetric about 4861 Å.

Almost all previously reported horizon profiles have shown the asymmetry that this profile exhibited before removal of the VK 2-15. Several authors have debated whether light scattered from the magnetic zenith may cause the enchancement usually observed on the blue side of the profile. However, the required amount of scattered light always seemed rather large compared to what might be expected on the basis of scattering theory. (See Eather, 1966). Here, an alternative and more plausible source of enhancement of the blue side of the horizon profile has been offered: The Vegard Kaplan 2-15 band.

Fig. 2.4 H-beta emission doppler profile observed at magnetic horizon. Dashed profile represents sum of approximately 70 spectrophotometer scans across the wavelength interval shown. The duration of each scan was 8 seconds. The solid line profile represents the result of subtraction of the N_2 VK 2-15 band from the dashed profile. The profiles have been normalized.

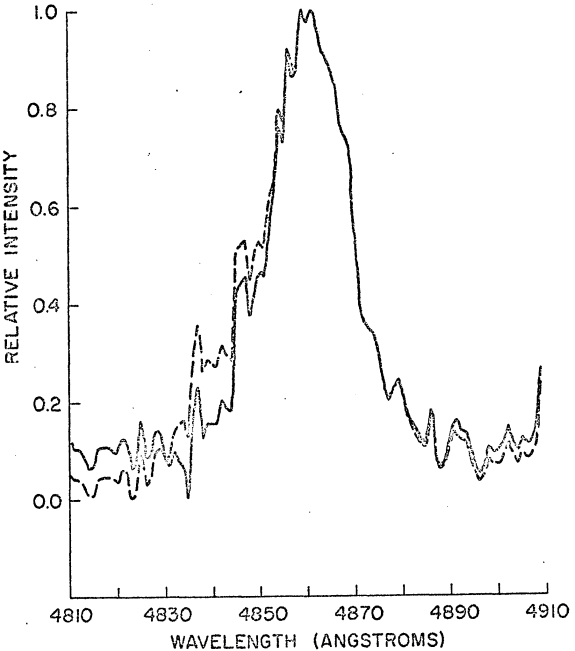

2.4 H-beta Profile Analysis

2.4.1 Pitch angle distribution

Chamberlain (1961) developed a method by which independent proton pitch angle and energy distributions could be obtained from analysis of the moments of simultaneous horizon and zenith hydrogen line profiles. The analysis assumes that the pitch angle distribution is the same for all energies and vice versa. Further, the pitch angles deduced are those of the neutral hydrogen atoms that are emitting quanta.

The pitch angle distribution is determined by superposition of functions the first order of which have the form:

$$n(\theta) = \frac{(n+2)}{2\pi} \quad F\ (\cos^{n}\theta) \qquad (n > -1)$$

where $n(\theta)$ is the "intensity" of protons/cm^2 sec sterad and where the unit area is taken perpendicular to the velocity vector. We can define another quantity,

$$N(\theta) = n(\theta) \cos \theta$$

where $N(\theta)$ is the number of protons/cm^2 sec sterad, θ is the angle of the proton velocity vector measured from the unit normal, and where the unit area is taken normal to the magnetic field lines. This later quantity is the true flux per steradian of protons into the atmosphere. (Complete discussion of these terms is provided in Appendix B).

The quantity n can be found through the ratio of the first moments of the horizon and zenith profiles taken about the undisplaced line position. Chamberlain (1961) published a table giving values of the ratio for integral values of n from -1 to 6. The ratio of horizon to zenith moments for the two profiles analyzed here was found to be between 0.8 and 0.9. This yields a value of n of approximately 0.7.

Fig. 2.5 Result of subtraction of convoluted OII lines from H-beta horizon profile and deconvolution of Ebert spectrophotometer instrument function (solid line). Dashed line profile represents smooth curve fit to uncorrected (but deconvoluted) horizon profile.

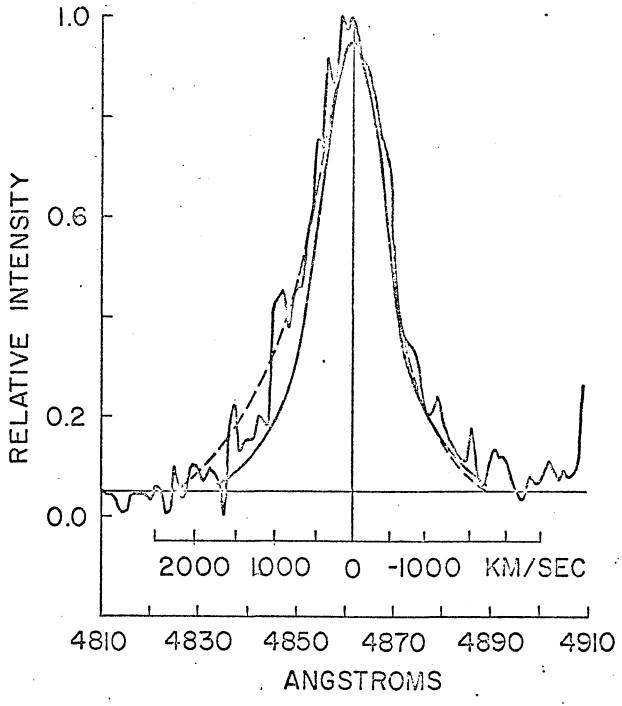

A value of $n = -1$ corresponds to isotropic flux per steradian. A value of $n = -1$ yields $N(\theta) = (n(\theta)\cos\theta) = (\cos^{-1}\theta\cos\theta) = 1$. That is, the number of protons per solid angle passing through a unit area perpendicular to the field is independent of the direction of the solid angle chosen. Care should be taken not to confuse this isotropic flux per steradian with the concept of $n(\theta) = \text{constant}$, which is an isotropic intensity.

Omholt (1956) noted that in the case of $n = -1$ (isotropic flux per steradian), the total intensities of the zenith and horizon profiles are the same and the zenith profile is identical to the corresponding semi-horizon profile. (Except that, of course, the intensity of the semi-horizon profile is half that of the zenith profile since the horizon profile is symmetric). In this case, the zenith profile has a peak intensity at the undisplaced line position. Omholt did not consider the existence of a red tail in the H-beta profile.

Eather (1966) showed that in the case of $n = -1$, one could expect a red "tail" on zenith profiles due to magnetic mirroring. Precipitation of protons of 10 kev energy and isotropic flux per steradian yields a red tail indicating maximum recessional speeds of 500 km/sec, which is consistent with the zenith profile shown here.

Eather (1966) also computed that for *momoenergetic* protons, a zenith profile maximum near 250 km/sec required

$$-1 < n < 0$$

Although it is recognized that the proton flux reported here was very likely not mono-energetic, it is reasonable to expect a value of $n = 0.7$ to yield both a zenith profile maximum displaced from $\lambda 4861$ and a significant red tail.

CHAPTER III

Contamination of H-beta Photometric Signals

3.1 Introduction

This chapter relates the intensities of the auroral emissions found to contaminate H-beta line profiles to the contamination of H-beta measurements obtained by interference filter photometers. The result is an analytical expression for the contamination of auroral H-beta photometric observations.

3.2 Contamination in Interference Filter Photometry

There are two general categories of possible contamination of the desired signal in an interference filter photometer: 1) intense emissions outside the maximum pass band of the filter, but still within its transmission "wings". 2) Other spectral features such as weak molecular bands, atomic lines or continuum underlying the emission of interest and passed by the filter (Eather, 1967).

All filters used in this observational program had transmissions of approximately 0.01% at wavelengths $\pm$ 70 Å from the peak wave length of the filter to the limits of sensitivity of the S-20 detectors. The peak of transmission of the H-beta interference filter used in the observation was approximately 45%; above 4930 Å and below 4800 Å the transmission was less than 0.01%. Since no strong auroral emissions occur within $\pm$ 70 Å of the H-beta line, no wing contamination can be expected. All other emissions monitored by the photometer system utilized filters of similar quality.

A search for sources of contamination of the second type revealed these possible contributors: the VK 2-15 band (Chamberlain, 1961; Eather,

1967), certain OII lines (Wiese, et. al, 1966 ; Vegard and Kvifte, 1945 ; Gal'perin, 1959), possibly some atomic neutral lines of nitrogen (Remy, et. al., 1960) and the general stellar continuum and galactic hydrogen.

3.2.1 Galactic background

There are several regions in the sky which are bright in H-beta to the extent that a scan across them by a photometer would be interpreted as a narrow arc of several hundred rayleighs intensity. These bright regions are contained in our galaxy and lie in the "Milky Way". There is not always one such bright region in the field of view nor will one always come into view during any particular night. The solution to this source of contamination is to be aware of its existence and avoid using data thus contaminated. Because of the extensive use of H-beta photometric data in this thesis, a simple analog device was constructed to quickly determine at any time the field of view of a photometer scanning in the dp 256° meridian in relation to the Milky Way H-beta background. This device is described in Appendix D.

3.2.2 Atomic spectra

After a thorough search of line strength tables, it was concluded that the only atomic lines likely to have sufficient intensity to contaminate H-beta photometric signals are those due to ionized oxygen and neutral nitrogen.

Contamination of H-beta photometric signals due to NI lines

Lines of neutral atomic nitrogen are listed at 4846.7 Å and 4850.5 Å but have never been observed in the laboratory (Remy, et. al. 1960) and are below 5% and 12% respectively on the transmission curves of the filters used in photometric studies reported here. These lines have never been

observed superimposed on the H-beta profile. However, if their intensity were the same as that of the H-beta profile at those same wavelengths, they could contribute up to 30 R of equivalent H-beta photometric signal at times when H-beta =1KR.

Contamination of photometric signals due to OII lines

Multiplying the OII lines in Table 2.1 by the filter function used in the photometric measurements yields a total of approximately 20 R measured by the H-beta photometer which, when converted to equivalent H-beta signal, yields approximately 100 R total maximum possible contamination due to OII. Again, this 100 R contamination represents the contamination during the brightest auroras (H-beta ~ 1000 R) and therefore the value of 10% has been adopted here for the maximum percentage contribution of contamination.

3.2.3 Contamination of H-beta photometric signals due to molecular band systems

As mentioned in Chapter II, a search for molecular band contaminants of H-beta photometric signals revealed only the Vegard-Kaplan 2-15 band of molecular nitrogen. Based on the results of Chapter II an estimate of false H-beta photometric signals due to this source can be made.

Application of the H-beta profile analysis

If the peak intensities (R/Å) of the VK 2-15 band and H-beta profile are equal, the total emission of the VK 2-15 band is 70% of the total emission of H-beta. In Chapter II it was found that the peak intensity of the contaminating VK 2-15 is actually 20% of the peak intensity of H-beta. Hence the actual total emission of the VK 2-15 is 14% of the total emission of H-beta.

Convolution of the corrected H-beta profile and the VK 2-15 band with the passband function of the H-beta filter normally used in this study shows that if equal intensities are emitted from both sources, the ratio of measured signals is VK 2-15/H-beta = 1/2. This implies that the contamination of H-beta photometric intensity measurements due to VK 2-15 emissions is half the total intensity of the VK 2-15 band. Since the ratio of VK 2-15 to H-beta was found to be 14%, the contamination of H-beta due to VK 2-15 is approximately 7%.

This result was obtained at times when the H-beta intensity was approximately 350 R. Lower intensities require integration times which are too long, and higher intensities are found only in auroral forms which are active and are 1) hard to track and 2) do not remain in the magnetic zenith or horizon long enough to permit a profile measurement.

Theoretical estimate of VK contamination

The VK 2-15 intensity discussion of section 2.2.1 is based on auroral emission measurements when H-beta intensities were on the order of 1 KR. Under these conditions the VK 2-15 band intensity of 450R contributes 225 R to H-beta photometric measurements performed with the filters utilized here. Hence, theoretically under these conditions, the contamination of photometric measurements due to the VK 2-15 band, can be as high as 25%.

Quantitative expression for VK 2-15 contamination of H-beta photometric measurements

In order to determine the relationship between H-beta intensities and N_2^+ 4278 intensities during times of bright, active aurora, several minutes of consecutive photometric scans along the dipole meridian over College were scaled in these wavelengths. Figure 3.1 shows the H-beta

Fig. 3.1 Simultaneous H-beta and N_2^+ 4278 intensities during the "break-up" phase of a substorm. All measurements were made within 20 degrees of magnetic zenith. Intensities were measured under the various auroral conditions indicated.

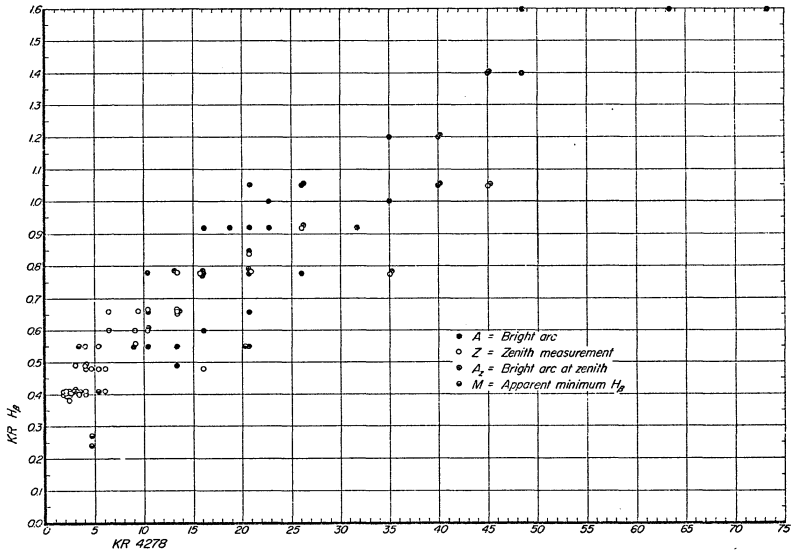

intensities plotted against simultaneous 4278 Å intensities. To minimize effects of aspect geometry, all readings were taken within a few degrees of magnetic zenith at times when a bright active arc occupied part of that region of the sky. Readings were taken according to three criteria: the most intense emissions in the sky (the bright arc) indicated by A, the zenith intensity indicated by Z (if the brightest region was in the zenith the point is indicated by A_Z), and regions near magnetic zenith where it appeared that H-beta might exhibit minimum values (indicated by M). Note that these three groups of points blend together indicating that regardless of how the point is chosen, the relationship between H-beta and 4278 follows the same general pattern.

Several useful conclusions are drawn from this diagram:

1) for 4278 intensities greater than 50 KR, a generally linear relationship can be found between 4278 and H-beta. This relationship is given roughly by

$$R\ (4278) = \frac{(H\text{-beta})-350}{0.0195}$$

2) a general rule for H-beta contamination can be found reconciling the two estimates given earlier for VK 2-15 contamination of H-beta.

Assuming that N_2 VK 2-15 is proportional to N_2^+ 4278, the large 250 R contamination of H-beta corresponds to N_2^+ 4278 intensities near 30 KR and uncorrected H-beta intensities of 1KR. On the basis of figure 3.1, it appears that there is a background of 350 R H-beta during bright auroras. Above this background, H-beta and N_2^+ 4278 are roughly linearly

related by

$$R_{4278} = \frac{[R_{H\text{-beta}} - 350\ R]}{0.02}$$

The values obtained earlier for VK 2-15 contamination can be derived by multiplying these values by 0.0075:

$$R^*_{(VK\ 2\text{-}15)} = (0.008\ (R_{4278}) = 0.4\ (R_{H\text{-beta}} - 350\ R)$$

Note that for

$H\text{-beta}^{\dagger} = 1$ KR, VK 2-15* = 260 R (267.)

and

$H\text{-beta}^{\dagger} = 400$ r, VK 2-15* = 20 R (5%)

This last figure corresponds roughly to the 7% contamination of H-beta by the VK-15 band found by profile analysis while the former corresponds to the theoretical estimate for the VK 2-15 contamination during periods of bright auroras.

3.2.4 Auroral background

No real auroral background continuum has ever been detected. It is usually described as a combination of the entire Vegard-Kaplan band system and other low level emissions previously discussed. Eather (private communication) has obtained empirically an average value of 0.2 R/A per KR (N_2^+) 3914 for the intensity of the auroral background in the H-beta region. In the event studied here the intensities of 4278 Å (N_2^+) and 4861 (H-beta) were 28 KR and 1 KR respectively. The transmission of Eather's background intensity through the H-beta filter yields a value of 500 R for

† = uncorrected intensities

* = this is the amount of contamination due to the VK 2-15 band

the total contamination of the peak H-beta signal. Subtracting the previous estimates of the VK, OII and NI intensities leaves approximately 150 R unaccounted for, and presumably due to either a true continuum or other unresolvable emissions. No data are currently available to check this value.

There is, however, one possible source of contamination which has never been evaluated. It is the intensity of continuum level emissions which occur during electron-capture processes. Only a crude estimate of their effect is made here. The effective ionization rate has been estimated at 2×10^6 ion pairs/cm^3 sec for a very bright aurora arc (Chamberlain, 1961). Taking 10 km as the effective depth of the light-producing column yields a column of 10^6 cm. In equilibrium, the recombination rate equals the ionization rate. In this case 2×10^{12} recombinations occur per cm column/sec. It seems reasonable to assume that associated with each of these recombinations at least one quanta of "continuum" level emission results. These emissions are then distributed in some fashion over several thousand angstroms. It is most likely that the great bulk of these emissions will be in the ultraviolet and only a very small fraction will contribute to a continuum in the visible region of the spectrum. A continuum of 1R/Å spread across two thousand angstroms in the visible region requires only 3×10^9 quanta/column cm^2 sec or 0.1% of the estimated quanta.

A continuum of 1R/Å yields a photometric signal through the filter used here which is interpreted as 30 R H-beta.

Since most auroral emissions due to electron impact are roughly proportional to N_2^+ 4278, this source of contamination will probably

behave in the same way as the VK 2-15 system. On this basis an estimate of 50% of the VK 2-15 contamination appears to be a reasonable value of H-beta signal contamination by aurorally associated continuum emissions. Contamination of this magnitude would require a continuum of 4 R/Å during the brightest of auroral conditions.

3.3 Conclusions

Chapters II and III have demonstrated that photometric measurements of auroral hydrogen emissions are subject to contamination by various auroral and astronomical sources. These contaminating sources and the relative amount of contamination are estimated to be:

Source	Amount
1) Galactic background	Negligible outside the milky way
2) Atomic nitrogen	3%
3) Ionized atomic oxygen	10%
4) VK 2-15	R(VK 2-15) = 0.4 (R(H-beta)-350)
5) Auroral background	1/2 (VK 2-15)

Hence, an H-beta measurement of 400 R is adjusted to approximately 325 R, while a H-beta measurement of 1 KR is adjusted to approximately 550 - 600 R. The 1600 R H-beta intensities of figure 2 are adjusted to approximately 650 - 750 R. This estimate of contamination yields what is thought to be the most conservative estimate of true H-beta intensity.

The analytical expressions which have been derived and tested in this chapter permit a reasonably accurate determination of the contamination of H-beta photometric measurements over a large range of auroral intensities. Applying these corrections to photometric data provides a means of relating hydrogen emissions to proton precipitation quantitatively and with a high degree of confidence. The dynamic behavior patterns of auroral emissions produced by precipitated protons and electrons can now be compared directly.

CHAPTER IV

The Consequences of Experiments Relating Auroral Proton Measurements and Simultaneous Photometric H-beta Observations

4.1 Introduction

Knowledge of the absolute intensities of hydrogen emission observed in the aurora makes possible an estimation of the number flux and energy distribution of injected protons. This estimation can be made by means of theoretical estimates for photon production by protons based on atmospheric densities and laboratory cross section measurements. Direct measurements of protons in the aurora make possible another method of relating injected protons to hydrogen emissions. Calculations based on laboratory measurements usually depend on assumed energy distributions for the protons. Direct measurements of protons (see section 1.3) can be used to determine the general form of a portion of the energy distribution but usually do not allow determination of the total number of protons because of the difficulty in detecting low energies.

By comparing simultaneous hydrogen emission observations and direct particle measurements through the theoretical estimates, the range of validity of the directly measured energy spectrum can be expanded and a more accurate determination of the total number of injected protons be made.

On March 17, 1969, an electron and proton-measuring rocket payload was launched into an intense pulsating aurora from the Poker Flat rocket range of the Geophysical Institute, (see Johnstone, 1970). Launch occurred approximately one hour after an auroral substorm onset and two hours after local magnetic midnight. Unfortunately only eight thousand protons were actually counted due to the combination of detector efficiency and field of view as well as the relatively low particle flux.

4.2 Proton Measurements

Within the range of the detector (2 to 20 kev) Johnstone found a very strong indication of a power-law particle energy distribution: AE^{-r} where r varied from 2.1 to 2.9.

4.3 Photometric Measurements

During the particle measurements, an auroral scanning photometer was operated from the Ester Dome auroral observatory located to the southwest of Poker Flat. The angle between the plane of the scan of the photometer and the plane of the rocket trajectory was 10°. Thus the photometer viewed the rocket on the upleg of the flight altitude of 200 km. It is estimated that the payload was in the volume swept out by the rotating photometer's field of view for approximately 30 sec. Because of the 10 sec. scan rate of the photometer, the payload was actually in the field of view twice. The photometer was operated on the 10 second horizon-to-horizon scan mode for the following reasons:

1. The intensity of H-beta was so low that poor photon statistics were being encountered on high speed scans.

2. The H-beta intensity was fairly uniform over the sky and in time.

Hence, very little spatial and temporal intensity resolution would be lost while the signal-to-noise ratio would be greatly enhanced by a slower scanning rate.

After the payload passed from the field of view of the photometer, no significant changes in auroral intensities were observed in that sector of the sky by the photometer. It is safe, considering the proximity of the payload to the field of view and the uniformity of the emissions, to assume that no great changes in auroral luminosity

occurred in the region of the payload for the duration of the flight (except for the fast pulsations).

Using the calibration technique described in Appendix A, the photometer current output is interpreted as 120 R assuming either the Veissberg (1962) zenith profile or the zenith profile used in Chapter II for pitch angle determination. However, considering the intensity corrections discussed in Chapter III for contamination due to other auroral emissions, the intensity of H-beta measured at the photometer is placed between 80 and 100 R.

4.4 Photon Production by Protons

Eather (1966, 1967) considered the problem of total photon (H-beta) production caused by entry of a high-speed proton into the atmosphere. His numbers were obtained by up dating the calculations of Chamberlain (1961). Briefly, since a pure proton beam very quickly comes to charge-exchange equilibrium and the change of atmospheric density with altitude is sufficiently gradual that an equilibrated beam stays in equilibrium, only an equilibrated beam need be considered. An incoming proton beam is degraded to zero energy by considering the statistical process of energy loss in the atmosphere, using the total cross sections for all possible interactions of protons and neutral hydrogen with atmospheric constitutients, the density of these constitutients as a function of altitude, and the equilibrium fraction as a function of atmospheric density. H-beta production is determined by the probability of that transition occuring during cascading due to both electron-capture and neutral excitation. Generally, the data used only extended down to a few kev. The shape of the curve generated is very likely valid; however, as Eather noted, the scale value is rather uncertain. Considering

all the data available, Eather chose to adjust the scale value so that a 300 kev proton produced 10 photons of H-beta during degredation.

4.5 Photon Production Per Proton

Because of the analytical form of the proton energy spectra, the temptation was great to attempt to fit the data obtained by Eather to some analytical form. For energies below 30 kev (shown to be of major consideration here) it was found that

$$\frac{\text{photons}}{\text{proton}} = 0.1\ E^{1.1} \qquad 4.1$$

where E is the initial energy of the proton in kev. Some preliminary calculations were made using this form. However, this being the age of modern high-speed computers, it was thought that the proper effort would not be made until an attempt at fitting Eather's data with at least a second degree polynomial was tried. The following is the result of this attempt:

$$\frac{\text{photons}}{\text{proton}} = 0.0102 + 01253\ E - 0006\ E^2 \qquad 4.2$$

The data used for this fit did not extend below 3 kev. The program cannot be made to fit any given point. Hence, the zero-order term 0.0102 photons per proton represents the extrapolation of the best fit down to zero energy. The only way to cause the best fit to go to zero at zero energy is to make this term equal to zero. Obviously, this only shifts the curve downward a small amount and does not affect the fit significantly. The small coefficient of the second-degree term causes this term to be significant only for energies near 100 kev. This negative term only insures that the dwindling proton population at these energies contributes even less to total photon production. This leaves the first-degree term which agrees closely with the data-

fitting curve found earlier by solving simultaneous equations to derive an analytical expression. It has been found that use of either of these expressions for photons per proton yields very nearly the same result.

4.6 Total Photon Production

The power law spectra were multiplied by the modified best fit to the photon/proton data and integrated:

$$I(\text{rayleighs}) = \frac{\pi}{10^6} \int_0^\infty (AE^{-r}) \; (0.125E) \; dE \qquad 4.3$$

The values of r used were 2.1, 2.3, 2.5, 2.7, 2.9. The coefficient A is held to a value of 10^7 for this analysis. The object here is to compare the behavior of this integral for the different values of r. Using these values of r the integrand vanishes for the upper limit, and obviously does not converge for a lower limit of zero. The cross section for even neutral excitation drops to zero at a few electron volts. Therefore the range of definition of the photon production function should terminate at a few ev. It is very likely that this abrupt "chopping" of the function does not represent its true detailed behavior at low energies any more than does modifying the function to exhibit uniform convergence to zero at a few ev. What ever the true shape of the photon production curve, concern here is with the general effect that changing the exponent in the power law energy spectrum has on the integral of the two functions. Twenty ev (near the ionization potential of hydrogen) is assumed to be the effective cutoff energy for H-beta production. It will be seen that this is reasonable enough for the comparisons made here. Evaluating the integral at this lower limit assumes that the power law energy spectrum is valid to this energy.

At first, this may not appear to be a sweeping assumption. However, depending on the power law exponent r, this extension can imply changes by orders of magnitude in the total number of protons precipitated.

Cutting off the power spectrum at the detector threshold (2 kev) in cases where no tendency toward attenuation is indicated at that energy is not valid. Comparison of the power laws observed with simultaneous groundbased measurement of optical H-beta emission gives some idea of the range of validity of the power law spectrum. It is also possible to determine whether the power-law exponent r can vary as reported and, if it cannot, what the most reasonable value for it is.

Table 4.1 shows the result of evaluating the integral (eq. 4.3) for various values of r and several lower limits.

4.7 The Power Spectrum of Protons

4.7.1 Power spectrum cutoff energy

For the lowest cut-off energy, the total photon output is a very sensitive function of r, varying by orders of magnitude. On the other hand, for cut-off energies on the order of 1 kev the total photon production varies by only a factor of two throughout the range of r. Also, it is apparent that for low values of r total photon output is not a sensitive function of cut-off energy. For high values of r, the assumption that the energy spectrum continues to low energies implies a total photon emission of great magnitude. Johnstone's (1970) experimental evidence indicates that the energy spectrum varies over this entire range of r. Johnstone (1970) noted that this variation could be the effect of inaccurate data to correct the particle flux for energy losses while passing through the atmosphere; this was thought

to be possible because the observed spectra tended to show a systematic variation with altitude. However, other experimental evidence indicates values of r on either side of the range of exponential values reported by Johnstone (See Eather, 1966). Because of this evidence, we should consider the implications of the possibility that this reported variation is real.

It is obvious that if the power law spectrum varies over this entire range, either 1) the cutoff energy has to be very near 1 kev, or 2) it has to vary so as to approach 1 kev for high values of r. Otherwise great variations in H-beta intensity would have been observed. The first possibility is unlikely because no tendency toward cutoff was indicated at detector threshold. Further, other observations using similar particle detectors (Wax and Bernstein, 1969 ; Chase, 1969 ; Reasoner et. al., 1968) indicate that a power law energy spectrum continues to at least 1/2 kev. The second possibility is even more remote because added to the argument above is the objection that such a fortuitious variation of cut off energy with r appears contrived.

4.7.2 Numerical evaluation of power of energy spectrum

The systematic variation of r with altitude considered in view of the previous discussion leads one to reconsider the possibility that the wide range of r values observed did represent an error and that the problem is to identify the correct value. Because the error is suspected to reside in an altitude-dependent correction, the r values of 2.1, 2.3, and 2.5 obtained at apogee, where these corrections are smallest, are likely to be the most accurate.

The reported proton energy spectra can now be compared with the intensity of H-beta as measured from the ground. The number quoted

Table 4.1

r	E_o = 25	2	1	.5	.05	.02	KEV
2.1	3.127	4.023	4.31	4.62	5.82	6.38	
2.3	1.940	4.123	5.09	6.27	12.56	16.48	
2.5	1.176	4.158	5.88	8.32	26.30	41.58	
2.7	.7004	4.102	6.66	10.83	54.26	103.05	
2.9	.4111	3.991	7.45	13.90	110.38	251.85	

Values are tabulated (arbitrary units) to illustrate the behavior of the photon/proton production integral (eqn. 4.3) for observed values of proton spectral exponent, r, and various cutoff energies, E_o, of the proton energy spectrum. For these values the coefficient, A, of the proton energy spectrum has been held equal to 10^7.

Table 4.2

r	A x 10^7	E_o = 25	2	1	.5	.05	.02	KEV
2.1	2.5	7.83	10.0	10.6	11.5	14.5	15.9	
2.3	5.5	10.7	22.7	27.0	34.6	68.8	90.6	
2.5	7.2	8.3	29.9	42.4	59.9	189	299	
2.7	10.3	7.22	42.3	68.6	111	558	1060	
2.9	12.7	5.21	50.7	94.5	176	1410	3100	

Values are tabulated in rayleighs for photon production by protons. Photon/proton production integral (eqn. 4.3) is evaluated for observed values of proton spectral exponent, r, and various cutoff energies, E_o, of the proton energy spectrum. The coefficients, A, of the proton energy spectrum are values interpolated from those given by Johnstone, (1970).

earlier, 80-100 rayleighs, is considered to be as accurate as is possible to obtain for the light emitted from the atmospheric column energized by the protons. Recently, Condal (1971) found that the absorption correction for even this zenith angle (20°) may very likely be as high as 1.5. This value places the true column emission rate at between 120 and 150 rayleighs.

In order to compare this number with the predicted intensity, it is necessary to have knowledge of the values of the coefficient A. Unfortunately, Johnstone (1970) has only provided this number for r values of 2.1 and 2.5. These are 2.5×10^7 and 7.2×10^7. Table 4.2 provides intensities for these r values using the interpolated values of A. Included also are intensities for other r values assuming a linear extrapolation for A.

It is apparent that a 1 kev cutoff energy will not provide sufficient emission for any of these energy spectra. It also appears that an r value of 2.1 or 2.3 will not provide the required emission even if the energy spectrum continues to energies below the threshold for H-beta production.

Values of r = 2.5 and higher require cutoff energies between 0.05 and 0.5 kev. It has already been determined that the spectral exponent is between 2.1 and 2.5. An exponent value of r = 2.5 could produce the required emission and requires a cutoff energy slightly lower than 0.5 kev. Within the range of observed intensity (120-150 R), it appears that a value of r = 2.4 would also be satisfactory for a cutoff at 0.02 kev, the threshold energy for H-beta production.

4.7.3 Charge Neutrality

It is interesting to examine the question of precipitated flux neutrality on the basis of these investigations of proton energy dis-

tribution. Johnstone (1970) reported an electron flux near 0.21×10^9/ cm^2/sec. The value of 10^9 electrons per cm^2/sec is not unusual.

The wide range of experimental values r, coefficients A, and possible cutoff energies for the proton spectra allow some speculation. Table 4.3 shows the expected proton flux for several cutoff energies E_o and exponents, r, and the coefficient, A. The values of A used are extrapolated from values given by Johnstone..

Table 4.3

r	$A \times 10^7$	E_o = 25	2	1	.5	.05	.02	kev
2.1	2.5	.22	3.6	8.6	17	208	574	
2.3	5.5	.26	7.2	23.	43	840	2940	
2.5	7.2	.18	8.0	29.	64	2020	4060	
2.7	10.3	.13	10.	55.	1050	5300	6300	
2.9	12.7	.08	11.	76	1490	7000	67700	

Values are tabulated of total proton flux (protons/cm^2) produced by power law energy distribution $N = A \int_{E_o}^{\infty} E^{-r}\, dE$. The values of A used are extrapolated from those given by Johnstone.

Examination of Table 4.3 shows that taking 2 kev as the particle spectrum cut-off energy yields fewer protons than electrons for all values of the power spectrum exponent.

It can also be seen that for r = 2.5, the observed emission requires a cutoff energy, E_o, slightly higher than 0.05 kev. The power law spectrum produces 20×10^9 protons at E_o = 0.05 kev and 0.64×10^9 protons at E_o = 0.5 kev. Thus, it appears that within the uncertainties in these measurements the total particle flux in this aurora was neutral or positive. Note that this is true only for altitudes >400 km because

the concentrated flux of low energy protons is spread out below that altitude due to charge-exchange spreading.

If the cutoff energy E_o actually is near 0.05 kev, very great numbers of precipitated protons become possible. Hence, during times of very great electron flux, even though H-beta emissions do not increase greatly the total particle flux in the aurora could be neutral simply due to the existence of many low energy protons which have a very low cross section for photon production. For this reason, the morphology of hydrogen emissions in the aurora assumes a greater importance.

CHAPTER V

Morphological Relationship Between Auroral Emission Patterns Associated with Injected Electrons and Protons.

5.1 Introduction

Visible hydrogen emissions are characteristically on the order of 1% of the intensity of the brightest visible auroral emissions. The bright auroral features have been linked to precipitation of energetic electrons. Auroral morphology has concentrated on analysis of the behavior patterns of these bright electron-linked auroral features. Auroral hydrogen emissions can be tied directly to injected protons through the doppler broadened hydrogen line profiles. However, on the basis of the relatively low intensity of the hydrogen emissions, the role of protons in terms of particle precipitation patterns in the aurora might be considered small.

The previous chapter demonstrated that the total flux of protons is considerably greater than formerly thought, and that the total particle flux may be neutral for many auroral features. For these reasons, the role of injected protons takes on a new significance in the study of auroral morphology. In this chapter, H-beta and N_2^+ 4278 Å auroral emissions are analyzed to produce patterns of proton and electron associated emissions in the auroral substorm model.

The utility of H-beta as a measure of proton precipitation has been established. The other emission considered here, N_2^+ 4278 Å, is actually the peak emission of the P-branch of the 01 (electronic transition) band of the N_2^+ first negative system. The ionization potential of N_2^+ is 16 volts, and the cross section for ionization of N_2^+ by electrons peaks at 100 ev and drops off to less than one third the peak value at 1 kev,

and to a few percent of the peak value at 10 kev. Hence, for moderately "hard" electron energy spectra, the N_2^+ 4278 emission is relatively concentrated at the lowest altitudes of electron penetration.

5.2 Data Collection

The emission data used here were obtained by means of a chain of three meridian scanning photometers (MSP) located along the dipole 256° meridian at College (dp. lat. 64°36'), Fort Yukon (dp. lat. 66°37') and Bar-I (dp. lat. 70°12'). These photometers scanned the meridian from horizon to horizon in one second every every two seconds. Six auroral wavelengths were measured simultaneously by utilizing six telescopes each with its own filter and photomultiplyer. The scan was provided by a rotating mirror. The field of view of each telescope was circular with a diameter of 1 1/2 degrees.

5.3 Data Format

Among the virtues of the MSP data are high time resolution and absolute intensity measurements. When the MSP system was designed it was anticipated that the data of greatest value would be that of absolute intensity. For this reason a large amount of the experimental effort was applied to that purpose. However, complicating factors were imposed by the magnitude of the observational task which made subsequent data analysis of absolute intensities cumbersome.

One very great value of the MSP data is that all emissions were measured simultaneously. However, since most auroral emissions normally range over several orders of magnitude during an auroral display, the recording of six emissions each over three orders of magnitude requires the ability to record eighteen linear signal channels. Because of

expense, a recorder of this size was out of the question. The alternative was to construct amplifiers which would convert the linear photometer signal output to a logarithmic signal so that each photometer's output could be recorded on a single tape recorder channel. This technique imposes the necessity of later converting the recorded signal back to a linear scale.

When the original data was recorded on magnetic tape two photometric channels, H-beta and OI 5577 Å, were displayed on an oscilloscope. The oscilloscope trace was photographed three out of each five scans (because of certain limitations) onto 16 mm movie film. It was planned that these films would later yield "quick look" data for selection of taped data for automatic processing. The oscilloscope amplitudes were of necessity also logarithmic, and care was taken to calibrate the amplitude of the recorded trace.

Subsequent experience has shown the oscilloscope movie films to be of much value. Many dynamic features of auroral displays become apparent only by cinematic viewing of the films. The chief drawback is that the viewer must mentally convert the viewed amplitudes to linear scales. For this reason, many important relationships between proton and electron precipitation cannot be determined from these films. Furthermore, during times of rapid intensity changes or motions, the half-second lifetime of the OI 5577 Å transition leads to erroneous first conclusions.

In this chapter plots of absolute intensity of H-beta and N_2^+ 4278 along the dipole 256° meridian, using simultaneous MSP sky scans from College, Fort Yukon and (when available) Bar-1, are used to illustrate

a study of auroral displays using the oscilloscope films and all-sky camera films from the Alaskan all-sky camera network.

5.4 Data Preparation

In order to produce the intensity plots, the recorded logarithmic signal was displayed on a strip chart. Base lines were drawn under the sky scans to be analyzed based on the periods when the photometers were looking downward into a black box to provide dark current recordings. Next three such sky scans were digitized for each 1/10 degree and an average for each degree for all three scans was produced. Each plot therefore represents an average of auroral intensities over a six second period. The intensities were then converted from zenith angle to horizontal distance scales assuming a 125 km altitude. This proved to be reasonably satisfactory, and when triangulation was possible correction could be made by visual inspection.

At this point the H-beta intensities were corrected according to the conclusions of Chapter III, and then both intensities were corrected for geometric effects and the combination of absorption and scattering. The obvious geometric factor to apply to H-beta emission was the Van Rijn correction. After some consideration it was determined that the same correction applied to N_2^+ 4278 would most nearly preserve the total intensity of the emission — even though it would have the effect of laying arcs with vertical extent "on their side". Further correction by assuming vertical profiles for arc-line structures would increase data preparation time by orders of magnitude. It should be noted however that absolute intensities and especially their ratios will generally be calculated only near the zenith of photometer locations.

The absorption and scattering corrections were taken from an opacity table prepared and used by members of the Geophysical Institute over a number of years. Although this work is currently being updated, it has been found to produce results interpreted as satisfactory. Both the Van Rijn and opacity corrections are rather severe for angles more than 50° from zenith and they have a countervailing influence. A poor choice for either one would have a decided effect on their product. Yet, when applied to early evening data which contains only background continuum emissions, the result of the opacity values used is a "flat" intensity plot indicating that the correction must be very nearly accurate. This also indicates that the zenith correction which is not unity is also correct. The latter result is important for later computation of the ratio of N_2^+ 4278 to H-beta.

By this means intensity versus range (from the photometer location) plots were prepared. To construct the intensity plots presented here the intensity plots from each station were overlaid and the best fit to the three plots was traced. It is significant that very often the intensity values for the location midway between photometers exhibited agreement. These "intensity plots" offer a basis for a morphological description of the substorms of January 20-21, 1966.

5.5 The Use of the Substorm as a Model of Auroral Morphology

Statistical studies are useful to point out general trends where analyses of specific events might merely lead to confusion. On the other hand, statistical studies tend to blend details and might lead to erroneous conclusions if the limitations imposed by the statistical process are not kept well in mind (see Davis, 1967). The history of

auroral research has followed a pattern from the most general study (Loomis, 1860) wherein the auroral zone was determined over a many-year average and the greatest number of parameters were held constant, to the substorm model of Akasofu (1964, 1965) where the greatest number of parameters were allowed to vary. Yet at each stage of development of the morphological picture of the aurora, it was only after the previous statistical average of events was fully comprehended that the next parameter could be changed from a constant to a variable (again, see Davis, 1967).

Since its inception in 1964, no author has seriously disagreed with the auroral substorm as a model of the dynamic behavior of auroral events generally centered around a "break-up". The study presented here adds a few details to that model in terms of electron and proton precipitation and suggests some possibilities for further study.

5.6 The Night of January 20/21, 1966

The two and one half years of operation of the scanning photometer system produced a great quantity of photometric data. Although it was realized that simultaneous photometric data from two adjacent locations would be of maximum utility, the photometers were operated when the moon was below the horizon on locally cloudless nights regardless of conditions at other stations. This was a fortunate decision for otherwise significant data would have been lost.

For the study attempted here it was necessary to have data from College, Fort Yukon and (hopefully) Bar-1, all night on a long night near mid-winter with active auroral conditions. There were only 10 nights with even partial data from all three photometer systems, and

the other criteria imposed reduced the number of nights suitable for analysis even farther. Finally, due to a combination of reasons, only one night was selected for detailed intensity analysis.

The night of January 20/21, 1966 AST was selected for detailed analysis because of a) its length, b) the College and Fort Yukon meridian photometers operated all night and the Bar-1 scanning photometer operated in the crucial morning period, and c) this was the second night after a storm sudden commencement and three (or possibly five) identifiable substorms occurred, affording a view of three substorms each from a different sector, yet under generally similar conditions. The analysis of this night's data is, as far as possible, broken down into discussion of each substorm.

Analysis of the Auroral Intensity Plots

Auroral and magnetic substorms are centered near the dipole midnight meridian. The activity originates and is generally the most identifiable in terms of the substorm model in this sector. Therefore, the analysis of the intensity plots begins with the first clearly identifiable substorm using magnetometer data from the midnight meridian for identification. All subsequent substorms will be considered, progressing to the early morning sector. After developing a picture of the relationship of proton and electron precipitation behavior in the pre-midnight to early morning sectors, attention is refocused on the details of a well-documented substorm occurring in the midnight sector.

Preceding the intensity plots, the horizontal component of the magnetic field measured at College during this period is reproduced as figure 5.1. Following figure 5.1 is Table 5.1 listing six-minute scalings of the magnetogram.

Figure 5.1

Shown here is the horizontal component of the magnetic field measured at College during the night of January 20/21, 1966. Baseline shown is the instrumental baseline of the magnetometer. For convenience, both local time (bottom) and universal time (top) are shown.

Although specific features of this magnetogram are discussed and related to auroral activity in the text which follows, figure 5.1 gives on a single page a record of the night's substorm activity. For this reason it is worthwhile discussing the general characteristics of the magnetogram before presenting the night's auroral data.

The Akasofu substorm model (section 1.5) relates positive bays in H in the evening sector and negative in the morning sector to substorm activity centered near the midnight meridian. Accordingly, here in the evening sector two positive bays are indicated which correspond roughly to the model in terms of duration and magnitude. In the morning sector, there is a large negative bay which appears to be the result of a running together of several consecutive substorms. It will be seen that in the morning sector the individual substorms are more easily identified from all-sky camera films than from the magnetogram.

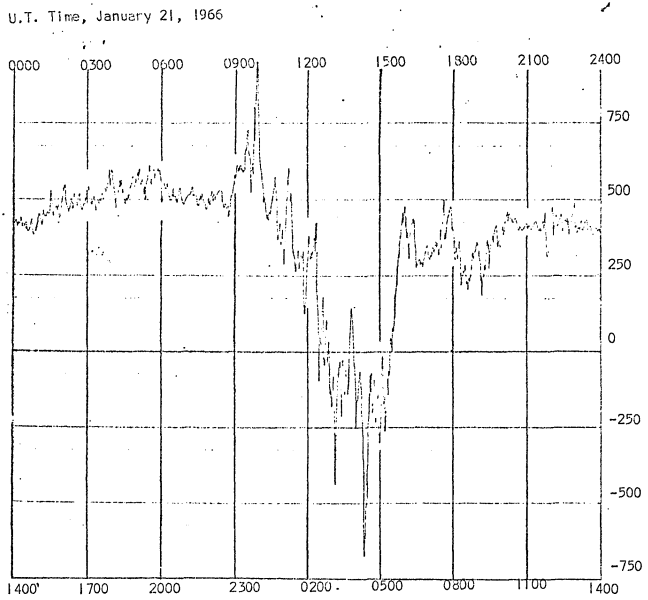

Horizontal component of the magnetic field measured at College during the night of Jan. 20/21, 1966. Baseline shown is the instrumental baseline of the magnetometer.

Six-Minute Interval										Hour	Date
1	2	3	4	5	6	7	8	9	10		
418	419	418	432	412	41m	394	429	384	391	0000	012166
444	432	458	443	448	517	445	473	476	460	0001	012166
518	526	466	498	501	498	500	489	472	496	0002	012166
532	482	498	476	491	494	514	529	552	575	0003	012166
578	515	505	548	524	503	530	533	566	539	0004	012166
558	591	558	525	565	541	568	582	586	593	0005	012166
536	543	539	516	502	509	499	517	506	480	0006	012166
498	510	533	509	500	498	501	486	465	495	0007	012166
518	500	502	521	525	472	472	440	505	535	0008	012166
568	596	598	586	656	716	644	600	742	724	0009	012166
623	552	501	441	453	498	535	508	385	372	0010	012166
346	426	593	464	552	289	328	311	325	175	0011	012166
374	306	348	366	066	022	019	-043	-034	-112	0012	012166
-178	-135	-182	-049	-108	-064	-080	-081	135	003	0013	012166
-159	-073	-178	-474	-564	-362	-131	-112	-166	-144	0014	012166
-301	-019	-259	-100	035	039	149	294	362	454	0015	012166
449	385	369	416	395	264	299	268	316	341	0016	012166
305	332	352	355	328	344	440	414	455	456	0017	012166
390	305	323	328	241	268	260	266	323	338	0018	012166
283	259	230	286	349	329	376	405	373	356	0019	012166
405	430	452	436	428	435	415	408	401	411	0020	012166
415	414	412	423	418	401	421	451	356	389	0021	012166
476	428	432	429	436	430	430	412	442	484	0022	012166
392	405	418	419	414	408	395	388	421	399	0023	012166

Table 5.1 6 minute scalings of horizontal component of College magnetogram for Jan. 21, 1966 U.T.

Fig. 5.2 Parts a through n. Pairs of plots of simultaneous absolute zenith intensity vs. latitude of N_2^+ 4278 (top) and H-beta (bottom) prepared at fifteen minute intervals for the night of Jan 20/21 (L.T.) 1966. The plots were prepared by averaging three successive one-second meridianal photometric scans (when available) from each of the three stations indicated. Generally, College and Fort Yukon data are available throughout the night. The Bar-1 photometer did not contribute data until 0414 150° WMT.

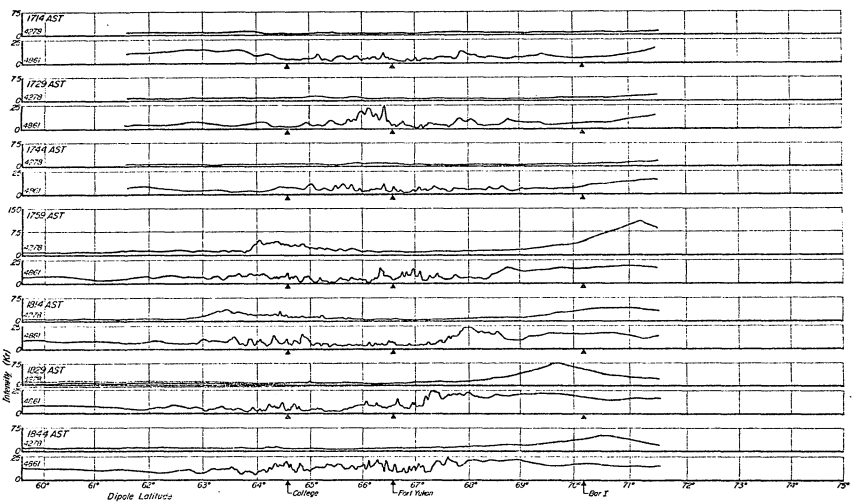

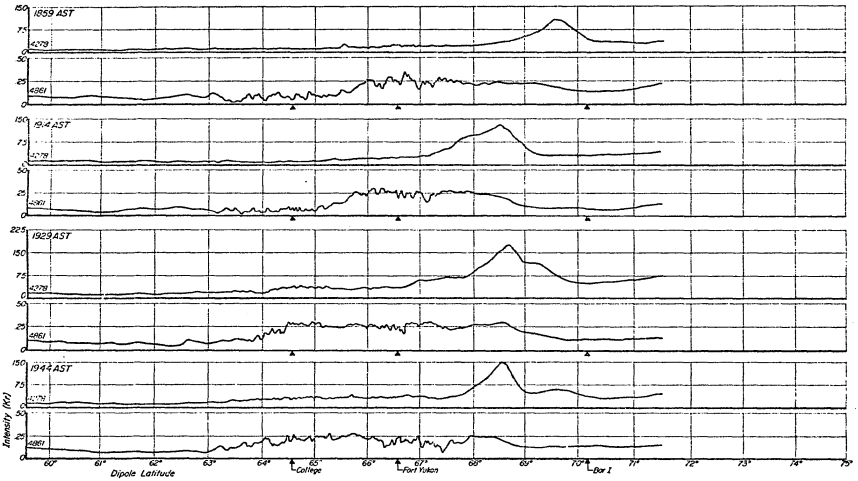

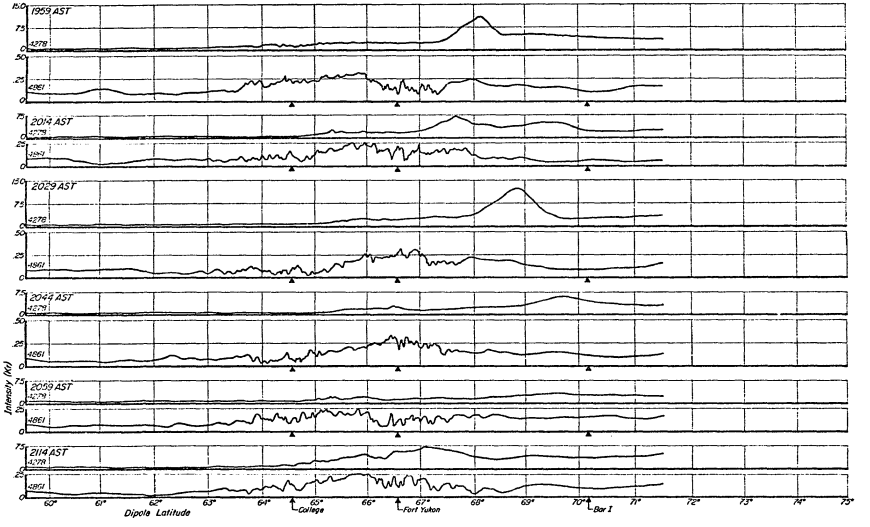

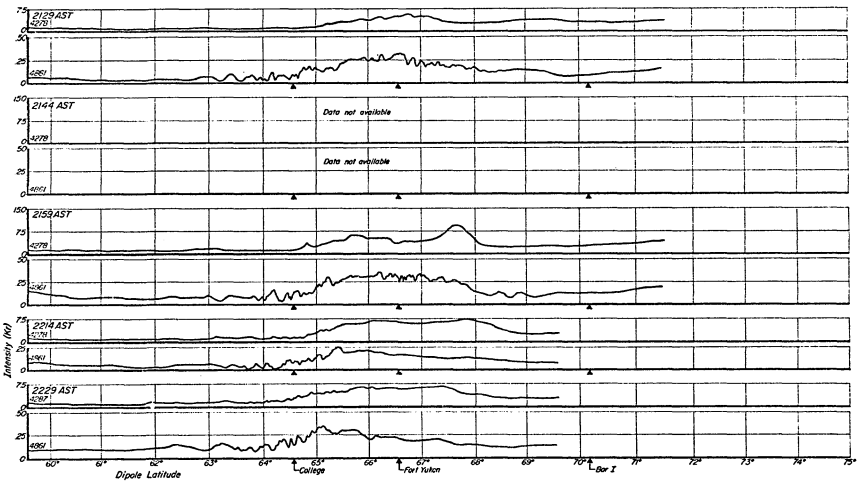

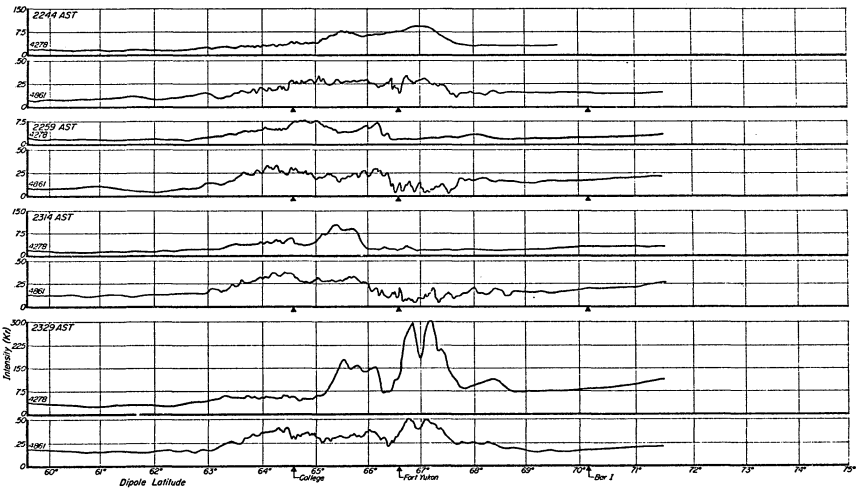

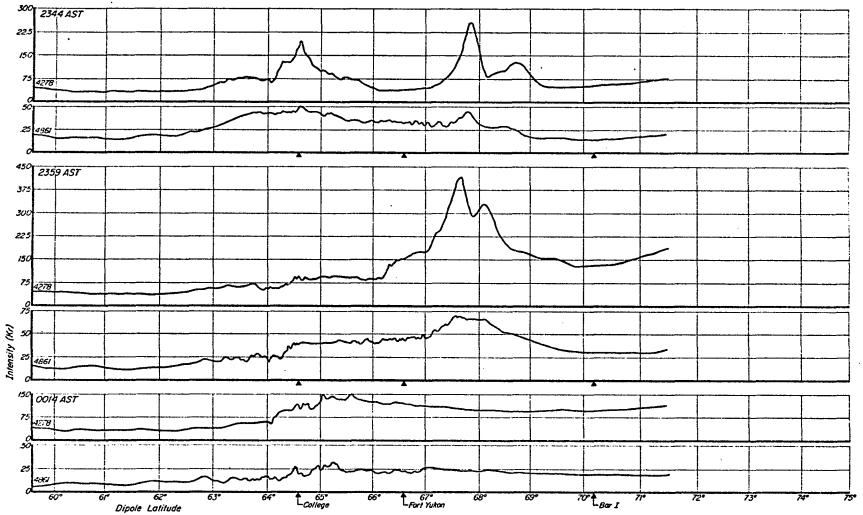

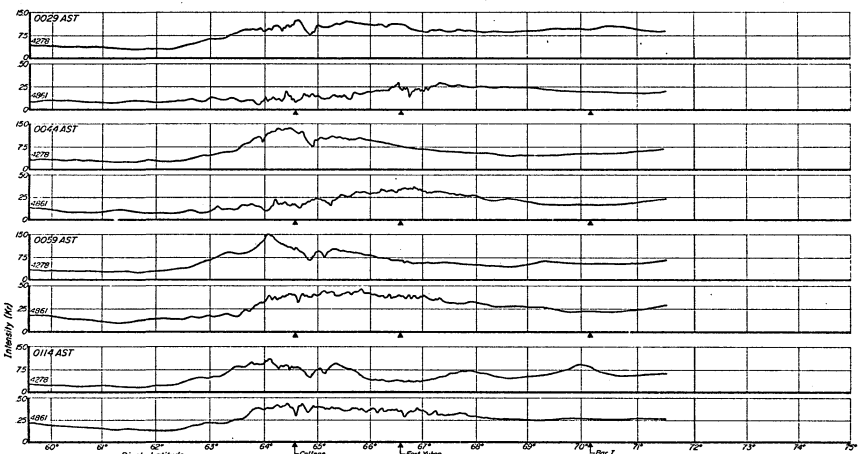

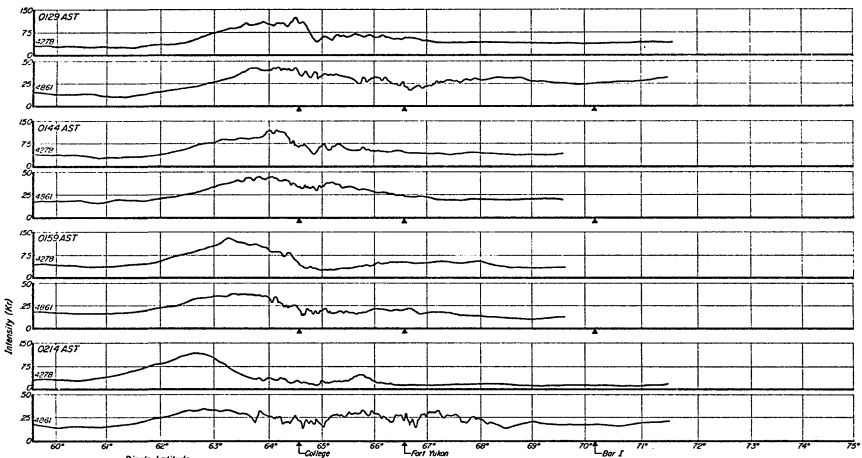

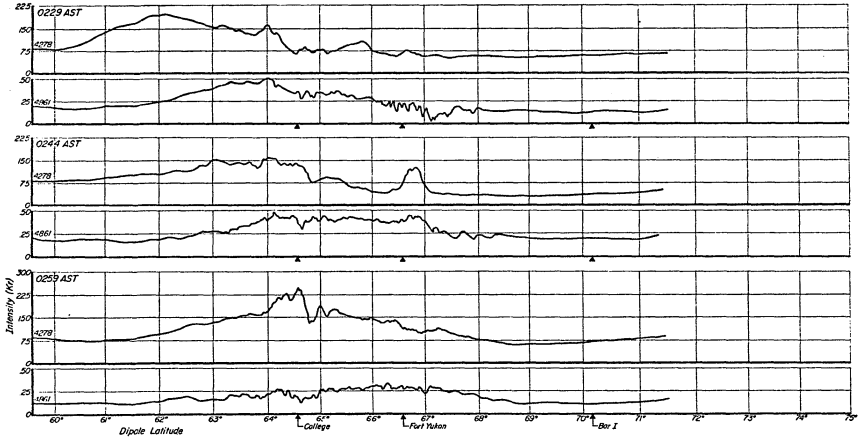

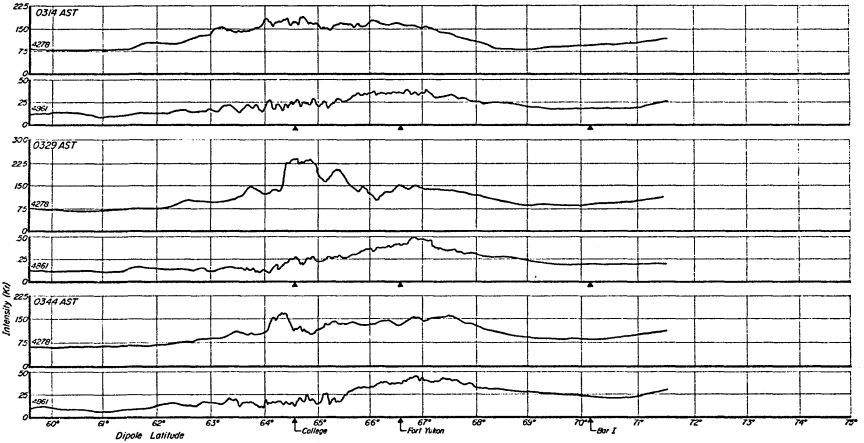

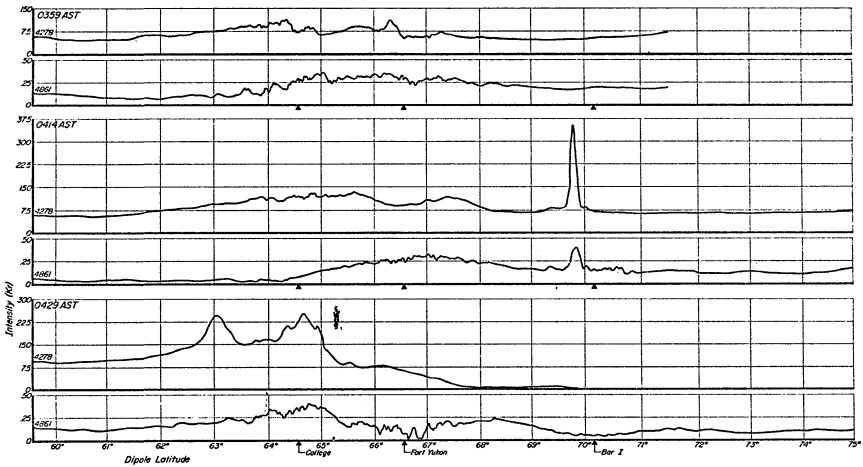

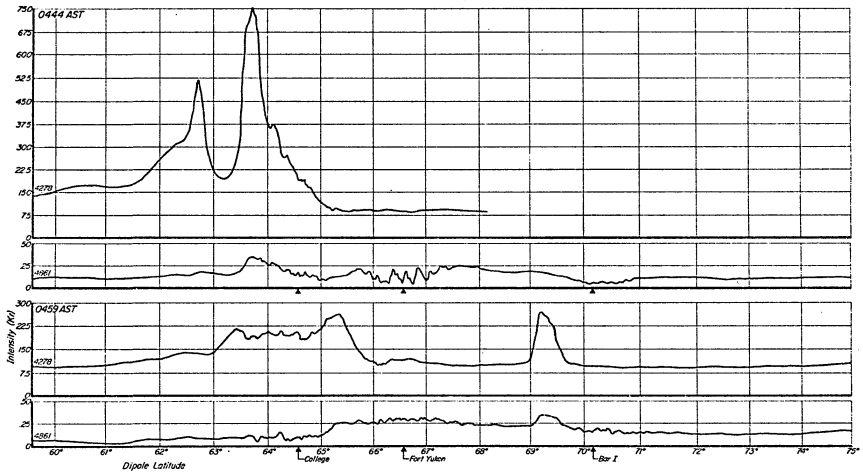

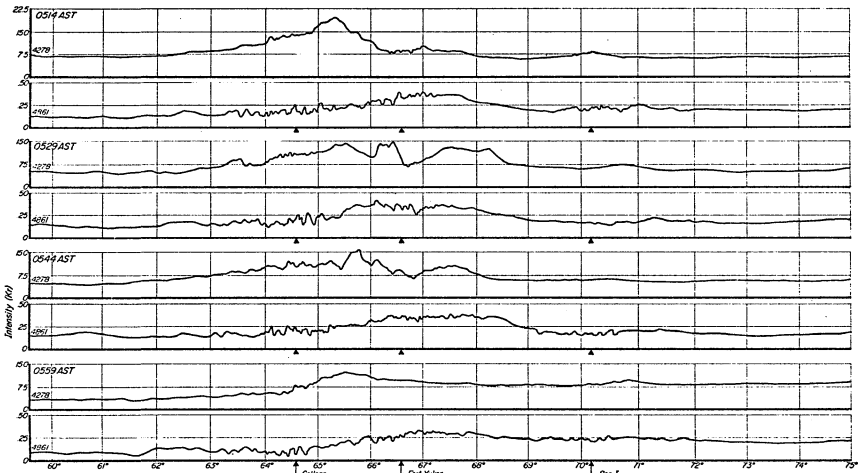

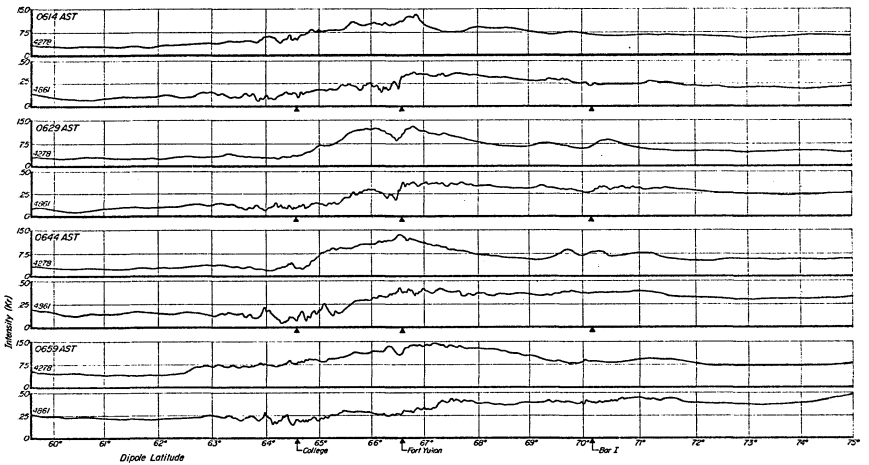

Preliminary remarks

a. Pure proton precipitation

Pure proton precipitation produces auroral emissions other than hydrogen lines chiefly through secondary electrons produced by the primary protons. Eather (1967) predicts intensity ratios for incident protons with an exponential energy distribution:

$$N = N_o e^{-E/E_o}$$

where E_o = 20 kev for E < 100 kev, and E_o = 100 kev for E > 100 kev. The predicted ratio of N_2^+ 3914/H-beta is from 20/1 to 30/1. The normal ratio of N_2^+ 3914/N_2^+ 4278 is generally 3/1 in the aurora (Chamberlain, 1961). Hence, the predicted N_2^+ 4278/H-beta ratio is from 7/1 to 10/1 for pure proton precipitation. Eather (1967) called an aurora which appeared to be due to pure proton precipitation through exhibiting this ratio a "proton aurora". This terminology will be retained here.

b. The "hydrogen arc"

The general usage of "the hydrogen arc" varies from a term denoting the entire region of auroral hydrogen emissions having a width as great as 10° of latitude or the narrow (~2° wide) region of brightest (>50% maximum intensity) hydrogen emission within the hydrogen emission region. This latter definition is generally only applied to quiet conditions in the evening and midnight sectors. Here, "hydrogen region" will refer to that portion of the sky from which hydrogen emissions greater than background levels can be detected. "Hydrogen arc" will have a specialized meaning, developed from the >50% maximum intensity criterion. From these definitions it is possible that portions of the "hydrogen arc" or "hydrogen region" can be "proton auroras". Portions of the

"hydrogen arc" which exhibit N_2^+ 4278/H-beta ratios indicating mixed electron and proton precipitation are referred to as "(electron) contaminated".

5.7 Early evening behavior

The Fort Yukon scanning photometer was placed into operation slightly before the first intensity plot shown here for 1714. The flat N_2^+ 4278 trace (top) supports the assertion made earlier that the geometric and opacity corrections must be nearly correct. Note that both N_2^+ 4278 and H-beta rise slightly toward the south. The dipole meridian is aligned 30° west of geographic south. The southwest horizon is still slightly light at this time. The 30 to 1 ratio between scale factors for N_2^+ 4278 and H-beta is partially reflected by the greater apparent deflection of H-beta shown here.

By 1729 both intensities have diminished in the south. The large H-beta amplitude south of Fort Yukon is thought to be due to an unusually bright region of hydrogen emission in our galaxy passing through the Fort Yukon photometer's field of view at this time (see Appendix D).

Between 1744 and 1759 a very dim arc can be seen traveling south on the College all-sky camera. This dim arc is evident on the N_2^+ 4278 traces for 1759 and 1814. The H-beta emission from Fort Yukon south is thought to be noise and galactic contamination. The dim arc mentioned here was noticed on all-sky films only after a search had been initiated on the basis of its apparent existence exhibited here. It is not known if a dim southward-traveling arc in this time sector is a general morphological feature. If so, it may only be associated with SSC's. It is not known at this time if there were any low latitude red arcs

associated with this storm. However Montbriand (1969) and Berkey (1971) have observed patches on all-sky films at this local time during very active periods.

The H-beta traces for 1714 through 1744 indicate enhanced emission in the far north. By 1759 this emission enhancement region has moved south and the N_2^+ 4278 trace also shows the presence of enhanced emission in the north. Note that H-beta actually preceeds N_2^+ 4278 southward. The Bar-1 photometer was not operating at this time so that zenith intensities are not available for this region. However, on the basis of the discussions of the substorms which followed later, it is very likely that the equatorward portion of this emission region is due to pure proton precipitation. The auroral feature being discussed here is the "hydrogen arc" which has been described by others (Romick et al., 1961; Montbriand, 1969).

It is difficult to determine which features of the morphology of the hydrogen arc shown here are associated with the rotation of the quiet auroral oval - and hence migration to more southerly latitudes - and which features are associated with substorms centered near the midnight meridian. Based on the descriptions of auroral behavior in other time sectors, it seems that the proton precipitation region moves southward at a somewhat uniform rate. Superimposed on this is an electron precipitation region with maximum precipitation on the poleward edge of the hydrogen arc. During quiet times the equatorward edge is very likely pure proton precipitation. The ratio of N_2^+ 4278 to H-beta on the southward one degree segment of this arc from 1814 through 1914 indicates this.

The Great Whale River magnetogram has been examined in order to identify magnetic behavior in the midnight sector during this time. At 1900 L.T. College, this magnetometer is located at local midnight. In terms of College local time, the Great Whale River magnetogram shows a moderatley flat H-component from 1700 to 1800. Starting at 1800 there is a gradual decrease, until approximately 1930 when there is a sudden impulse followed by a negative bay which persists until 2010 and recovers by 2030. It is then flat until 2100 and decreases slightly again until 2130, when a positive bay begins.

The intensity plots show that as magnetic activity increases on the midnight meridian, first electron precipitation increases on the poleward edge of the hydrogen arc (1859 and 1914) and finally electron precipitation increases across the entire hydrogen arc and it is "contaminated" (1929, 1944). This is indicated by the change in the N_2^+ 4278/H-beta ratio over Fort Yukon from 8.5/1 at 1914 to 13/1 at 1929. The entire hydrogen arc also moves abruptly equatorward at this time which corresponds to substorm onset in the midnight sector as indicated by the Great Whale River magnetogram.

As activity on the midnight meridian decreases, first the electron precipitation diminishes leaving the equatorward portion of the hydrogen arc uncontaminated (1959, 2014), and as the recovery continues, the entire arc moves poleward (2029) - or at least resumes a "quiet time" position that reflects the general expansion of the auroral oval dependent on overall auroral activity. (During a large storm, one expects a generally expanded oval.)

Even for quiet periods it seems there is a maximum local dipole time for which the equatorward portion of the hydrogen arc will remain uncontaminated. The southern sector of the hydrogen arc shown here was clearly contaminated after 2114, yet the next identifiable substorm did not occur until 2317.

5.8 The Substorm of 2317.

This event is referred to as the substorm of 2317 because this is the local time at which the aurora viewed from College started behaving in the manner characteristic of substorm onset as documented by Akasofu (1964). The event most probably originated a few minutes earlier at a point as far as 45° longitude east of College. Hence, this description deals with behavior on the evening side of the substorm. Note the positive bay in H which occurs at this time in accordance with the substorm model.

5.8.1 Pre-onset phase

In describing this event it is difficult to separate events related to previous substorms far to the east from those events more directly related to the onset of the substorm of 2317 - if indeed such a distinction can be made. However, note that at 2014 the intensity plots show proton precipitation to peak approximately two degrees equatorward of electron precipitation. The situation at 2029 very nearly resembles that described by Romick and Sharp (1967) for L.T. 2208, November 9, 1965. On this date simultaneous satellite and spectrographic data were compared to relate proton and electron precipitation as measured by a polar-orbiting satellite with H-alpha and OI 5577 Å emission as measured by a spectrograph located at College. The results

of their study are shown in figure 6.6. Note that the lower threshold energy for proton detection was 10 kev and hence the exponential fit of $N \sim N_o e^{-E/16}$ kev may not be valid for energies much lower than 10 kev. This tie-in does give us some idea of electron and proton energies and precipitation patterns and the validity of H-beta representing actual proton precipitation at this time.

By 2044 electron precipitation has diminished. By 2059 both electron and proton precipitation have diminished, and also the proton region has moved equatorward to span the region 64 3/4° to 66°. This is very nearly the width of a zone of maximum proton emission due to the injection of 10 kev protons along a single field line with an isotropic pitch angle distribution as calculated by Davidson (1965). (See figure 1.3.) It is interesting that while N_2^+ 4278 intensity at the same location is 1.6 KR, the average H-beta intensity during this period is approximately 190 R, or a ratio of 8.5 to 1. At this time the H-beta emission centered between College and Fort Yukon represents what has come to be described as a "proton arc": pure proton precipitation injected along a narrow line with widespread photometric emissions due to charge-exchange spreading of the primary protons before their proton production and secondary electron production become large. It is interesting that only the slightest hint of an auroral arc can be seen in this region of the sky on the College all-sky camera photographs.

By 2159, the ratio of N_2^+ 4278 to H-beta has changed to 15/1 and there is an electron arc located at 67 1/2°. There may be some electron contamination of the proton arc at this time, but it is also possible that light scattered in the troposphere from the electron arc in the north contributed to the N_2^+ 4278 emission observed.

During the next hour there is evidence of electron encroachment on the proton arc. At 2244 the arc overhead at College exhibits a 4278/H-beta ratio of 10/1. At 2259 the ratio just south of College is approximately 12/1, and it is likely that there is some electron precipitation at this time.

The positive bay shown on the College magnetogram began just before 2257 and corresponds to the southward motion, intensification and contamination of the hydrogen arc between 2229 and 2259. Note that throughout this period the peak emission of H-beta has been equatorward of the peak emission of N_2^+ 4278, indicating proton precipitation equatorward of electron precipitation. This precipitation pattern will produce a poleward electric field, which will in turn produce a Hall current resulting in an eastward electrojet and a positive bay in H. (Additional evidence for this precipitation pattern is presented in Chapter VI.)

5.8.2 Onset

By 2314 the electron arc to the north of College has brightened, yet the zenith ratio of N_2^+4278/H-beta remains 12/1. This electron arc is located on the poleward edge of the hydrogen arc. At 2317 it brightens and becomes active. The bright electron arc remains north of the College zenith while at 2329 the zenith ratio of 4278 to H-beta is 16/1. If the obvious increase in the N_2^+ 4278 background is subtracted, this value is 12/1. It is possible then that during this break-up the southern edge of the proton arc remains very nearly pure proton precipitation. This could be, as will be discussed later, largely due to the natural charge-exchange width of the proton arc.

The large positive spike in College H corresponds to the intensity plot for 2344. Note that in the College zenith, H-beta has reached an intensity of 500R - the greatest value until this time. The N_2^+ 4278 intensity of the electron arc or the poleward edge of the hydrogen arc is 20 KR - also a maximum until this time. Hence, one would expect the greatest Hall current thus far.

During the next hour or so, there is auroral activity in the north consisting of bright rayed arcs. Most analyses might concentrate on that region of the sky; note here is made only that those arcs are obviously electron arcs. H-beta enhancements in these arcs are discussed later.

At 2344 the region south of College exhibits a 4278/H-beta ratio of 19/1. The H-beta intensity in this region has increased to 400 R. The appearance of this arc remains the same - diffuse with the possibility of consisting of thin filaments or striations.

By 2359 and 0014 both the H-beta and N_2^+ 4278 regions move poleward. At 0014 the ratio of N_2^+ 4278/H-beta in the region south of College is nearly 30/1. The ratio is even greater to the north. There is without any doubt simultaneous electron and proton precipitation at all latitudes at this time.

Between 0014 and 0029 H-beta intensities drop abruptly to around 75 R while N_2^+4278 increases to 10 KR or a ratio of 130 to one in the region over College. During this time, patches appear in this same region and remain until around 0044. The patches remain as long as proton precipitation is virtually absent. At this time the peak emission of N_2^+ 4278 is equatorward of the peak emission of H-beta - hence, a cross-over of peak emission of N_2^+ 4278 and H-beta from times previous to this.

5.8.3 Recovery phase

Between 0044 and 0114 the region of overlap of proton and electron precipitation is rapidly changing from pulsating patchy aurora to a broad striated arc. When viewed in cine fashion, the College all-sky camera indicates many parallel arcs with E-W alignment passing southward and tending to sweep the patches further south. These arcs move southward faster than the patches and there is a very strong indication that the arcs pass into the patch region for some distance before becoming indistinct. By 0114 the striated arc can be seen far to the south of College. From Talkeetna patches can still be seen on the southern edge of this region.

In general, from this description and from examining the intensity plots for 0044, 0059, and 0114, one has the impression that the broad region of parallel arcs moving into the patch region is associated with the equatorward extension of proton precipitation at this time.

During the next hour (0114-0222) the proton region becomes coincident with electron precipitation by 0144, and remains so until the breakup at 0222. Also during this time the broad region of parallel arcs becomes narrower and very likely is a striated arc, a broad arc composed of many parallel arc-like filaments.

5.9 The Substorm of 0220

5.9.1 Preonset phase

It is rather difficult to determine at what time the after effects of the previous substorm (2344) diminish and the precurser events of the next begin. Examination of all-sky camera films shows that by 0144 events are occurring which can be ascribed to the substorm in that they

do not follow the pattern established for post-substorm behavior in this sector. The intensity plot for 0114 shows electron precipitation extending approximately 1/2 degree equatorward of proton precipitation. The hydrogen emission resembles a plateau rising abruptly at approximately 63 3/4° to 375 R and sloping to 330 R at 66.5° (over Fort Yukon). The N_2^+ emission rises abruptly to 8.5 KR at 64 1/4°, shows more structure than H-beta, remains more-or-less constant to about 65 1/2° and drops to 4 KR over Fort Yukon. The 4278/H-beta ratio changes from 23/1 at College to 12/1 at Fort Yukon.

To the north there is other auroral activity which, according to the substorm model, is related more to the last stages of the previous substorm than to the beginning of the substorm of 0220. From Mould Bay at 0116 a bright arc can be seen briefly in the far southwest. No other aurora can be seen until 0221 (to be described later). To the south of Mould Bay, the Barrow sky is filled with westward traveling active arcs. One of these, to the north, is moderately bright. This westward motion along E-W arcs continues until 0058 when the arcs themselves start migrating southward. The last of these pass overhead at 0200. By 0220, arcs can only be seen in the 30 degree segment above the southern horizon. At 0223 the bright arcs associated with the 0220 substorm can be seen in the south.

From Allakaket, between Barrow and College (just to the west of Fort Yukon), the southward migration of arcs can be seen starting at 0044, when parallel arcs sweep into the patches remaining from the last substorm. The southward motion of striations continues and at

0201 a bright arc can be seen 20° above the northern horizon. This bright, active arc reaches zenith at 0216 and remains there until the break-up arc passes overhead.

Again examination of the intensity plots shows that between 0029 and 0044 the proton precipitation region moved southward past the latitude of Fort Yukon and Allakaket, following the pattern described for College during the time period 0014-0044.

5.9.2 Onset

The description of the actual onset phase of this substorm begins at Kotzebue, 600 km west of College. At this universal time, Kotzebue is located close to dipole midnight. Starting at 0200 a broad, diffuse arc in the south becomes increasingly more discrete. Its intensity remains more or less uniform. Suddenly, at 0219 the entire sky is so bright that no auroral structure can be seen, due to over exposure of the all-sky camera film. The all-sky camera base plate which is also in the camera's field of view is lighted well enough to show construction details.

On the Talkeetna all-sky camera picture for 0221 active bright folds are seen traveling eastward along the broad arc between Talkeetna and College.

The College all-sky camera for 0221 shows no change from the previous few minutes; the frame for 0222 shows the entire arc with bright, wavy folds. The accuracy of all-sky camera picture frames is $\pm$ 30 seconds. At this time there is a sudden decrease in H at College. This magnetic behavior agrees with that documented by Akasofu (1964) for the overhead onset of a substorm.

The detailed behavior of spectral emissions during a substorm onset at this local time has been documented by A. E. Belon and G. J. Romick (private communication). The origin of the substorm onset described by Belon and Romick was situated more nearly overhead at College than that of January 20/21, 1966, so that the details at the first few minutes of the event can be more clearly seen. This event occurred during the night of October 1/2, 1965; it is described in section 5.12.

Briefly, an electron arc travels rapidly poleward following 0222. The hydrogen arc and considerable N_2^+ 4278 remain south of College. Between this time and 0229 there is a 500 γ decrease in H at College. Corresponding to this decrease in H, N_2^+ 4278 brightens and moves equatorward while H-beta brightens and moves poleward. Hence where at 0214 these emission regions were nearly coincident, at 0229 proton precipitation is clearly poleward of electron precipitation. A Hall current produced by the equatorward electric field due to this precipitation pattern would cause a decrease in H as seen.

The intensity plots for 0255 through 0344 show a general poleward motion of both N_2^+ 4278 and H-beta, with the N_2^+ 4278 peak emissions remaining equatorward of the peak emission of H-beta.

5.9.3 Recovery phase

Between 0344 and 0359 the H-beta region returns equatorward. Films of the monitor oscilloscope show that during the time proton precipitation advanced overhead at College, pulsations within the aurora diminished considerably in that region.

5.10 The Substorm of 0406

5.10.1 Substorm onset

At 0406 the first identifiable signs of a substorm to the west of College can be seen in the College all-sky camera films. These indications generally are a change from patch-like structures moving in a westward direction to more arc-like patches moving in an easterly direction. By 0414 there are many wavy pulsating arcs overhead. The waves are traveling eastward. Examination of the Allakaket all-sky film shows that the bright arc in the far north on the intensity plot for 0414 is traveling very rapidly equatorward, sweeping patchy pulsating aurora equatorward before it. (Fortunately for this analysis, the Bar-1 photometer started operation just before 0414.) When this arc reaches Allakaket zenith at 0423 it takes on the configuration of the omega band. At 0431 an omega band with active eastward traveling folds comes into view at College from the north. It is likely that the substorm occurred several minutes before 0400 at a location 45° longitude to the west. Note the large, 500 γ magnetic bay which occurs at this time.

The intensity plot for 0429 shows two regions of bright N_2^+ 4278. The poleward arc is the southward traveling omega band while the arc on the equator side is a brightened band which more-or-less collected out of the region of the patches. The H-beta emission region seems to be more closely related to the omega band than the band to the south. From this time on the sky is filled with eastward drifting arc segments. The intensity plots show that the proton region moves poleward but also becomes wider in width again as before the appearance of the bright omega band at 0429.

The omega band moves southward past College zenith. The patches and arc segments recede before it. The intensity plot for 0444 shows the result of the photometer scanning across the arc-like portion of the omega band in the south, and across the north-south segment of a 180° bend in an omega extending northward from the arc-like portion of the omega band. The high H-beta emission in this portion of the sky may be due to excitation of atmospheric hydrogen (see section 6.1).

The large magnetic bay between 0414 and 0429 can be explained in terms of a Hall current; the precipitation pattern is that which is required. However at 0444, the N_2^+ 4278 intensity is the greatest observed during this night yet the H-component has recovered completely. The lack of a Hall current can be explained as the result of very little proton precipitation in the region north of the bright electron arc.

By 0459 the omega band has diminished in intensity and moved northward. The bright N_2^+ 4278 emission region just north of 65° is the omega band and the emission to the south is due to eastward-traveling patches. Note the great variation in ratio of H-beta to N_2^+ 4278 over the sky. The bright arc overhead at Bar-1 appears to be one particularly bright rayed arc of many arcs passing overhead in a northerly direction in this time sector.

The intensity plot for 0514 shows for a relatively quiet period a definite cross-over of electron- and proton-produced emissions in the early morning sector. The omega band is spreading northward and at 0529 passes over Fort Yukon.

5.10.2 Recovery phase

At 0544 there are many active rayed bands between College and Fort Yukon. Again the region of N_2^+ 4278 is located equatorward of the H-beta region. This occurs during the 700 γ recovery in H shown on the College magnetogram.

At 0559 the N_2^+ 4278 region north of College is composed of many parallel bands which appear to be pulsating. It is important to note that at both 0544 and 0559 the H-beta intensity is relatively small (250R) in the region of peak N_2^+ 4278. Note that between 0544 and 0559, H-beta and N_2^+ 4278 decrease by 50% at College zenith. By this time the recovery in H is nearly complete.

5.11 Early Morning Quiet Period

During the next 45 minutes, starting at 0614, there is very little or no displacement of H-beta from N_2^+ 4278. All during this time there are no patches.

At 0659 patches appear just at dawn over College. The enhanced H-beta is very likely due to twilight.

5.12 The Substorm Onset of 0132, October 1/2, 1965 AST

Much useful insight can be gained from a comparison of the substorm occurring on this evening with those of January 20/21, 1966. This substorm occurred at almost the same local time as the January, 1966 storm and can therefore be compared with it directly. As stated earlier, the October 1/2, 1965 substorm offers the advantage that it occurred nearly directly overhead at College and can provide more details than the January 20/21, 1966 substorm. This discussion makes use of a figure prepared by Romick and Belon (private communication).

Figure 5.3 is broken down into subfigures showing all-sky camera photographs and photographs of an oscilloscope display of the H-beta emission and the OI 5577 Å emission as measured by the Meridian Scanning Photometer. North is on the right, and the vertical scale is logarithmic in both cases.

Subfigures 1a and 1b show what is very likely a pure proton arc far to the north of College. Subfigures 2a and 2b show the same arc displaced slightly to the south with an electron arc to the north. This is not too unlike the situation for 2029, January 20/21, 1966. Later, the proton arc moves abruptly southward (subfigures 3a and 3b).

Note that the rayed arc to the north shows up as a definite structure on the oscilloscope photograph. The rayed arc followed the proton arc south, and shortly after this time moved even closer to the proton arc. However, instead of actually merging with the proton arc, the oscilloscope film shows this arc diminishing in intensity to background levels.

Subfigures 3c and 3d show the situation shortly after the rayed arc discussed above died out. The northern edge of the striated electron-contaminated proton arc increases in intensity. The rayed arc in subfigure 3c is located over Fort Yukon and has moved in from the north.

Subfigures 3e and 3f show both the brightened poleward edge of the proton arc and the brightened rayed arc to the north. Actually, the rayed arc brightened abruptly two to three minutes before the arc at zenith. It is difficult to determine the earliest stage of a substorm onset which can definitely be identified a priori as leading to a substorm onset.

Fig. 5.3 Parts 1a through 6b. Corresponding all-sky camera photographs and photographs of oscilloscope display of horizon-to-horizon scan of 5577 [OI] (top trace) and H-beta (bottom trace) illustrating various phases of a substorm which occured as a "break-up" at zenith at L.T. 0132, Nov. 2, 1965. (Belon and Romick, private communication).

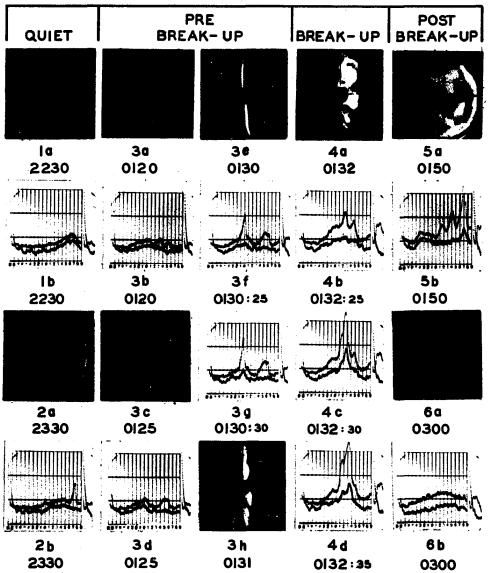

However, once the striated proton arc has the appearance shown in subfigure 3e, substorm onset is inevitable and will occur within one or two minutes.

Subfigures 3g and 3h show that the region of enhancement has brightened considerably but has not changed location. From subfigure 3g, it is clear that the region of enhancement is still located on the northern edge of the preexisting proton arc.

Subfigure 4a shows that by 0132 the bright arc overhead has taken on the appearance of what is generally termed "break-up" and is called "substorm onset" here. The three oscilloscope photographs associated with this time period show several interesting features:

1) The intensity of the arc is quite great and variable (5577 OI intensity of 100 KR in subfigures 4c and 4d).

2) H-beta shows arc-like structure (to be discussed in section 6.1).

3) The intensity of H-beta is increased over the entire hydrogen arc.

4) The bright, active electron arc remains on the northern edge of the hydrogen arc.

Subfigures 5a and 5b show the situation after break-up. It is particularly interesting that although the poleward expansion of the substorm activity has taken place, the hydrogen arc has shifted equatorward and H-beta intensities are quite large.

Subfigures 6a and 6b show the beginning of electron cross-over and the diminishing and poleward migration of the hydrogen region. Note that its latitudinal extent was greatly extended during the poleward expansion of the substorm (subfigure 5b).

5.13 Conclusions

5.13.1 Hydrogen emission in the auroral substorm model

Based on the previous discussions, a model of hydrogen emission in the auroral substorm will be superimposed on Akasofu's (1964) model of the auroral substorm.

Six figures prepared by Akasofu (1964) to illustrate the dynamic behavior of the aurora are used here as a basis for a model of hydrogen emission during a substorm. One of Akasofu's figures is used two times with minor modifications to illustrate certain subtle features in the latter stages of the substorm.

The Akasofu model was developed on the basis of IGY auroral data, and the model used represents auroral activity for an active period similar to the night under study.

Figure 5.4 is composed of Akasofu's substorm model figures and the modified drawing superimposed by a plastic overlay to show the regions of hydrogen emission. The drawings are generalizations based on the previous descriptions and examination of MSP oscilloscope films from numerous other nights. As with all generalized models of the aurora, it should be emphasized that these sketches should not be taken too literally. They are presented only to give a general picture of the association of hydrogen emissions and substorm activity. Facing each figure is a page containing the figure caption and a discussion of features shown in the figure. Many of the conclusions drawn from the intensity plot analysis are presented in these discussions.

In these figures, relative contours for H-beta emission in approximately 100 R increments above background will be indicated. The light dotted line shown on these diagrams separates the region of pure proton precipitation (proton aurora) from the region of 'mixed' electron and proton precipitation.

Figure 5.4 A Presubstorm-Onset Quiet Phase

Taking the instant just before the sudden brightening of an electron arc on the poleward edge of the hydrogen arc as T = 0, or substorm onset, this figure could represent times up to an hour before T = 0. H-beta intensities increase gradually before the sudden brightening, tending to add a new intensity contour within the existing hydrogen arc, and in the evening sector, an over-all narrowing of the >50% maximum intensity of the hydrogen region. Although there are no clearly identifiable events which would allow a prediction of the instant sudden brightening, a tendency has been noticed for rayed arcs to the north of the hydrogen arc to migrate rapidly southward just before the sudden brightening. Akasofu (1964) has indicated this behavior as indicative of the final stage of a previous substorm.

It should be emphasized that these drawings refer only to a period of generally great auroral activity and that under less active conditions, the auroral oval would be less expanded and H-beta intensities correspondingly lower.

Figure 5.4 A shows large H-beta intensities to occur in the morning sector. This again is a condition which may be linked to periods of continuing magnetic activity.

There are two features of this drawing which should be emphasized. Even during quiet periods between substorms the hydrogen arc is electron contaminated before midnight and the electron and proton regions are superimposed in the dawn sector. The auroral oval - particularly in the dawn sector - was somewhat expanded during the night analyzed so the location of hydrogen intensities have been slightly adjusted in this sector to correspond to the Akasofu model.

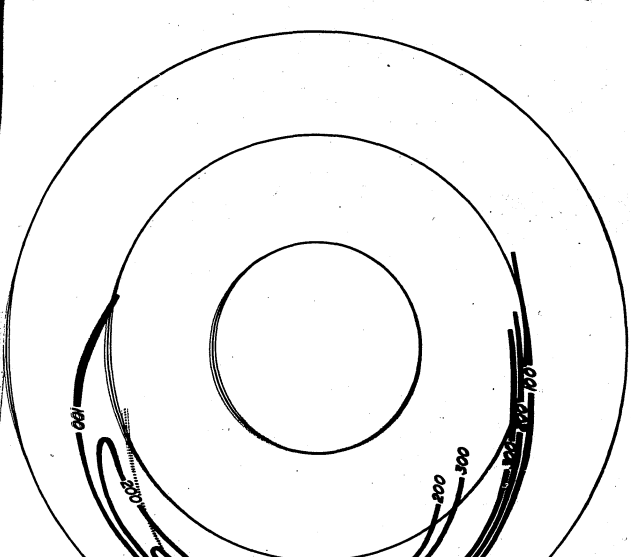

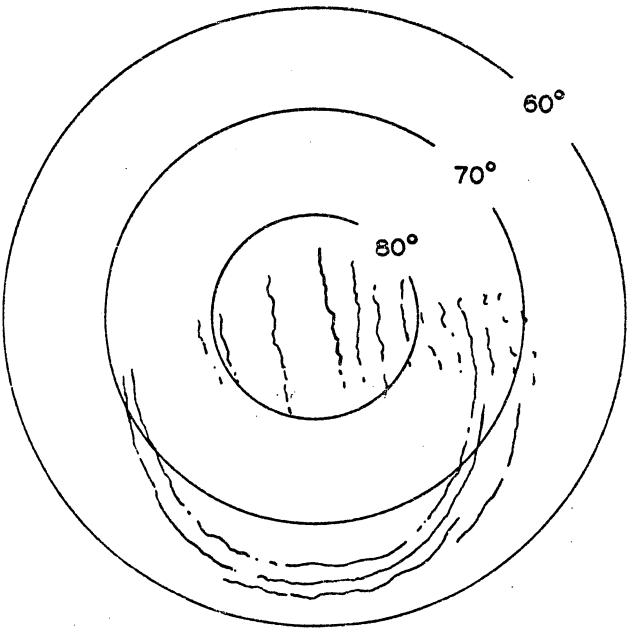

T=0

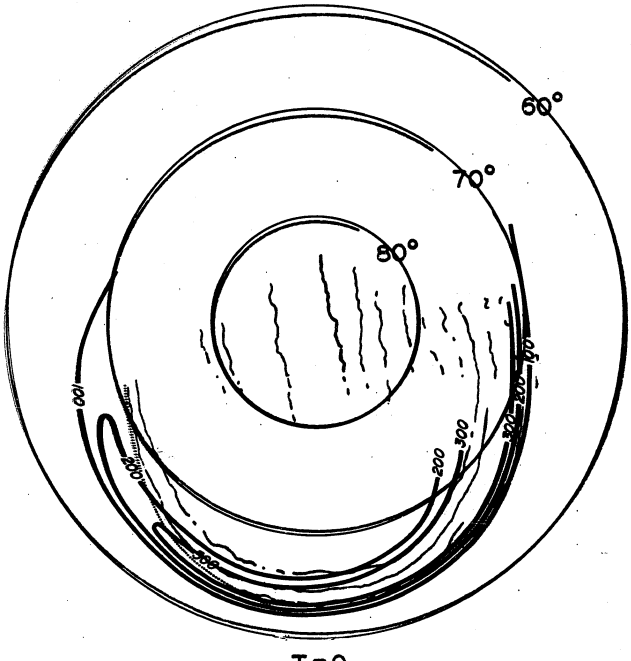

Figure 5.4 B Substorm Onset

This figure represents conditions at or very soon after (1 min.) the instant of sudden brightening or substorm onset. The Akasofu model shows the brightening as occurring within the southernmost auroral arc. At the time of substorm onset the southern-most clearly identifiable auroral arc is the region of enhanced electron precipitation at the poleward edge of the striated hydrogen arc. In the dipole midnight meridian, this arc often appears as a new arc just equatorward of a pre-existing most equatorward electron arc. This bright arc is shown here just polewards of the 300 R intensity contour of the hydrogen arc.

Accompanying the sudden brightening of this very narrow discrete arc is a narrow, bright H-beta arc which is not shown on the contour diagram. The intensity of this narrow H-beta arc can be several hundred rayleighs. Note that this may not be due to precipitating protons, but rather electron excitation of atmospheric hydrogen.

The H-beta contours shown here are much the same as in the previous contour plot except that the width of the hydrogen arc has been narrowed and the region of contamination continued somewhat westward. The entire hydrogen arc (approximately the region for which H-beta > 200 R) has moved equatorward.

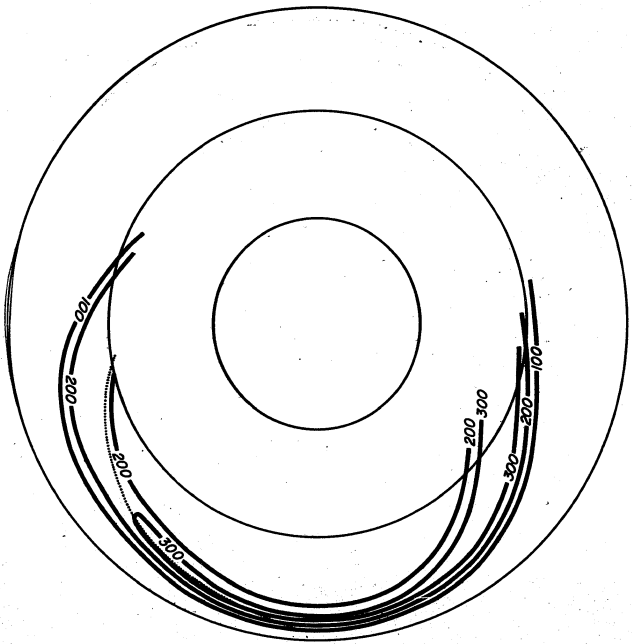

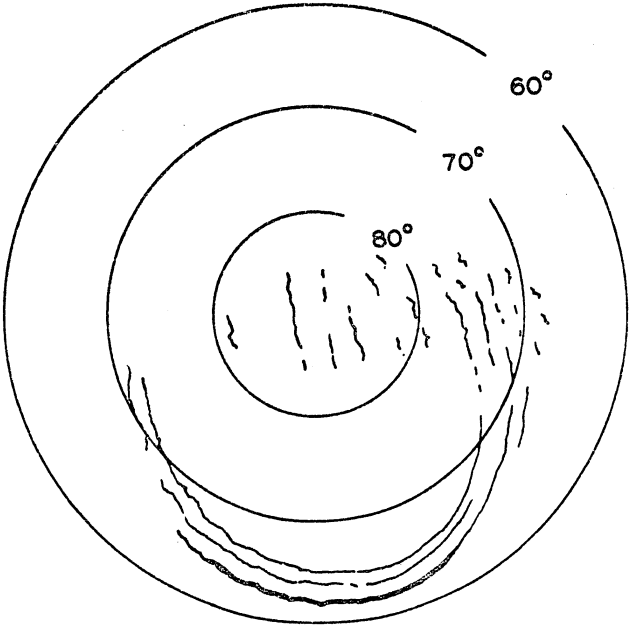

T=0~5 MIN

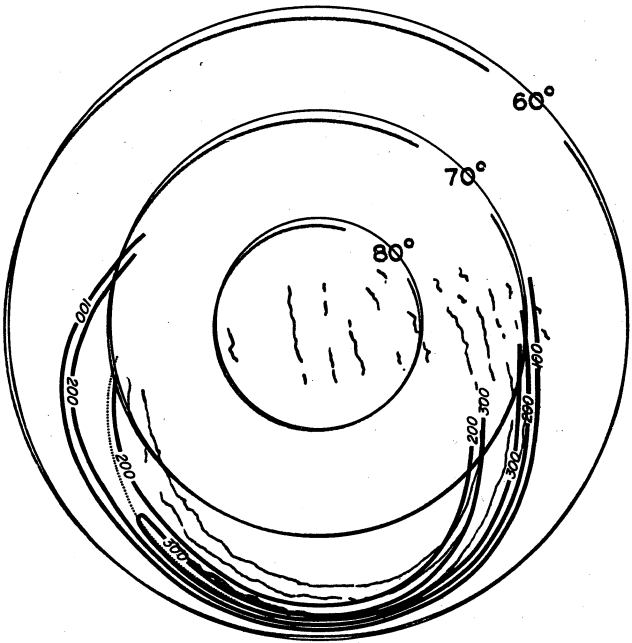

Figure 5.4 C The Poleward Expansion

During the early expansive stages of the substorm shown here in figures C and D, the location of equatorward portion of the hydrogen emission region remains largely the same. The poleward portion does expand and contains bright discrete arcs corresponding to the bright discrete auroral arcs which are found at this time.

The intensity contours of this figure indicate general intensities as high as 500 R. With discrete regions of emissions marked as lines corresponding to the auroral features indicated on the Akasofu diagram. Actually, on the night scaled H-beta intensities corrected for all possible sources of contamination were somewhat higher. For the sake of clarity only the east and west portions of the 400 and 500 R contours have been shown.

Note that the dotted line denoting the boundary between pure proton precipitation and mixed electron and proton precipitation has moved equatorward in the evening sector to indicate that in the late evening sector, the entire hydrogen arc is electron contaminated. This is the beginning of electron-proton "cross-over".

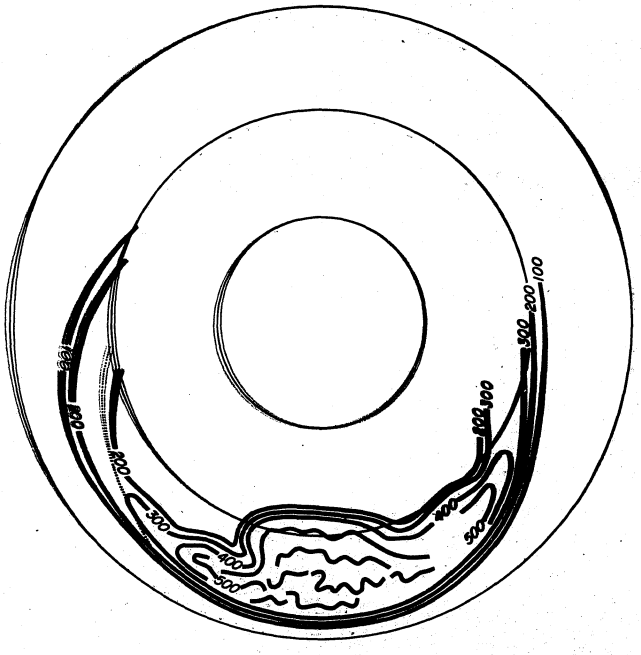

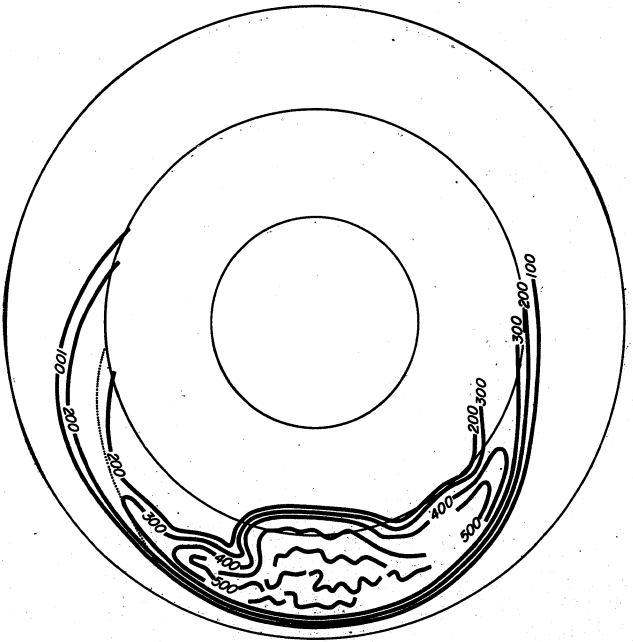

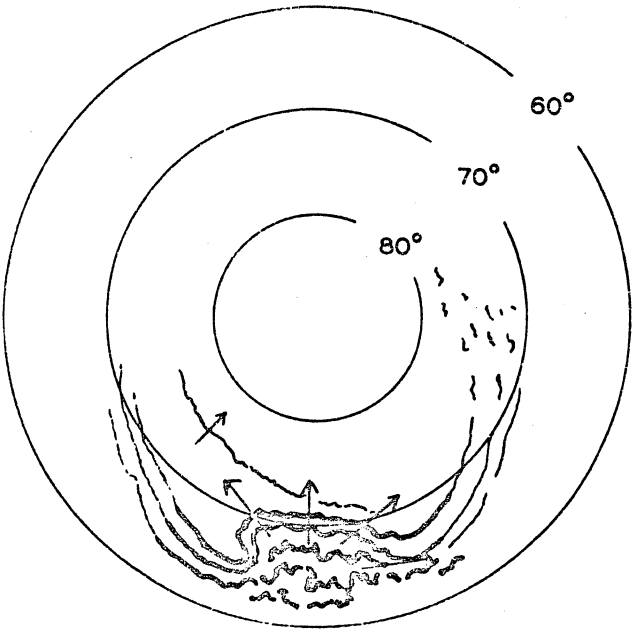

T=5~10 MIN

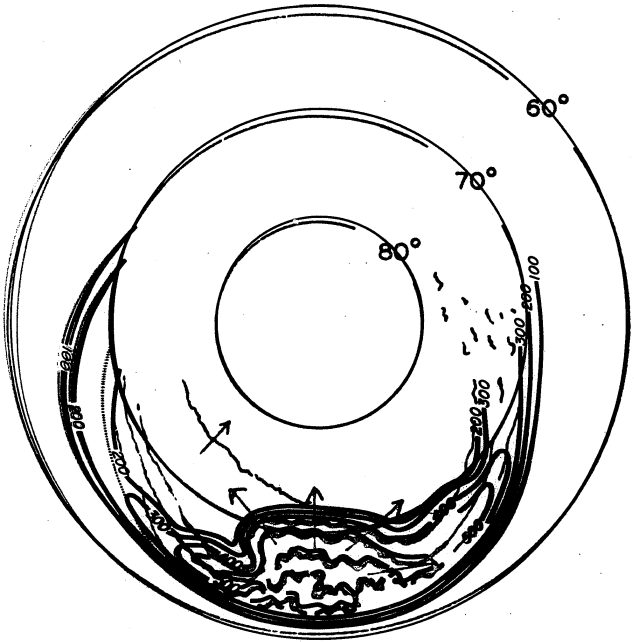

T=5~10 MIN

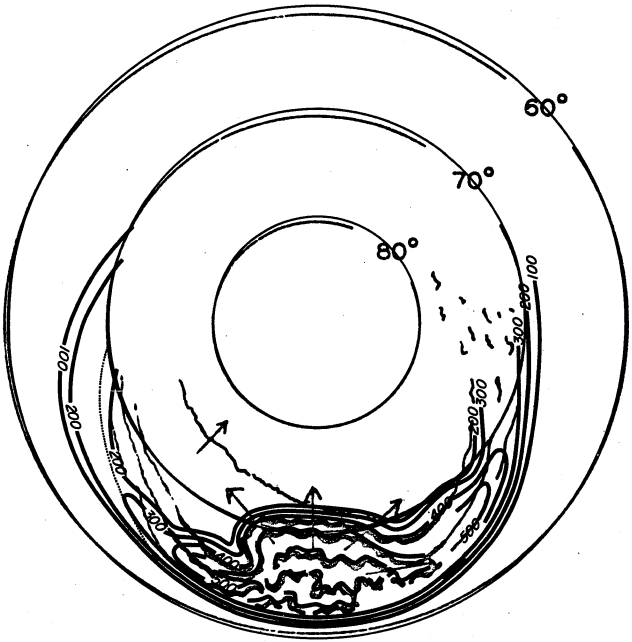

T=5~10 MIN

Figure 5.4 D The Poleward Motion of the Hydrogen Region

Approximately 30 minutes after the substorm onset the poleward expansion phase of the substorm is well underway and the region of hydrogen emission begins to move poleward. In the region equatorward of the hydrogen emission are electron-produced patches and arc segments. The dotted line denoting the boundary between pure proton precipitation and mixed electron and proton precipitation has moved slightly westward. Here again bright, discrete regions of H-beta corresponding to discrete electron arcs are shown as solid lines. A single contour open polewards indicates the region where H-beta intensities are > 300 R above background. No hydrogen data are shown above 74° because of the limitation of coverage.

Particular attention has been given to the behavior of hydrogen emission in the region of the bright wavy omega band shown in the morning sector of the Akasofu diagram. The solid contour lines indicate intensities as shown on the intensity plots. However, on the basis of section 6.1, it is believed that the small amount of H-beta observed at this time is produced entirely by electron excitation of atmospheric hydrogen. The dashed H-beta contours for this sector show what is the true region of proton precipitation in this sector.

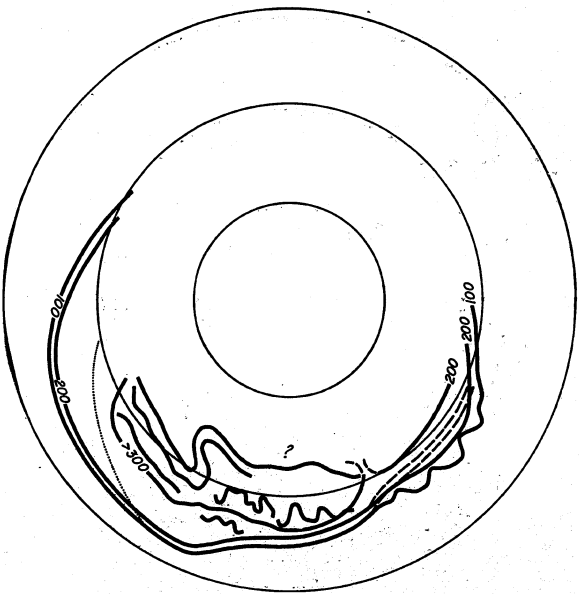

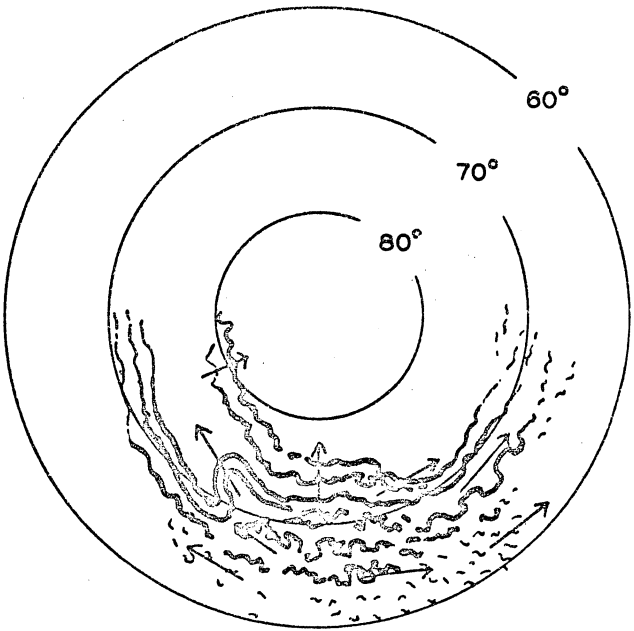

T=10~30 MIN

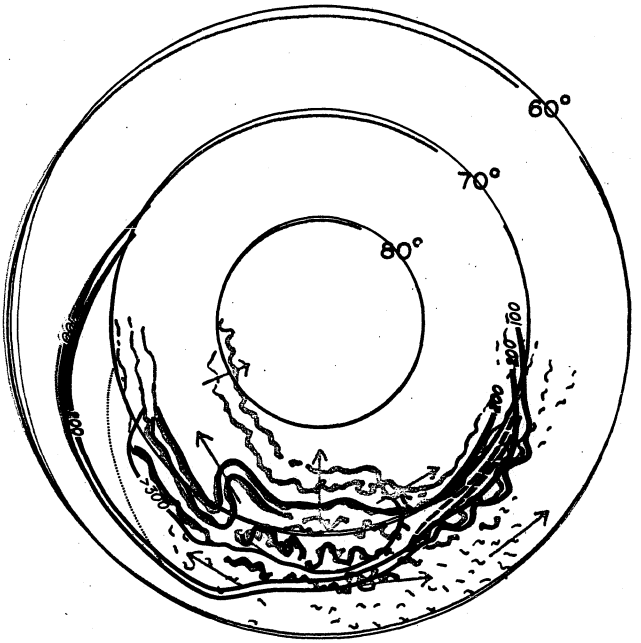

T=10~30 MIN

Figure 5.4 E Maximum Poleward Expansion

This figure represents the time of maximum poleward motion of hydrogen emission. The region equatorward of the hydrogen emission contains eastward drifting patches. The evening sector of the hydrogen region begins to closely approximate the quiet time configuration and intensity. However, the region of electron contamination of the hydrogen arc has reached a maximum and does not represent quiet conditions.

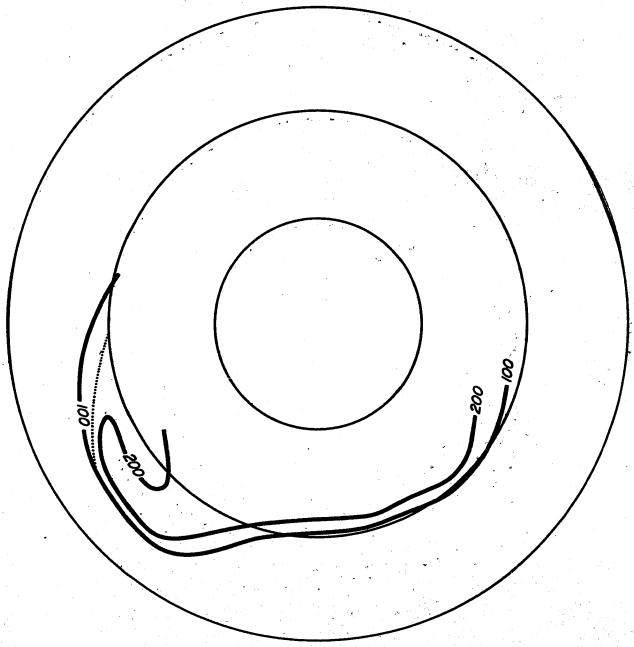

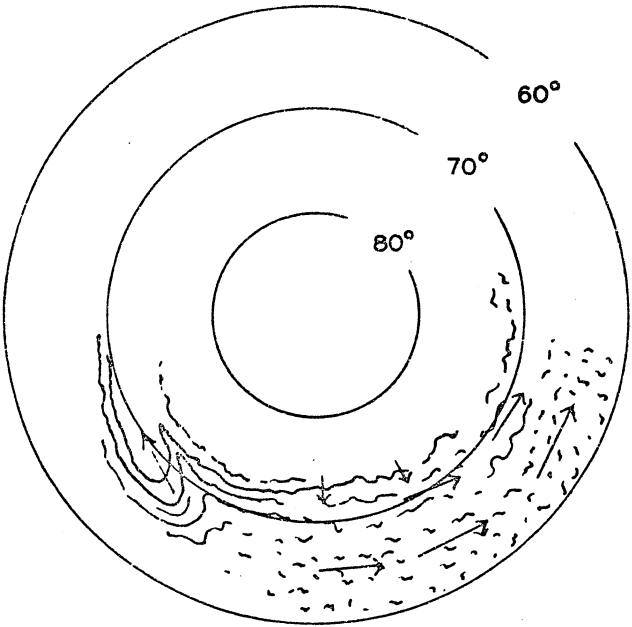

T=30 MIN~1 HR

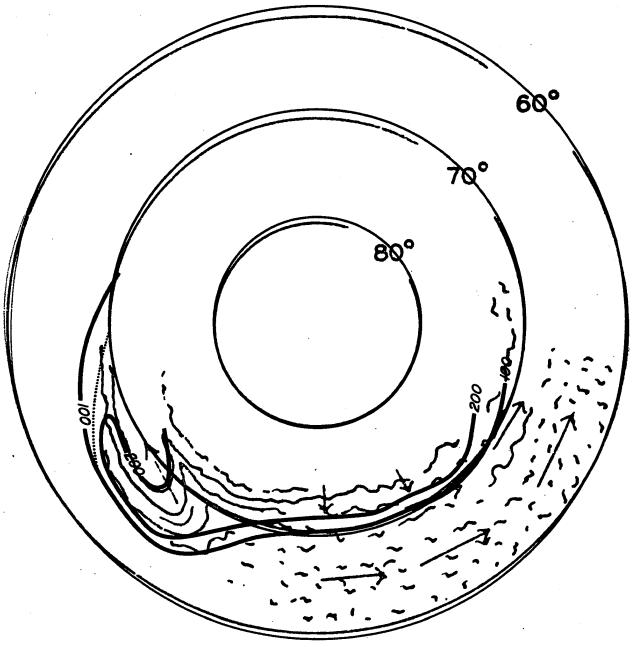

T=30 MIN~1 HR

Figure 5.4 F Beginning of Recovery Phase

The substorm configuration for this time was obtained by slightly modifying the Akasofu drawing shown for the maximum expansion configuration. The purpose of this additional detail is to illustrate the return of hydrogen emission to lower latitudes, which is a significant feature at this time.

In this drawing patches are located equatorward of the region of hydrogen emission. The equatorward motion of the hydrogen region is accompanied by many broad parallel auroral bands as described in section 5. These are shown here as dark lines just equatorward of hydrogen emission in the midnight and early morning sectors.

At this time the region of pure proton precipitation in the evening sector expands polewards as shown by the light dotted line.

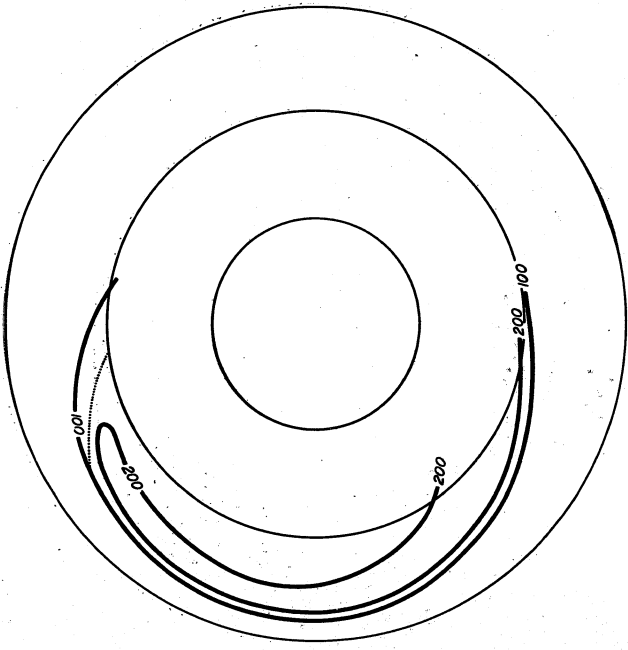

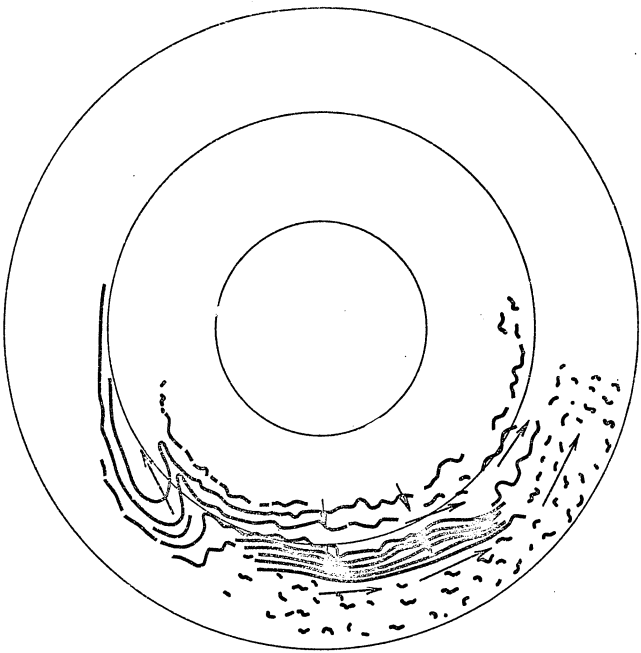

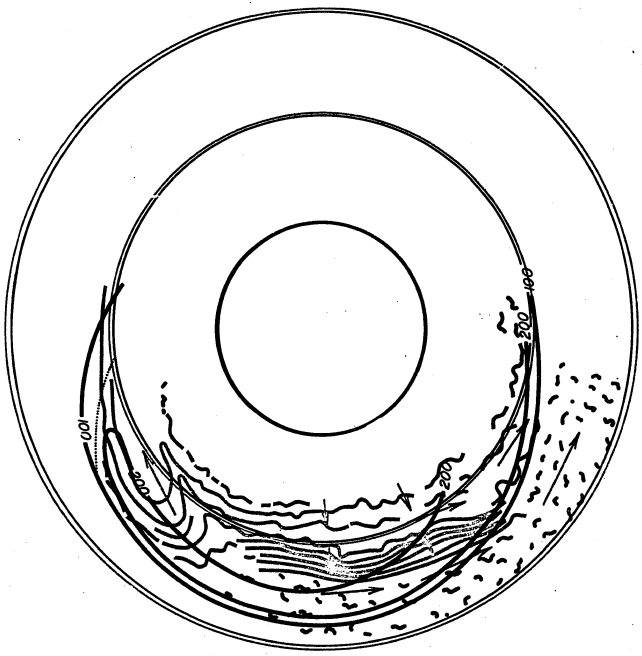

Figure 5.4 G End of Recovery Phase

By this time the aurora has almost completely returned to its quiet time configuration. The region of pure proton precipitation in the hydrogen arc has begun to expand in the evening sector, and the hydrogen region has regained its position on the equatorward edge of the auroral oval.

The hydrogen region shown here is broad and of low to moderate intensity. The many broad parallel bands of figure F have migrated equatorward with the hydrogen region and formed a broad striated arc which contains the zone of maximum hydrogen emission.

During the next half-hour to two hour period, many rayed arcs move equatorwards from higher latitudes as shown by the arrows on the Akasofu diagram. The maximum hydrogen intensity increases and the width of > 50% peak intensity narrows.

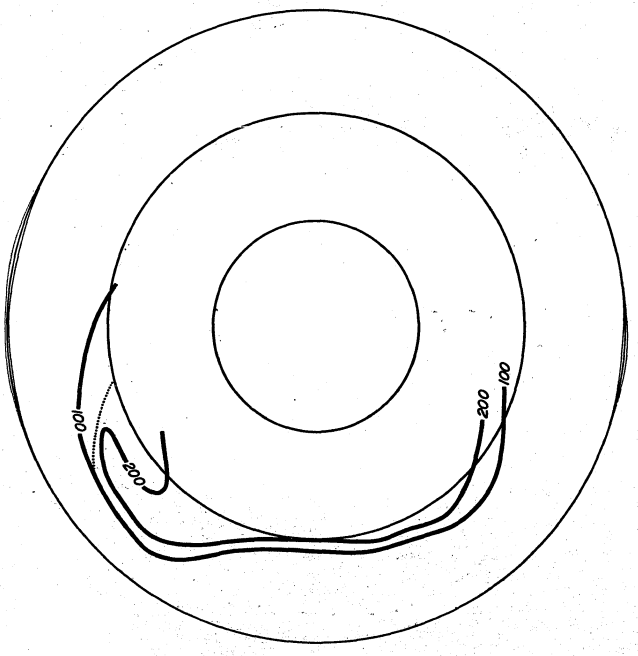

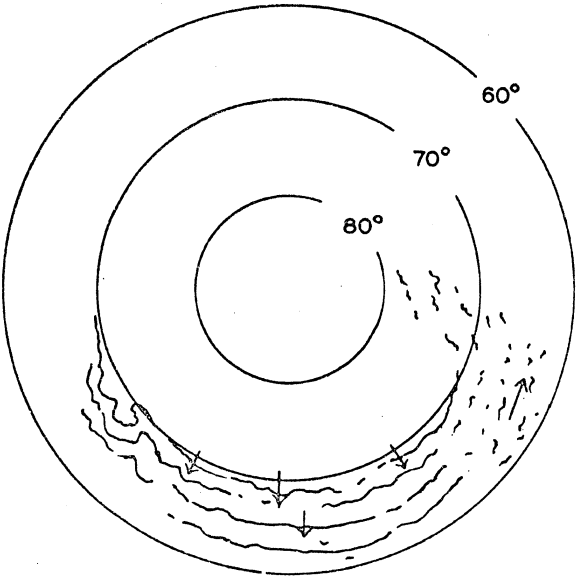

T=1~2 HR

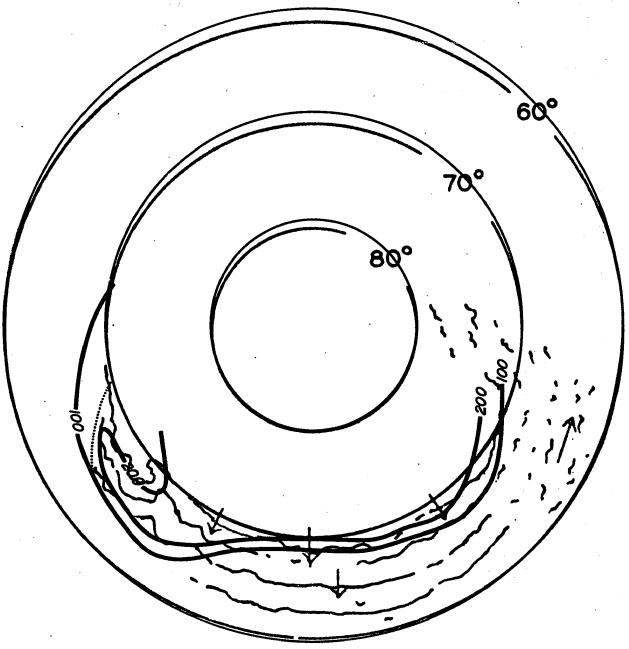

5.13.2 Interpretation: electron-proton "cross-over"

It seems clear that during the time T + 30 to about T + 90 during substorms, there is a true crossing of hydrogen peak emission to a location polewards of the peak of electron-produced emission in the midnight-to-dawn sector of the auroral oval. It also seems clear that during quiet times the two regions, while separate in the evening sector, merge in the midnight-to-dawn sector. Hence, a statistical average over all times would show a cross-over.

A quiet-time auroral model needs only to explain charge separation in the evening sector. While a substorm-time model must explain the charge separation cross-over. The fact that patches occur equatorward of the proton region following a substorm has been known and "re-discovered" for some time. This may be significant and should be investigated.

In Chapters IV and V charge balance in precipitating particles has been discussed at various points. Charge balance may or may not play a major role in the origin of the sudden brightening of an auroral arc signaling the onset of a substorm. However, the sudden brightening always takes place just poleward of the region of maximum proton precipitation.

Future research should probably concentrate in detail on the few minutes surrounding the sudden brightening of the "breakup" arc. The short duration of this period makes it particularly hard to study, yet any successful substorm theory must explain this period.

CHAPTER VI

The Interpretation of Some Features of Auroral Hydrogen Emission

6.1 Discrete Regions of H-beta Emission

Ever since the discovery of doppler-broadened hydrogen emission profiles in auroral spectra the temptation has been great to ascribe all hydrogen emission observed in the aurora as that due to incoming energetic protons. While this is probably valid in general, there may be exceptional cases.

Very soon after the operation of meridian scanning photometers began and oscilloscope films were available for viewing H-beta and OI 5577 Å, it was noticed that coincident with very bright (>100 KR), narrow regions of OI 5577 Å there was a narrow, bright (≈1 KR) region of H-beta (see figure 5.3, subfigures 4a, b, c).

One possibility is contamination of the photometric signal due to other auroral emissions. The conclusion of Chapter III is that there is no contaminant or combination of contaminants bright enough to create this effect.

Another possibility is that protons of very hard characteristic energy (100 kev), steep ($>\sin^{-1}$) pitch angle distribution, or a combination of both are precipitated coincidently with the electrons in the narrow bright arc.

Figure 6.1 shows sequential H-beta and N_2^+ 4278 scans of such an arc which occurred overhead during the evening of October 11, 1969. The author was observing the arc visually when the measurement was made. The arc was very active and rayed. The photometer producing the data for figure 6.1 is one of a generation of photometers produced after the MSP.

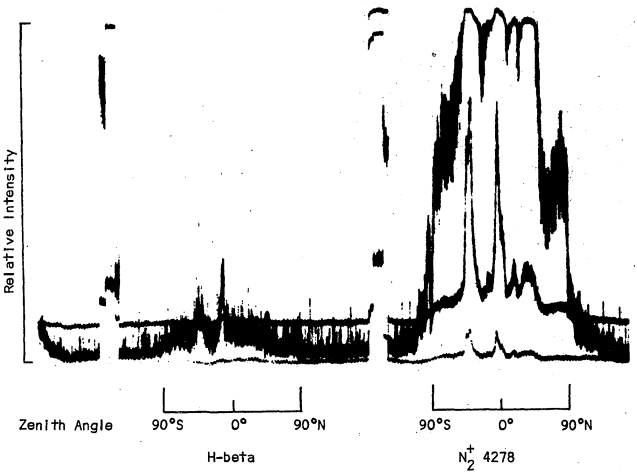

Fig. 6.1 Horizon-to-horizon photometric scan in H-beta (left) and N_2^+ 4278 (right) obtained at College near local midnight, Oct. 29, 1970. The photometer output is displayed in three linear gains for each emission. The narrow, bright region of H-beta shows a deflection of .75 inch on the most sensitive gain while N_2^+ 4278 shows a deflection of 2.5 inches on the next highest gain. Hence the ratio of N_2^+ 4278 to H-beta is approximately 30 to 1.

The trace amplitudes are linear, several decades of response being displayed simultaneously. However, to achieve this linear recording, the different wavelengths were observed sequentially. Hence there is a time lapse between observations. This operation was performed by rotating a wheel containing the various pass-band filters in front of a single photomultiplier. An additional benefit of this arrangement is that intensities can be compared directly for ratio measurements without the necessity of absolute calibration that different photomultipliers for each wavelength require.

The narrow H-beta arc shown in figure 6.1 has a half-intensity width of approximately 10 km. The half-intensity width of the N_2^+ 4278 emission is also approximately 10 km. Individual features of the arc were much smaller than this but the arc was moving rapidly, highly folded (rayed) and the field of view of the photometer is around 3 km at auroral altitudes. Hence individual features of the arc were very likely blurred together to produce the 10 km overall width.

The gyro radius of a 100 kev proton is approximately 1 km. If the proton precipitation pattern within the arc is structured, then very little spreading has taken place. At the most, with protons being injected in the center of the observed arc, an average spreading of 5 km to each side of the injection has taken place. This result very likely requires a combination of high energy and steep pitch angle distribution.

Generally speaking, it is the mean free path for re-ionization at the altitude that most protons first neutralize that determines the order of magnitude of proton-spreading in the hydrogen arc. Reference

to Table I.I shows that for 5 kev protons, at 500 km the mean free path for neutralization, (490 km), is nearly the same as the altitude. By the time the proton has reached 400 km, the mean free path is 98 km, or the distance to the 300 km level where the mean free path is 19 km. It is apparent that most of the incoming protons will not charge exchange before reaching 400 km but most will have charge exchanged by a short distance below that level. The mean free path for reionization changes from 2000 km at 400 km to 300 km at 300 km altitude. It is principally the mean free path for reionization in this region that determines the width of the 5 kev proton arc.

Using a similar argument, it appears that for 100 kev protons, most incoming protons will originally neutralize at an altitude between 300 and 200 km. The order of magnitude for reionization of 100 kev hydrogen atoms at that altitude is on the order of tens of kilometers.

It is emphasized that, even with an isotropic pitch angle distribution, very few neutralized protons travel horizontally. Since the neutrals follow a trajectory determined by their pitch angle, they tend to spread less than the mean free path for reionization because 1) only part of the motion is horizontal and more importantly 2) the vertical component carries the atoms to lower altitudes and thereby greatly enhances the probability of reionization.

Comparison of Davidson's plotted intensity distributions, figures 1.3 and 1.4, with the table of mean free paths indicates that 100 kev protons with isotropic pitch angles spread too much to produce an arc as narrow as reported here. Either the energy must be greater than

100 kev (and limited to high energy protons) or the pitch angle distribution must be "steeper" than $\sin^{-1}\alpha$.

These narrow regions of H-beta emission only arise when electron-induced emissions are quite bright (5577 OI $\sim$ 100 KR) at times during and just after "break up". Study of the oscilloscope films shows that as the narrow electron arcs develop, rising out of the auroral background, the narrow H-beta regions only appear and grow after what appears to be a "threshold" intensity of the electron-induced emission. The narrow H-beta arcs show no tendency to change in width as one might expect if an originally "soft" energy spectrum changed into a "hard" spectrum. Nor do they show any horizontal displacement from the N_2^+ 4278 emission under static or dynamic conditions - even when the arc is moving so quickly in a north-south direction that the OI 5577 Å emission peak trails that of the N_2^+ 4278 Å due to the half-second lifetime of the "forbidden" transition producing OI 5577.

Figure 6.2 was prepared by G. J. Romick. This figure represents a detailed scaling as a function of zenith angle the narrow H-beta region shown in figure 5.3, subfigures 4b and 4c. The narrowest region occurred just after 4b and is best represented in part 4c. In figure 6.2, H-beta, 5577 OI and N_2 6704 are plotted against N_2^+ 4278. The fact that all three emissions maximize at the peak intensity of N_2^+ 4278 indicates that all these emissions peak at the same zenith angle from the photometer. Additionally, the fact that no horizontal displacement of enhanced H-beta regions has ever been seen when these bright arcs are directly overhead indicates that the obviously electron-induced emissions peak in intensity at the same altitude as the hydrogen emission. It seems

Fig. 6.2 Scalings in relative intensity of 6704 (N_2), 5577 [OI] and H-beta against 4278 (N_2^+) of the bright arc in figure 4.3, parts 4b and 4c. Arrows indicate sequence of scalings from bottom of arc through peak emission to high altitude portions of arc.

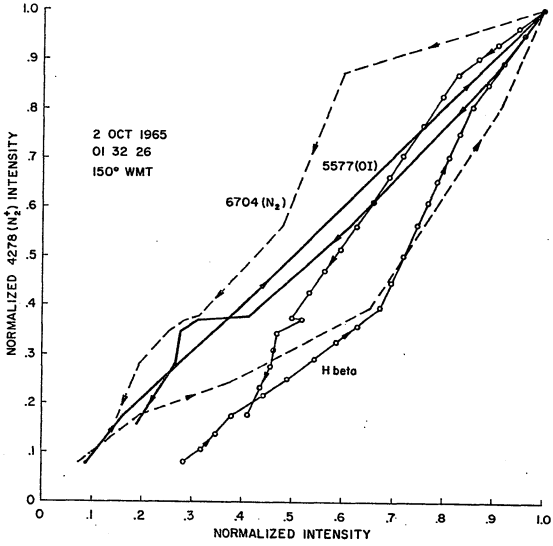

strange indeed that the production of H-beta due to high energy protons maximizes at the same altitude as emissions due to energetic electrons.

The details of the behavior pattern of these discrete H-beta regions seems to rule out their production by energetic injected protons, unless many fortuitous circumstances combine to produce the behavior pattern observed. This possibility again raises the spectre of photometric or emission contamination. However, there remains yet another possibility to explore: excitation of atmospheric hydrogen due to energetic electrons.

6.2. Possible Intensities of H-beta Resulting from Excitation of Atmospheric Atomic Hydrogen by Energetic Electrons Penetrating to Low Altitudes.

6.2.1 Introduction

This exposition is intended to show that it is at least possible that the narrow regions of H-beta emission under discussion here can be due to energetic auroral electrons penetrating to low altitudes. While admittedly speculative in nature, this explanation of narrow H-beta arcs appear worthy of serious consideration.

6.2.2 Hydrogen concentration

Various authors, (Bates and Nicolet, 1950; Bowman, et al., 1970) have indicated rather large atomic hydrogen densities (10^{10}, 10^{9} /cm^{3}) at altitudes near 80 km, (see figure 6.3) and densities diminishing for higher and lower altitudes. These figures represent estimates based on calculations solving diffusion and continuity equations. Direct measurements by means of mass spectrometer are very difficult at these altitudes.

6.2.3 The excitation of H-beta by collisions of electrons on atomic hydrogen

H-beta production cross section

Figure 6.4 shows the differential cross section for H-alpha production due to electron bombardment (Kieffer, 1969). Except for the spike near

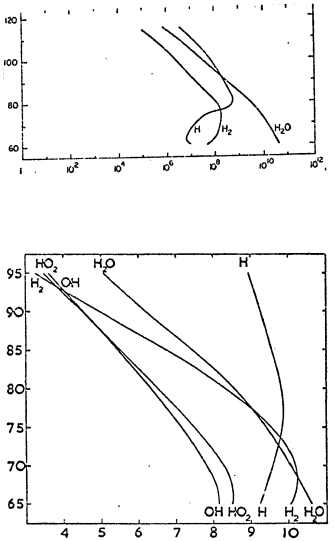

Fig. 6.3 Estimated densities of atmospheric hydrogen from Bates and Nicolet, 1950, (top) and Bowman et. al., 1970 (bottom).

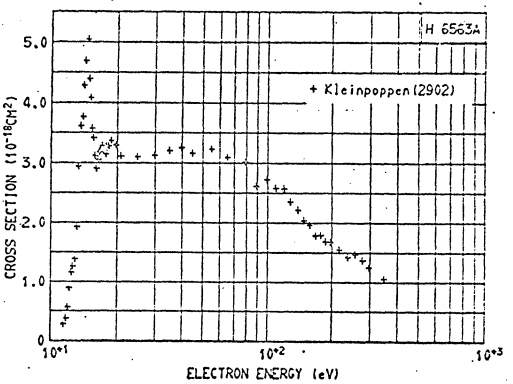

Fig. 6.4 Differential cross section for H-alpha production due to electron bombardment. (Kieffer, 1969).

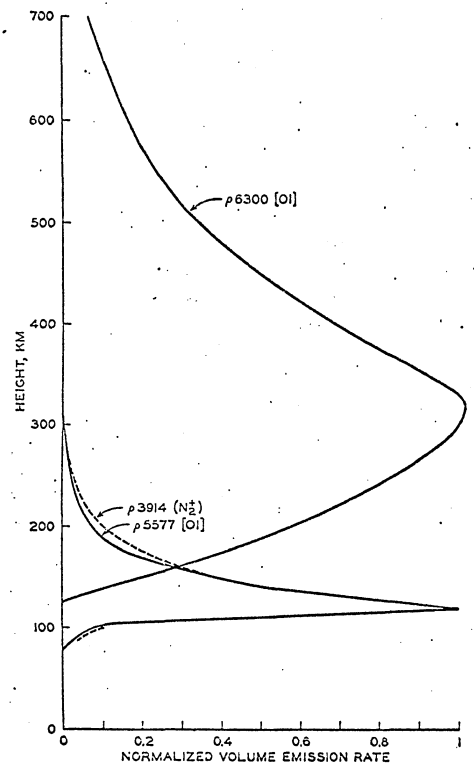

Fig. 6.5 Profile showing normalized volume emission rate of λ 5577 [OI], λ 6300 [OI] and λ 3914 (N_2^+) versus altitude for a narrow auroral arc with peak emission at 110 km and lower border at 100 km altitude. (Romick and Belon, 1967).

15 ev, this cross section is generally uniform at 3×10^{-18} cm^2 to energies as high as 100 ev. It then drops off for higher energies. The observed H-beta/H-alpha ratio in the aurora is roughly 1/3, giving an approximation for the H-beta production cross section a value of 1×10^{-18} cm^2 from 15 to 100 ev.

6.2.4 The thickness of the H-beta producing region.

In order to estimate the number of hydrogen atoms excited by electrons, it is necessary to estimate the depth of the column within which the electrons possess energies sufficient for H-beta production. If, for the purpose of a lower estimate of H-beta production, the differential cross section for H-beta production by electrons with energies from 15 to 100 ev is used, then the assumption is implicitly made that every electron-hydrogen atom encounter within that column has that cross section. All energetic electrons must degrade through this energy range. If electrons of higher energy are ignored, then part of the total precipitation column where the electrons possess these higher energies must also be ignored. In arriving at a first approximation to the depth of the atmospheric layer in which electrons have energies of this magnitude, note the following.

Romick and Belon (1964) have shown that for a narrow arc with peak emission near 110 km and lower border near 100 km (such as the arcs under discussion here) that the depth of the emission vs. height profile at 50% peak emission is near 30 km for both λ5577 and λ3914 (see figure 6.5).

The calculations here assume that the depth of the column in which electrons have their most efficient energies for hydrogen excitation is 1/3 this previous value or 10 km.

6.2.5 Electron flux

Belon, et. al, (1966) showed that for a vertical intensity of 30.6 KR of N_2^+ 3914 and a luminosity profile with lower border at 100 km and peak emission at 120 km, the corresponding electron flux is between 6.6 x 10^{10} and 1.2 x 10^{11} electrons /cm^2 sec. The magnitude of N_2^+ 4278 during the bright arc under consideration here (figure 3.1) varied from 50 to 80 KR for uncorrected H-beta intensities near 1.6 KR. Using the ratio of $\frac{3914}{4278} = 3$ and taking 50 KR for 4278, this corresponds to 150 KR 3914 or 5 times the value for the quiet stable arc measured by Belon, et. al. Taking 8 x 10^{10} e/cm^2 sec as the electron flux in the 30.6 KR (3914) arc the 150 KR arc would require an electron flux at 4 x 10^{11} electrons/cm^2 sec.

6.2.6 H-beta intensities produced

Denoting the atmospheric density by D, the number of photons emitted by a column of 1 cm^2 cross section and 10 km depth, is given by

$$\text{photons} = 10^6 \times 4 \times 10^{11} \times 1 \times 10^{-18} D = 4 \times 10^{-1} D$$

The calculated atmospheric hydrogen densities fall off to about 1/10 of its maximum value at 100 km. Hence D values from figure 6.3 range from 10^9 to 10^8 atoms /cm^3. These values yield from 40 to 400 rayleighs of H-beta emission for N_2^+ 4278 values near 50 KR.

Hence, it is possible to have a region of enhanced H-beta emission corresponding to a pure electron precipitation arc.

6.3 Possibilities Related to the Hydrogen Arc Near Break-up

There is an identifiable recurring feature of the spectral morphology which may be of significance in terms of particle processes related to substorm onset: It has been noted in Chapter V that at times near

onset, the proton arc has superimposed on its northern edge a broad electron arc.

The object of this section is to relate this stage of development of the hydrogen arc to measurements which have been made by rocket and satellite.

The similarity between the hydrogen arc at 2029 Jan 20/21 1966 and the hydrogen arc of 2209 Nov. 9, 1965 studied by Romick and Sharp (1967) has already been pointed out. Figure 6.6 shows schematically the results of their observations.

Recently Cloutier et al. (1970) have published results of rocket-borne measurements that may be related to this same auroral situation. From the description they give, it is very likely that the auroral arc involved in their measurements was a hydrogen arc in the configuration described above: the rocket was fired from Fort Churchill at 2000 L.T. over a homogeneous, stable, well-defined arc. This arc was the only one which had been observed before the time of firing and later it moved southward over zenith, and following a small magnetic bay, became structed and "split".

The rocket payload consisted of a vector magnetometer system and particle detectors. The results of their analysis are shown in figure 6.7. They concluded that: (1) The magnetic vector profile data could best be reproduced by a horizontal arc-aligned current (electrojet) combined with two equal anti-parallel geomagnetically aligned current sheets lying in planes parallel to the visible auroral arc. (2) The maximum flux of precipitated electrons was detected near the center of the observed visible arc, and the horizontal electrojet was roughly coincident with the region of precipitated electron flux. (3) The upward geomagnetically aligned sheet current inferred from the magnetometer data was approximately

Fig. 6.6 Schematic representation of satellite measurements of precipitating protons and electrons and simultaneous spectographic observations of H-alpha and λ 5577 [OI] at L.T. 2208 Nov. 9, 1966. (Romick and Sharp, 1967).

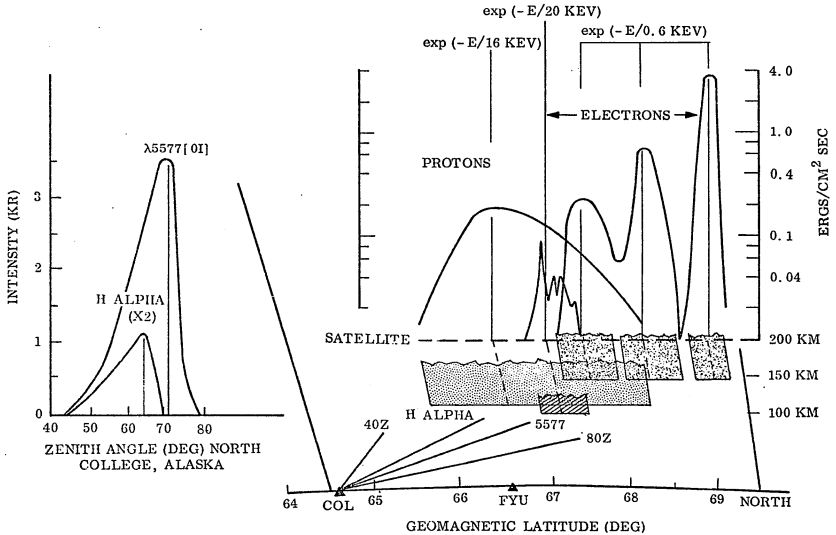

coincident with the detected precipitated electron current. (4) The precipitated electrons in the energy range from 2 to 18 kev represented a significant energetic particle flux, and were observed in the region of the downward (equatorward) current sheet inferred from magnetometer data.

Whereas the rocket in the latter experiment passed through the auroral form just above the altitude of peak emission, the satellite in fig. 6.6 crossed over the auroral zone at an altitude of approximately 200 km.

In order to relate these two observations, the following model has been constructed based on the Davidson picture of charge-exchange spreading of the proton beam. Figure 6.7 shows an idealized composite of the Romick and Sharp figure, the Cloutier figure, the intensity plots during this type of auroral situation, and the Davidson charge-exchange proton spreading added to which are proposed processes responsible for the Cloutier observations.

The principal Cloutier et. al. (1970) observation which demands explanation is the equatorward downward-directed current sheet which was not associated with energetic particles, either proton or electron. If the Davidson charge-exchange picture is correct then: (1) High above the atmosphere (500-600 km) there is a concentrated stream of incoming protons which later charge-exchange spread to create the proton arc. (2) Starting about 500 or 600 km this stream will begin to diminish due to charge exchange spreading. Below approximately 300 km, a) virtually all protons have charge-exchanged once, and b) spreading has ceased. (3) There will be a region below the 500-600 km level and above 300 km on the same magnetic field lines occupied by the incoming protons where electrons will be depleted due to the initial charge exchange reaction of the protons.

Fig. 6.7 (Top, right hand) Current distribution based on results of vector magnetometer flight (shown as curved line) above an auroral arc. (Cloutier, et. al., 1970).
(Center) Explanation of current distributions based on observed and inferred particle precipitation patterns. The Davidson (1965) charge-exchange spreading calculations have been used to produce hydrogen emission contours.
(Bottom) Predicted pattern of H-beta and N_2^+ 4278 auroral emissions resulting from particle precipitation patterns indicated.

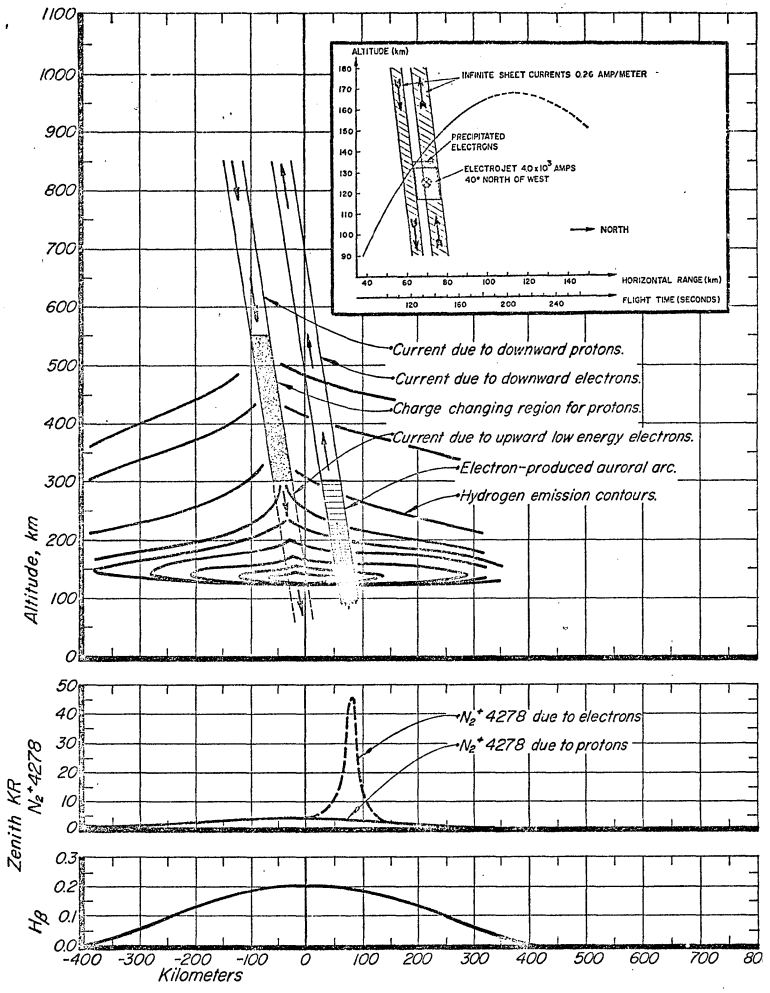

This region will be as narrow as the stream of incoming protons.

This positive space charge region will demand neutralization. It is postulated here that free ambient electrons would be drawn up the field lines from the ionosphere since the field lines are essentially conductors. The energy of the upward moving electrons would be too low to be measured as energetic particles. However, the current produced would be equal to the current of incoming protons above.

In order to check this possibility, the intensity of the H-beta emission produced will be calculated.

Cloutier, et. al. (1970) measured both low altitude sheet currents to be .26 amp/meter. By the postulates above, this would imply an incoming proton sheet current of the same magnitude. This reduces to a current of 1.6×10^{16} protons/E-W cm/second in the current sheet. The half-intensity width of the proton arc is nominally 250 km. If half the proton current sheet were spread uniformly over this width, the proton flux would be on the order of 3.2×10^{8} protons /cm^2/second.

Assuming that the proton energy spectrum is reasonably constant throughout the night and applying the conclusion from Chapter IV that the most reasonable spectral power for auroral protons is -2.4, we can extrapolate from tables 4.1 and 4.2 that a flux of $\sim 7 \times 10^{7}$ protons/cm^2 /sec would produce around 45R of H-beta if the energy spectrum cutoff were .5 kev. Under these conditions a flux of 3.2×10^{8} protons/cm^2/sec would create a H-beta intensity of 200 rayleighs. In Chapter V an intensity of 190 R was measured under these conditions.

CHAPTER VII

Conclusions and Areas for Future Study

The basic purpose of this thesis was to examine the relationship between proton and electron precipitation in auroral displays--particularly during periods of dynamic activity. However, there are many steps between measurement of light passed by an interference filter designed to detect light emitted by atomic hydrogen and interpretation of that signal in terms of precipitated protons. In the process of following these steps, many conclusions have been reached concerning the spectral purity of H-beta, its doppler profile, and the appearance of H-beta emission in the aurora. These have been discussed at the end of each of the previous chapters. Here the most important conclusions regarding hydrogen emissions in the aurora will be re-stated and broadened. Areas for future work will be pointed out.

Figures 5.4 A through 5.4 G represent what is felt to be a generalized picture of hydrogen emission during the dynamic auroral substorm. It is very possible that some of this hydrogen emission is not due to precipitating protons but atmospheric hydrogen excited by auroral electrons. The possibility of this is very great in omega bands. The further investigation of this possibility by means of high resolution (time and wavelength) H-beta profile measurements would certainly be useful.

The most interesting aspect of the conclusions represented by figures 5.4 A through 5.4 G is that regarding the manner in which hydrogen emission returns equatorward following a substorm. This appears to be the only time there is a true "cross over" of electron and proton precipitation. According to the description given by Cresswell (1968), this is the region of origin of fast auroral waves (when they occur). The rocket-

borne measurements discussed in Chapter IV were made in this region of the substorm. As illustrated in figure 5.4 F, there is a region where patches are being replaced by parallel bands as hydrogen emission returns equatorward. The boundaries seem to coincide. Examination of the College all-sky camera film taken during the Johnstone (1970) rocket measurements indicates that those measurements may have never been taken near such a transition zone. The results of Chapter IV showed that those measurements could indicate a neutral flux. There is the possibility that the broad striated (electron-contaminated) hydrogen arc which often forms after such occasions as described above results from a neutral or nearly neutral flux of protons and electrons.

It should be noted that this striated hydrogen arc is only the morning portion of the quiet hydrogen arc which appears to vary from pure proton precipitation in the dusk portion to a proton arc with an electron arc just poleward in the late evening sector. This latter situation was discussed in Chapter VI where some evidence for a neutral total flux was found.

The results of Chapter IV showed that large numbers of precipitated protons may have been undetected, thus due to the possibility of neutral total flux, it becomes imperative that the relationship of proton precipitation to the formation of stable, well defined auroral arcs be investigated.

The hydrogen arc appears to be a major feature of the pattern of auroral behavior. Perhaps if the processes responsible for its production were known, the substorm could be explained as a perturbation of, or resulting from, these processes. Certainly the substorm appears

to originate in the hydrogen arc, it is always present in auroral displays and it follows the most predictable behavior of all auroral features.

One promising area for future study would be the obtaining and analysis of hydrogen H-beta emission profiles. The possibility of excitation of atmospheric hydrogen needs serious study. It would be interesting to compare energy spectra derived from profile analyses with simultaneous particle measurements. Once the validity of the profile analysis method was established, profile measurements could monitor proton energies throughout the night.

The analysis begun here for comparison of emissions on a single night should be continued. The first step might be to plot OI 5577 along with H-beta and N_2^+ 4278. The ratio of OI 5577 to N_2^+ 4278 could yield information concerning the energy spectrum of precipitated electrons. In turn, once the electron spectrum is known, then that part of H-beta emission due to electron excitation of atmospheric hydrogen could be subtracted from the H-beta measurements.

Another area for study would be the few minutes immediately surrounding the sudden brightening in the hydrogen arc at break-up using simultaneous photometric and magnetospheric particle data.

APPENDIX A

Calibration of a photometer (for observation of an extended light source of discrete or broad-band emission) using a standard lamp (point source).

A.1 Introduction

Ultimately, all absolute photometric intensity calibrations lead back to a measurement of the light output of a standard (point source) lamp. In our case this standard lamp resides at the U.S. Bureau of Standards, Boulder, Colorado. Of course, photometric observations of the aurora concern observations of extended sources. (In fact, observers generally make the hopeful assumption that auroral intensity is uniform over their field of view.) The problem then, is to relate the absolute intensity of the light cast by a standard lamp at some given distance from that lamp to the surface brightness in photons/cm^2 steradian sec of an emitting region on the sky. The unit used in auroral intensity observations is the rayleigh which is one megaphoton/cm^2 (column) sec. The reader who is not familiar with this unit or the terminology of cm^2(column) is referred to Appendix II of Chamberlain: Physics of the Aurora and Airglow. It should be pointed out that the rayleigh is only a total surface brightness of the entire column or the total column emission rate and not a volume emission rate. The rayleigh permits unambiguous comparisons of observed auroral photometric intensities (with some tacit assumptions). The extension from surface brightness to volume emission rate involves either a great deal of calculation based on simultaneous observations from other locations or tremendous assumptions (see Romick and Belon, 1964). The rayleigh is, however, the

logical measurement unit with which to start to perform this extension.

Although nightly calibrations of the meridian scanning photometer system were made by means of full-field-of-view low brightness sources, the intensity calibrations are tied in with occasional observations of a standard lamp calibrated by the U.S. Bureau of Standards. This lamp was suspended from a tower 250' south of the photometer. The geometry was such that the standard lamp was observed against the sky and no ground or illuminated portion of the tower was in the field of view.

A.2 Units and Definitions

1 → $P_{(\lambda)}$ is the Lamp Power per square cm per Å measured at the photometer and given in microwatts/cm^2 Å;

2 → I_{B_λ} is the Lamp Power per square cm per 10 Å at distance d and operating current i as specified by the National Bureau of Standards in their calibration of the Lamp and is given in microwatts/cm^2 10 Å;

3 → $T_{(\lambda)}$ is the transmission of the filter as a function of wavelength;

4 → $T_{(\lambda_i)}$ is the transmission of the filter at wavelength λ_i;

5 → 10^{-6} watt = 1 microwatt = 10 erg/sec;

6 → $E = \int P_{(\lambda)} T_{(\lambda)} d\lambda$ = total power/cm^2 transmitted through filter band pass;

7 → x_i = number of quanta of λ_i per erg (from $w = hv_i = h\frac{c}{\lambda_i}$, $x_i = \frac{1}{w} = \frac{\lambda_i}{hc}$ where w is in ergs).

A.3 Relationships and Derivations

A.3.1 The definition of "B"

Now, $\frac{10E}{T_{\lambda_i}}$ is the equivalent monochromatic power/cm^2 in ergs/sec cm^2 at wavelength λ_i as measured outside the filter which would yield the same total power/cm^2, E, through the filter as the power/cm^2 A function $P(\lambda)$.

Hence $\frac{10E}{T_{\lambda_i}}$ = quanta/cm^2 sec at λ_i which would yield power/cm^2, E, through filter.

Now, for a field of view of Ω steradians, $\frac{10E}{T_{\lambda_i}} \frac{\chi_i}{\Omega}$ = B, the number of quanta / cm^2 sec steradian at the filter due to an extended source whose brightness integrated over Ω equals that of the standard lamp.

A.3.2 The relationship of B to the surface brightness of the extended source

Consider the following: if the photometer is moved to twice the distance from a source which fills the field of view at all distances considered, the amount of light falling on the filter surface due to that part of the surface formerly in the field of view is diminished by $\frac{1}{4}$. However, at the same time the total surface in the field of view is increased by a factor of 4. No matter where the photometer is located in relation to an extended uniform source at the same viewing angle, B will be the same. Hence B is the surface brightness.

A.3.3 The relationship of B to the column emission rate

Now B represents the number of quanta at the surface of a column per cm^2 per sec per steradian. The total number of quanta emanating per sec from that column is simply $4\pi B$. $4\pi B$ then has units of quanta per cm^2 (column) sec. The unit of one rayleigh, R, has been chosen to

represent this quantity: IR = 10^6 photons / cm^2 (column) sec. Obviously the volume emission rate of a column one cm long is the same as its column emission rate. Hence,

$$\text{volume emission rate} = \frac{4\pi \quad B}{\text{length of column}} = \frac{\text{photons}}{cm^3 \text{ sec}} .$$

A.3.4 Calibration for a monochromatic light source

What we want is the calculated value of $4\pi B$ at the front surface of the filter as a function of d, D (the distance from the lamp to the filter), Ω, x_i, $T_{(\lambda_i)}$ and I_{B_λ}. Hence

$$4\pi B = 4\pi \frac{10\ E}{T_{(\lambda_i)}} \frac{x_i}{\Omega} = \frac{40\pi(\int P_{(\lambda)} T_{(\lambda)} d\lambda)\ x_i}{T_{(\lambda_i)}\ \Omega}$$

However,

$$P_{(\lambda)} = \frac{I_{B_\lambda}}{10} \frac{d^2}{D^2}$$

so that

$$4\pi B = \frac{4\pi x_i}{T_{(\lambda_i)} \Omega} \frac{d^2}{D^2} \int I_{B_\lambda} T_{(\lambda)}\ d\lambda$$

This is the equivalent surface brightness of an extended source at wavelength λ, which covers the field of view of the photometer. This equation would be used for determining the intensity of a monochromatic light source.

A.3.5 Calibration for a light source with an emission profile

Since the $H_{(\lambda)}$ line is broader than the filters used, this problem reduces to determining the fraction of the total H-beta intensity measured by the photometer: given $H_{(\lambda)}$, the normalized relative intensity for the H-beta profile, we have

$$\frac{\int H_{(\lambda)} T_{(\lambda)}\, d\lambda}{\int H_{(\lambda)}\, d\lambda} = \tau$$

the fraction of the H-beta profile transmitted by the filter.

If we call Δ_H the current deflection obtained when observing hydrogen emission, Δ_H then represents τ of the true total profile intensity, I_H.

Calling Δ_λ the current obtained when observing the lamp with the filter, we have

$$10 \int P_{(\lambda)} T_{(\lambda)}\, d\lambda = 10E = \text{power/cm}^2 \text{ passing through filter in ergs/sec cm}^2.$$

Then,

$$\frac{\Delta_H}{\Delta_\lambda} = \frac{\tau(\text{times the total profile intensity})}{(\text{the lamp intensity})} = \frac{\tau I_H}{10E}$$

or

$$\frac{\Delta_H}{\Delta_L} = \frac{\left(\frac{\int H_{(\lambda)} T_{(\lambda)}\, d\lambda}{\int H_{(\lambda)}\, d\lambda}\right) I_H}{10 \int P_{(\lambda)} T_{(\lambda)}\, d\lambda}$$

or

$$I_H = 10 \frac{\Delta_H}{\Delta_\lambda} \frac{\int P_{(\lambda)} T_{(\lambda)}\, d\lambda}{\left(\frac{\int H_{(\lambda)} T_{(\lambda)}\, d\lambda}{\int H_{(\lambda)}\, d\lambda}\right)} \quad \text{in ergs/cm}^2 \text{ sec}$$

To obtain kilorayleighs we multiply by x_i (using the average value of the filter) and divide by Ω, the field of view of the photometer in steradians. Hence

$$\frac{4\pi 10^{-9} I_H x_i}{\Omega} = \text{kilorayleighs} =$$

$$\frac{4\pi 10^{-8} x_i \frac{\Delta_H}{\Delta_T}}{\Omega} \quad \frac{\int P_{(\lambda)} T_{(\lambda)} \, d\lambda}{\left(\frac{\int H_{(\lambda)} T_{(\lambda)} d\lambda}{\int H_{(\lambda)} \, d\lambda} \right)}$$

since

$$P_{(\lambda)} = \frac{I B_\lambda}{10} \frac{d^2}{D^2}$$

$$\text{kilorayleighs} = \frac{4\pi \times 10^{-9} d^2 x_i \frac{\Delta_H}{\Delta_\lambda}}{\Omega D^2} \quad \frac{\int I B_{(\lambda)} T_{(\lambda)} \, d\lambda}{\left(\frac{\int H_{(\lambda)} T_{(\lambda)} \, d\lambda}{\int H_{(\lambda)} \, d\lambda} \right)}$$

APPENDIX B

The relationship between intensity and flux and pitch angle distributions

Because there is a general confusion in the literature concerning the use of the terms "intensity" and "flux", an effort will be made here to define them. For background information, the reader is referred to pages 36, 258 and 342 of Chamberlain, "Physics of the Aurora and Airglow."

"Intensity" in particle measurements refers to the number of particles crossing a unit area per second from a unit solid angle where the unit area is oriented perpendicularly to the direction of the center of the unit solid angle.

"Flux" in particle measurements refers to the (net) number of particles entering the atmosphere per second, per unit area where the unit area is parallel to the earth.

Now, where intensity is denoted $n(\theta)$ we can see that the flux, N, is equal to

$$N = \int n(\theta) \cos\theta \, d\Omega = \int_{\pi}^{2\pi} \int n(\theta) \cos\theta \sin\theta \, d\theta d\phi$$

(In the case of particles spiraling around magnetic field lines it is often approximated that the field lines are perpendicular to the earth. θ and ϕ are the ordinary spherical polar azimuth and elevation angles where $\phi = 90°$ is the direction of a radial from the earth's center. In this way $n(\theta)$ is axially symmetric.)

From the definition of N, it is possible to define an intermediate term, $N(\theta) = n(\theta) \cos\theta$ which has been called the "flux per steradian."

Note that because of the cosine factor this quantity represents the number of particles per second passing through a unit area parallel to the earth from some given unit solid angle.

Often, "intensity" has been called "flux" and a particle intensity which is independent of unit solid angle has been called an "isotropic flux". Actually this term is meaningless. The term "isotropic flux per steradian" does have a meaning and is related to intensity by $\cos\theta$ as stated above.

The question arises as to which of the two quantities, "intensity" and "flux per steradian" has the more meaningful significance. Particle measurements by rocket and satellite measure "intensity" directly and usually report this quantity (often calling it "flux"). Obviously "intensity" is a measure of what particles are doing on space. However, "intensity" does not relate directly to the fraction of precipitating particles coming from a given steradian. This quantity is "flux per steradian".

Furthermore, if one wishes to determine the total percentage of precipitating particles with a given pitch angle, it is necessary to sum "flux per steradian" over the differential area of the unit sphere at a given pitch angle, θ.

Hence, flux per pitch angle $= \int_0^{2\pi} n(\theta)\cos\theta\sin\theta \, d\phi = 2\pi n(\theta)\cos\theta\sin\theta$. This quantity should be normalized to give the percentage flux per pitch angle, a quantity we shall here denote $F(\theta)$

$$F(\theta) = \frac{n(\theta)\cos\theta\sin\theta}{\int_0^{\pi} n(\theta)\cos\theta\sin\theta d\theta}$$

This later quantity represents what is probably the most meaningful term to use to relate pitch angles and number distributions of precipitating particles.

APPENDIX C

Photon statistics for the meridian scanning photometer system measurements of H-beta intensities

The MSP system utilized RCA 7265 photomultiplyers which had been chosen on the basis of high gain and low cost. Foord, Jones, Oliver and Pike (1969) evaluated several photomultiplyers including, the 7265 and concluded that the 7265 was rather poor in several respects which made it suitable for photon counting. However, in the MSP, the analog signal was used.

The 7265 utilizes an S-20 response cathode which is approximately 15% efficient in producing photoelectrons at λ 4861 Å (RCA). Foord et. al. claims that of these photoelectrons only 36% cause a cascade through the dynode chain to produce a current pulse. The overall quantum-counting efficiency, α is the product of these quantities. The value of α obtained from the above quantities is 5%. Foord, et. al. claim that in practice the maximum value of α = 1.7% is obtained at 2.7 kv across the tube. For the sake of calculations here we shall take $\alpha = 3 \pm 1\%$.

The product of the H-beta filter and H-beta line profile indicates that only 20% of H-beta photons are passed through the filter. The uncertainty in this figure is probably on the order of 17%. T=20±3%.

The filter area is approximately 48 cm^2 and response is rather flat across the field of view.

The field of view of the scanning photometer is 5.4×10^{-4} strad.

One rayleigh equals 10^6 photons/column/cm^2/second and equals $4\pi B$ where B is the surface brightness of the column/cm^2 per steradian.

The photons per rayleigh (R) collected by the photometer equals

$$\frac{\Omega \times 10^{6}}{4\pi} = \frac{5.4\times10^{-4}}{12.6}\times10^{6} = 4.3\times10^{-5}\times10^{6} = 4.3\times10^{1} \text{ photons/R/cm}^2\text{/sec}$$

Multiplying by the photometer area yields $\sim 2.1\times10^{3}$ photons/R/sec

Multiplying by the filter transmission yields 4.2×10^{2} photons/R/sec

Multiplying by α yields $1.2\times10^{3}10\times10^{-2} = 1.2\times10^{1}$ photons/R/sec

The MSP scanned 180° in 1 sec hence $\frac{1.2\times10^{1}}{1.8\times10^{2}}$ yields

.07 photoelectron pulses per degree of scan per R.

Analog signal

Foord, et. al. state that the 7265 has a gain of $.25\times10^{7}$ while RCA claims that it is 2×10^{7}.

$$1.2\times10^{1}\times2\times10^{7} = 2.4\times10^{8} \text{ electrons/R/sec} = \frac{2.4}{6.2} \times 10^{-10} \simeq 4\times10^{-11} \text{ amp/R}$$

The minimum detectable signal is believed to be $\sim$ 50 R which would be equivalent to 2×10^{-9} amp. Hence, 1 kR would yield a current of 4×10^{-8} amp. This generally agrees with experience. The dark current claimed by RCA is on the order of 10^{-8} amp.

Statistical Variation

The total short circuit current fluctuations will be given by

$$\delta i^2 = \frac{ei}{\tau}$$

where: e is the charge/anode pulse
i is the average current
τ is the transit time

For photomultipliers the transit time is characteristically 4×10^{-8} sec.

For 500 R the average current will be 2×10^{-8} amps

The charge/anode pulse will be $2 \times 10^{7}/6.2 \times 10^{-18}$ amp

Hence

$$\delta i^2 = \frac{2\times10^{-7}\times2\times10^{-8}}{6.2\times10^{18}\times4\times10^{-8}} = 1.6\times10^{-12} \text{ amp}$$

$$\delta i^{2\ 1/2} \simeq 1.3 \times 10^{-6} \text{ amp}$$

This is the average rms variation per photon cascade. At 500 R, there are 17 photons per degree of scan. Usually a time constant is used which corresponds to approximately a 5 degree running average. The data used here was summed for each degree over 3 scans. With such an integrating technique, over the long run the variation per degree would represent the average of the variations due to all the pulses. This would be $\frac{1.3}{250} \times 10^{-6}$ amp $.5 \times 10^{-8}$ amp or 25% of the signal. This agrees with experience.

Pulse Height Distribution

Another source of noise in photomultiplyer signals is the distribution of signal pulses collected at the anode corresponding to the emission of a single photoelectron at the cathode. In general, we would expect a poisson distribution broadened proportionally to the square root * of the number of times that the distribution is repeated i.e. the number of dynodes. In this way one would expect a photomultiplier with a large number of dynodes - like the 7265, with fourteen, to produce a large rather flat pulse-height distribution. The effect of the pulse-height distributions combined with the statistical variation due to random arrival times of photons would be to increase the noise level. The rise time of such pulses is on the order of 10^{-8} sec and hence with count rates on the order of 10^2 to 10^4 per second, there would be no overlapping of pulses to produce smooth signals as is observed.

*As the general rule with uncertainties arising from multiplied quantities.

APPENDIX D

Contamination of auroral H-beta photometric measurements due to galactic hydrogen emissions

Galactic hydrogen emissions can seriously contaminate auroral H-beta measurements (Eather, 1966). The best way to eliminate this source of contamination is to avoid it. If it cannot be avoided, then some accounting of it must be made.

Montbriand, et. al. (1965) have published an atlas of galactic hydrogen-emitting regions with apparent intensity contours based on a one-degree field of view. This atlas was transferred to a polar star chart for the northern hemisphere which was fastened to a small board. Mounted concentric with this star chart in a fashion such that they could be rotated independently were:

1) An hour angle chart so that upon placing the midnight hour at the appropriate position on the star chart, local times could be read for any night of the year chosen.
2) A plastic overlay with the projection of the plane of the field of view of the scanning photometer system plotted on the celestial sphere. Hence by aligning the geographic meridian with the local time on the hour angle chart, the field of view of the scanning photometer could be seen against the galactic contamination background.

The night studied in detail here was generally free from galactic contamination except for the early evening portion. Figure D.1 shows the scanning photometer field of view for the time around 1729, January 20/21.

Fig. D.1 Photograph of analog device constructed to show the field of view in the celestial sphere of a photometer scanning the 256° dipole meridian at a specified local time.

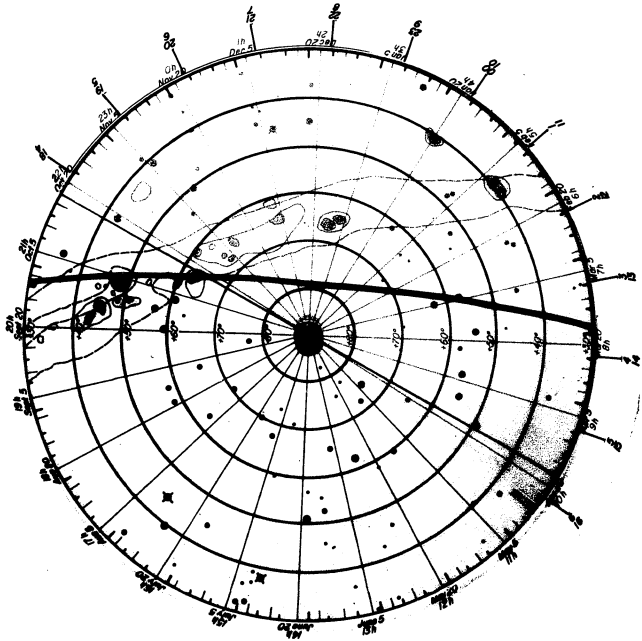

REFERENCES

Akasofu, S.-i., The development of the auroral substorm, Planet. Space Sci., 12, 273-282, 1964.

Akasofu, S.-i., Dynamic morphology of auroras, Space Sci. Rev., 4, 498-540, 1965.

Bates, D. R. and M. Nicolet, Theoretical considerations regarding the altitude of the layer responsible for the nocturnal emission of the sodium D-lines, J. Geophys. Res., 55, 235-239, 1950.

Belon, A. E., G. J. Romick, M. H. Rees, The energy spectrum of primary auroral electrons determined from auroral luminosity profiles, Planet. Space Sci., 14, 1966.

Berkey, F. T., A study of the auroral absorption substorm, Ph.D Thesis, University of Alaska, 1971.

Bernstein, W., G. T. Inouye, N. L. Sanders, R. L. Wax, Measurements of precipitated 1-20kev protons and electrons during a breakup aurora, J. Geophys. Res., 74(14), 1969.

Bowman, M. R., L. Thomas, J. E. Geisler, The effect of diffusion processes on the hydrogen and oxygen constituents in the mesosphere and lower thermosphere, J.A.T.P., 32, 1661-1674, 1970.

Bracewell, R. N., Simple graphical method of correcting for instrumental broadening, J. Optical Society of Amer., 45, 10, 873-876, 1955.

Broadfoot, A. L. and D. M. Hunten, Canadian Journ. Phys., Vol 42, 1212-1230, June 1964.

Chamberlain, J. W., Physics of the Aurora and Airglow, Academic Press, 1961.

Chase, L. M., J. Geophys. Res., 73, 3469, 1968.

Chase, L. M., Energy spectra of auroral zone particles, Ph.D. Thesis, University of California, Berkely, 1969.

Cloutier, P. A., H. R. Anderson, R. J. Park, R. R. Vondrak, R. J. Spiger, and B. R. Sandel, Detection of geomagnetically aligned currents associated with an auroral arc, J. Geophys. Res., 75, 13, 1970.

Condal, A. R., Effects of aerosol particles on tropospheric scattering, M. S. Thesis, University of Alaska, 1971.

Davidson, G. T., Expected spatial distribution of low-energy protons precipitated in the auroral zone, J. Geophys. Res., 70(5), 1061-1068, 1965.

Davis, L. R., D. E. Berg and L. H. Meridith, Space Research I., 721, North-Holland Pub. Co., Amsterdam, 1960.

Davis, T. N., Variables involved in descriptions of worldwide auroral morphology, Geophysical Institute Report, UAGR-187, 1967.

Eather, R. H., Red shift of auroral hydrogen profiles, J. Geophys. Res., 71, 5027, 1966.

Eather, R. H., Auroral proton precipitation and hydrogen emissions, Rev. Geophys., 5(3), 207-285, 1967.

Eather, R. H., Spectral intensity ratios in proton-induced auroras, J. Geophys. Res., 73, 119-126, 1968.

Eather, R. H. and F. Jacka, Auroral hydrogen emission, Australian J. Physics, 19, 241-284, 1966.

Eather, R. H. and B. P. Sandford, The zone of hydrogen emission in the night sky, Australian J. Physics, 19, 25-33, 1966.

Fastie, W. G., Journal of the Optical Society of America, 42, 641, 1952.

Foord, R., R. Jones, C. J. Oliver, E. R. Pike, The use of photomultiplier tubes for photon counting, Applied Optics, 8(10), Oct. 1969.

Gal'perin, Yu. I., Hydrogen emission and two types of auroral spectra, Aurora and Airglow, 1, 1959.

Gartlein, C. W., Auroral spectra showing broad hydrogen lines, Trans. Am. Geoph. Union, 31, 18-20, 1950.

Gartlein, G. W. and G. Sprague, Hydrogen in auroras, J. Geophys. Res., 62(4) 521-526, 1957.

Johnstone, A. D., Measurements of low energy protons in a pulsating aurora, Ph.D Thesis, University of Alaska, 1970.

Kieffer, L. J., Low energy electron collision cross section data, Atomic Data, 1, 121-287, 1969.

Loomis, E., The great auroral exhibition of August 28 to September 4, 1859; and the geographic distribution of auroras and thunder storms, American Journal of Science and Arts, 30, 79-100, 1860.

McIlwain, G. E., J. Geophys. Res., 65, 2727, 1960.

Meinel, A. B., Doppler-shifted auroral hydrogen emission, Astrophys. J., 113, 50-54, 1950.

Miller, J. R., Optical measurements in hydrogen aurora, Ph.D Thesis, University of Saskatchewan, 1969.

Montalbetti, R., Photoelectric measurements of hydrogen emissions in aurorae and airglow, J. Atm. Terr. Phys., 14, 200-212, 1959.

Montbriand, L. E., M.Sc. Dissertation, University of Saskatchewan, 1961.

Montbriand, L. E., Morphology of auroral hydrogen emissions during auroral substorms, Ph.D. Thesis, University of Saskatchewan, 1969.

Montbriand, L. E. and A. Vallance Jones, Studies of auroral hydrogen emission in west-central Canada. I. Time and geographical variations, Canadian Journal of Physics, 40, 1401, 1962.

Montbriand, L. E. J., B. A. Tinsley, and A. Vallance Jones, Galactic hydrogen as a hazard in auroral spectroscopy, Can. J. Phys., 43, 782, 1965.

Oldenberg, O., D. G. Bills, N. P. Carleton, Measurement of weak absorption by molecules, J. Opt. Soc. Am., 51, 526, 1961.

Omholt, A., Characteristics of auroras caused by angular dispersed protons, J. Atmospheric Terr. Physics, 9, 18-27, 1956.

Omholt, A., W. Stoffregen and H. Derblom, Hydrogen lines in auroral glow, J. Atmos. Terr. Phys., 24, 203-209, 1962.

Reasoner, D. L., R. H. Eather, B. J. O'Brien, Detection of alpha particles in auroral phenomena, J. Geophys. Res., 73(13), 1968.

Rees, M. H., A. E. Belon and G. J. Romick, The systematic behavior of hydrogen emission in the aurora, I. Planet. Sp. Sci., 5(2), 87-91, 1961.

Rees, M. H., A. E. Belon, G. J. Romick, Spectrographic development of the aurora I, J. Atm. Terr. Physics, 14, 1963.

Remy, L., C. Arpigny and B. Rosen, Identifications in the spectra of aurorae, Air Force Cambridge Research Center, Geophysics Research Directorate, Tech. Note NR-6, Contract NF AF 61(052)-24, 1960.

Romick, G. J. and A. E. Belon, The determination of the spatial distribution of auroral luminosity, University of Alaska Report, 1964.

Romick, G. J. and C. T. Elvey, Variations in the intensity of the hydrogen emission line H-Beta during auroral activity, J. Atmos. Terr. Physics, 12, 283-287, 1958.

Romick, G. J., and R. D. Sharp, Simultaneous measurements of an incident hydrogen flux and the resulting hydrogen Balmer alpha emission in an auroral hydrogen arc, J. Geophys. Res., 72, 4791, 1967.

Shemansky, D. E., N. P. Carleton, Lifetime of the N_2 Vegard-Kaplan system, J. Chem. Physics, 51(2), 682-688, 1969.

Sorass, F. and Trumpy, B., J. Atmos. Terr. Physics, 28, 1081, 1966.

Stoffregen, W. and H. Derblom, Auroral hydrogen emission related to change spearation in the magnetosphere, Planet. Space Sci., 9, 711-716, 1962.

Vegard, L., Hydrogen showers in the auroral region, Nature, 1944, 1089-1090, 1939.

Vegard, L., Composition, variations and excitation of the auroral luminescence spectra, Geofysiske Publikasjoner, 19, 9, 1955.

Vegard, L. and G. Kvifte, Spectral investigations of aurorae and twilight, Geofysiske Publikasjoner, 16, 7, 1945.

Veissberg, O. L., Spectroelectrophotometric studies of hydrogen emission in auroras, Aurora and Airglow, Results of Researches of I.G.Y., SSSR Acad. Sci., 8, 36, 1962.

Wax, R. L. and W. Bernstein, Rocket borne measurements of H_β emissions and energetic hydrogen fluxes during an auroral breakup, 1969 preprint.

Whalen, B. A., McDiarmid, I. B. and Budzinski, E. E., Canadian Journal of Physics, 45, 3247, 1967.

Wiese, W. L., M. W. Smith and B. M. Glennon, Atomic transition probabilities, Vol. I, National Standard Reference Data Series, National Bureau of Standards, 4, 1966.